AD A062264

DDC FILE COPY

ARO 12800.2-MSX

LEVEL II

ARO Grant No. DAAG29-76-G-0180 SMT-1-78

AN INVESTIGATION OF THE INFLUENCE OF SHOCK-WAVE PROFILE ON THE MECHANICAL AND THERMAL RESPONSES OF POLYCRYSTALLINE IRON

Final Technical Report, 5 April 1976 — 16 July 1978

Prepared For: U. S. Army Research Office - Durham
Box CM, Duke Station
Durham, NC 27706

Prepared By: G. A. Stone, G. T. Gray, A. R. Pelton R. N. Orava
Department of Metallurgical Engineering
So. Dakota School of Mines & Tech

DDC
RECEIVED
DEC 12 1978
F

Approved for public release; distribution unlimited.

Division of Engineering
South Dakota School of Mines & Technology
Rapid City, South Dakota 57701

410558

12 04 089

REPORT NUMBER SMT-1-78

Final Technical Report

on

AN INVESTIGATION OF THE INFLUENCE OF SHOCK-WAVE PROFILE ON THE MECHANICAL AND THERMAL RESPONSES OF POLYCRYSTALLINE IRON

by

G. A. Stone, R. N. Orava,

G. T. Gray, A. R. Pelton

Department of Metallurgical Engineering

South Dakota School of Mines and Technology

September 30, 1978

Prepared for

U. S. Army Research Office - Durham

ARO Grant No. DAAG29-76-G-0181

5 April 1976 - 16 July 1978

Approved for public release; distribution unlimited.

ABSTRACT

An investigation was conducted to determine the relative influence of shock-wave parameters on the strengthening of Magnetic Ingot Iron and AISI 1008 Steel. The shock-wave parameters include peak pressure, peak pressure duration, and rarefaction rate. An independent variation of one of these parameters with the other two held relatively constant provided an adequate source of comparison to determine the effect of each parameter on hardness, tensile properties, strengthening, and microstructure. Eighteen shock-loading conditions were studied with peak pressures of 8, 10, 13, 18, 25 and 35 GPa. As peak pressure was increased, an increase of the 0.2% offset yield stress, hardness, twin density and the degree of room temperature strain aging was observed. An increase of pulse duration caused an increase of twin volume fraction, yield strength, and strain aging. Rarefaction rate was found to produce no systematic changes in structure or properties.

A recovery study on the shock-hardened material was conducted and compared to samples which were cold-reduced to equivalent maximum shear strain. Isochronal (1 hr) anneals were conducted in the temperature range from 25 to 650°C. Recovery was monitored by hardness measurements, tensile tests, and optical and transmission electron microscopy. Annealing response is most influenced by peak pressure variations; however, increasing pulse duration can also effectively modify the recovery. Rarefaction rate shows no unifying trends on the softening of the shocked steel. One hour, 450°C recovery anneals eliminated work softening in the lower pressure shots, whereas the tensile properties of the higher pressure samples were only partially stabilized by aging. An additional effect of the recovery anneals was the appearance of upper and lower yield points in the shocked and cold-rolled AISI 1008 steel. The annealed low-pressure and cold-rolled samples showed improved tensile properties compared to the as-deformed properties. The tensile properties of the high pressure shots were not improved by aging at 450°C.

ACCESSION for
NTIS Section
DDC Section
BY
DISTRIBUTION/AVAILABILITY CODES
SPECIAL
A

TABLE OF CONTENTS

		Page
I.	INTRODUCTION	1
	1.1 Thermal Mechanical Treatments	2
	1.2 High Energy Rate TMP	4
	1.3 Shock TMT	6
II.	PROGRAM OBJECTIVES	11
III.	EXPERIMENTAL MATERIALS AND PROCEDURES	12
	3.1 Materials	12
	3.2 Shock-Loading Procedure	13
	3.3 Cold Rolling Procedure	15
	3.4 Thermal Treatments	15
	3.5 Hardness Testing Procedure	16
	3.6 Optical Metallography Preparation	17
	3.7 Quantilative Metallography	18
	3.8 Tensile Sample Preparation and Testing Procedure	18
	3.9 TEM Specimen Preparation	19
IV.	EXPERIMENTAL RESULTS	20
	4.1 Structure and Properties of The As-Shocked Material	20
	4.1.1 Optical Metallography	20
	4.1.2 Hardness and Room Temperature Strain Aging	21
	4.1.3 Tensile Properties	22
	4.2 Variation of Hardness with Recovery Anneals	23
	4.2.1 Effects of Peak Pressure	23
	4.2.2 Effects of Pulse Duration	24
	4.2.3 Effects of Rarefaction Rate	25

		Page
	4.2.4 Effects of the Mode of Deformation	25
	4.3 Influence of Recovery Anneal on Tensile Properties	25
	4.3.1 Effects of Peak Pressure	26
	4.3.2 Effects of Pulse Duration	27
	4.3.3 Effects of Rarefaction Rate	27
	4.3.4 Effects of the Mode of Deformation	28
	4.4 Optical Microscopy	29
	4.4.1 Effects of Peak Pressure	29
	4.4.2 Effects of Pulse Duration	29
	4.4.3 Effects of Rarefaction Rate	30
	4.4.4 Effects of the Mode of Deformation	30
	4.5 Transmission Electron Microscopy	30
	4.5.1 Effects of Peak Pressure	30
	4.5.2 Effects of Pulse Duration	31
V.	DISCUSSION OF RESULTS	33
	5.1 General Discussion of Structure and Mechanical Properties	33
	5.1.1 Substructure Development	33
	5.1.2 Mechanical Properties	38
	5.2 Purity and Grain Size	41
VI.	CONCLUSIONS	43
	References	46
	Tables	50
	Figures	71

0 I 009

I. INTRODUCTION

The industrial demand for materials with specific mechanical properties has stimulated research and development of new processing techniques. Some of these novel processes may not be immediately acceptable; although the design specifications may be met, the advantages of incorporating the techniques may be outweighed by the disadvantages. However, continued research should improve the processes so that they may become alternatives to conventional methods. A technique currently involved in this evolutionary trend is thermal-mechanical processing (TMP) using high energy rate forming (HERF). One of the more promising applications of using HERF in a TMP schedule is shock TMP.

The benefits of using high velocity shock waves as a strengthening mechanism, relative to strenthening by conventional straining, are well known. They are summarized as follows [1]:

1. Higher strengths per unit strain.
2. Little or no shape change, i.e., small residual strain.
3. Absence of anisotropy; no significant orientation dependence or directionality of properties.
4. Through-section uniformity of deformation and, therefore, uniformity of strengthening.
5. Possibility of the application of large strains where high initial strength, and/or minimal ductility, precludes other means of straining.

In addition to the above structural advantages of shock straining, there are also microstructural effects. Shock loading generates a higher concentration of excess vacancies which can aid in reducing

aging times. Also, there is generally a higher density of finer slip bands associated with this dynamic deformation [2]. Refinement of slip can influence strength, ductility, fatigue, and stress rupture [3]. These inherent advantages lead to potential benefits from using shock TMP.

However, there are still many factors involved with shock loading that remain unclear. For example, little is known about the influence of the shock-wave profile parameters other than peak pressure. Other important shock parameters are peak-pressure duration and rarefaction rate. Moreover, information on the effects of these three parameters on the thermal recovery of shock-loaded metals is scarce. This knowledge is critical to the understanding of shock TMP. Therefore, the present study was undertaken to partially fill this void for iron base alloys. The following sections will provide a background for a clearer understanding of shock TMP:

Section 1.1 Thermal Mechanical Treatments

Section 1.2 High Energy Rate TMP

Section 1.3 Shock TMP

1.1 Thermal Mechanical Treatments

Mechanical treatments are often applied in different sequences with thermal treatments. Depending on the order, the heat treatments are used to modify the microstructure by dislocation rearrangement, phase transformations, precipitation, or grain-size control.

In order to distinguish among the great number of thermal-mechanical treatments (TMT) or processes (TMP), a system of classification has been developed by Radcliffe and Kula [4]. Their system can

be summarized as follows:

Class I. Deformation completed before austenite transformation, i.e., the formation of martensite in strain-hardened austenite (e.g., ausworking).

Class II. Deformation during transformation of austenite, i.e., the formation of martensite during deformation (e.g., isoforming, TRIP Steels).

Class III. Deformation after transformation of austenite, i.e., strain aging of austenite transformation products (e.g., marforming, warm working).

Class III treatments also include: ferrous or nonferrous alloys which are precipitation-hardenable only; deformation plus aging; or pre-aging plus deformation sequences [1].

As an example of the possible advantages of TMP, consider the following: Bailey and Stevenson's [5] rationale in a recent investigation on the TMT of SAE 1010 Nitrogenized Steel was to capitalize on the inherent work-hardening effects during stamping of automotive components. By incorporating the forming operations into a TMT process, the researchers found that the tensile strengths were in excess of 600 MN/m^2 and total elongations were on the order of 18%. These properties are equivalent to those of a 980 micro-alloyed high strength, low alloy (HSLA) steel [5]. Other recent work done in conventional TMP include those by Koo and Thomas [6,7] with ferrous alloys, and Waldman, Sulinski and Markus [8] with aluminum alloy ingots.

Kula and Azrin [9] present a review of the major efforts where TMT steels have been used to produce specific items of hardware (e.g., jet engine bearings and armor plating). Finally, Zackay [10] provides a concise report on the effectiveness of the integration of physical and process metallurgy on the technological advancements made in TMT of superalloys, and possibly of aluminum and titanium alloys [10].

1.2 High Energy Rate TMP

Since forming processes depend, in part, on the kinetic energy imparted to the workpiece, it is worthwhile to consider the effects of the rate of deformation processes in TMP. There are essentially two variables that can be used to increase the input energy: mass and velocity. However, from the kinetic energy equation, $1/2\ mv^2$, it is obvious that the energy is more sensitive to variations in velocity than in mass [11]. Thus, by increasing the rate of deformation, the energy increases; a portion of this extra energy can be used to generate more lattice defects, such as dislocations, vacancies, stacking faults, and mechanical twins.

The benefits derived from using high energy rate forming (HERF) processes have been extensively reviewed by Orava and Otto [2], Orava [11], and most recently, by Orava and Wittman [1]. According to the above references [1,2,11], the mechanical properties of many metals can be improved by using HERF techniques. There is also the the possibility of gaining further improvements by HERF TMT.

In the decision to substitute HERF TMT in place of conventional, slower-rate deformation TMT methods, two factors must be considered [12]:

(1) Whether HERF TMT furnishes terminal properties over and above those obtained by conventional TMT or by mechanical or thermal treatments alone.

(2) Whether the shape or size of the material is convenient for HERF TMT.

The progress of employing dynamic TMP has been somewhat lethargic in the past. For example, in 1970, it was reported [2] that a greater

increase in terminal hardness could be obtained in aluminum alloys after HERF prestrain than after uniaxial static prestrain. However, in the intervening years, this research has not been completed; the strengthening of precipitation-hardenable aluminum alloys has not been experimentally determined [1,11]. Stein and Johnson [13] studied the properties of D6-AC tool steel and H-11 HSLA steel which had been ausformed by explosive forming. They found that the mechanical properties of the steels were not improved by using HERF in TMT. Their only encouraging conclusion was that it is possible to explosively ausform steels which transform too quickly to allow ausforming by conventional means. Orava [11] reports that other attempts have met with equally discouraging results: the benefits of TMP by explosive forming of 17-7PH stainless steel and Beta III titanium alloy were not sufficient to justify dynamic forming solely for this purpose.

In late 1970, Murr and Korbonski [14] presented some significant results on the thermal recovery of explosively formed Type 304 stainless steel. Unfortunately, the authors did not compare their results with statically deformed stainless steel. However, a qualitative comparison may be made between statically and dynamically deformed 304 stainless steel by using the results obtained by Murr and Grace [15] in 1969. In this paper, it was pointed out that simple static compression of the austenitic stainless steel led to dislocation pile ups; cold rolling the same material formed α-martensite, and shock loading produced twin faults. When the stainless steel was explosively expanded more than 25%, the resulting substructure was characterized by a high density of dislocations and deformation twins. It

was also determined tha' the subsequent thermal response of HERF expanded 304 stainless steel is essentially identical to that for shock-loaded stainless steel in terms of hardness and microstructure [14].

Although the results by Murr et al. [14,15] are encouraging, they are not complete. Optimization studies should be made, for example, on the terminal mechanical properties of Type 304 stainless steels, statically and explosively expanded, with subsequent aging in the recovery range (<700°C).

1.3 Shock TMT

As previously mentioned, a highly promising application of TMP by HER deformation is shock TMP. The effect of shock deformation is to increase the dislocation density and/or to form a polygonized substructure. Although the yield strength is increased by shock loading, the ductility may be greatly reduced [16]. Therefore, the recovery anneals are used to stabilize the shock-induced substructure. In this way, the terminal properties of metals can be improved.

Although several papers have discussed shock TMP, most of them were concerned only with monitoring the annealing response of shock-hardened metals. Few attempts were made to optimize the TMP. However, in order to obtain the maximum benefits from a shock TMP schedule, it is useful to review some of the earlier results obtained for iron-base alloys.

Leslie et al. [17] studied the effects of annealing temperature on the microstructure of α-iron shock loaded between 7 and 55 GPa and cold rolled 60 and 90%. It was found that the shocked iron recrystal-

lized more rapidly than the cold-rolled iron. This was attributed to the high concentration of point defects thought to be present in shock-strengthened materials. Also, there was little difference in the kinetics of recrystallization of specimens shocked between 15.5 and 31 GPa at annealing temperatures of 500°C below. Specimens loaded to above 13 GPa recrystallized to fine, equiaxed ferrite grains which confirmed an earlier observation by Zukas and McQueen [18].

The Soviets have also studied shock TMP of α-iron. Pressures of 11.5 and 21 GPa at 20 to 950°C were used for shock-loaded Armco iron in one investigation [19]. When the iron specimens were shock strengthened at different temperatures and a pressure of 21 GPa, it was found that the mechanical strength properties fall as the loading temperature rises, but then levels to a constant value at 700°C. They offer no explanation for this occurence. Specimens loaded to approximately 11.5 GPa at 700 and 900°C underwent the $\alpha \rightarrow \gamma$ phase transition. This process resulted in recrystallization with considerable grain refinement, disappearance of twin markings, and a drop in hardness. The same Soviet investigators studied the strength and ductility of Armco iron shock loaded to 13 GPa at 750 and 800°C [20]. By analyzing their data, it was found that after shock treatment at 750°C, there was an increase of 68% in the 0.2% yield strength and a decrease in ductility of only 3% from the original annealed state. After a second anneal at 300°C for two hours, the 0.2% yield strength dropped approximately 10%, but the ductility increased almost 6% over the values of the initial shock-thermal treatment. Similar results were obtained from shocking at 800°C. These Soviet findings must be used with caution as there were no measures taken in either investigation to prevent spallation

during shock loading.

The annealing response of shock-loaded Type 304 stainless steel was studied in the pressure range of 12 to 120 GPa, and compared with the response of the same material cold rolled 5 and 45% [21]. The recovery of the mechanically deformed stainless steel was monitored by micro-hardness measurements and by optical and transmission electron microscopy. The hardness data show that softening occurs at lower temperatures for heavily cold-rolled stainless steel than for shock-loaded stainless steel.

Electron microscopy of the shocked material revealed the presence of an increasing volume percent of twin-fault density with increasing pressures up to 42.5 GPa. This high density of twin faults was responsible for retarding the recovery and recrystallization processes. In contrast, the microstructure of the cold-rolled stainless steel was characterized by extensive martensite.

Optical microscopy showed that for the annealed, shocked material, complete recovery led to grain growth with no classical (intermediate) recrystallization stage. Recovery of the shocked stainless steel was also described as possibly resulting from a high density of point defects. Similar microscopic observations of the 45% cold-rolled stainless steel disclosed a typical recovery and recrystallization response. In addition, there was no evidence of grain refinement in the shocked stainless steel as was previously seen in the shocked iron [17,18]. According to the authors, "...this feature (lack of grain refinement) is indicative of the fact that the twin-fault structures in the shock-loaded stainless steel recovered without necessarily acting as prominent nucleation sites for new sub-grains..." [21].

Other work [14] on the annealing response of shock-loaded 304 stainless steel led to similar results.

Through electrical resistivity measurements of shocked (30 GPa) Fe-Mn alloys, Christou [22] observed three recovery stages, designated as Stages III, IV, and V: Stage III corresponds to the annihilation of interstitials through recombination with vacancies; Stage IV is interpreted as being due to the migration of vacancies to dislocations; and Stage V involves the annealing out of dislocations through a dislocation climb process which involves the self diffusion of vacancies. From these findings, it was concluded that the vacancy concentration after shock loading to 30 GPa is much larger than the interstitial concentration.

An investigation of the effects of shock loading on Young's Modulus of 1018 steel and of the activation energy of recovery was conducted by Huo and Ma [23]. They postulated that in 1018 steel shocked to approximately 10 GPa, carbon plays the dominating role in the recovery process, with nitrogen and vacancies having only a minor role. However, at approximately 30 GPa, the role of vacancies become more important. These speculations can be justified since the concentration of vacancies increases with increasing shock pressure. The activation energies for recovery also tend to confirm these hypotheses.

Stein and Johnson [13] directed their study towards the optimization of shock ausforming a 0.43% C, 3.0% Cr, 1.5% Ni and 1.5% Si steel. The material was shocked in three conditions: (1) in the metastable austenitic state, (2) in the tempered martensitic state, and (3) in the tempered martensitic state after prior ausforming. While shock loading increased the yield strength of the steel in

all three conditions, the maximum benefits were obtained from shock loading a sample tempered at 212°F (100°C) for one hour. The ultimate tensile strength increased from 250 ksi (1724 MN/m^2) to 398 ksi (2745 MN/m^2), and the ductility increased from 1% to 21% reduction in area.

II. PROGRAM OBJECTIVES

The experimental approach was designed to achieve the following objectives:

1) To correlate the specific shock-wave parameters: peak pressure, pulse duration, and rarefaction rate with hardening, microstructure, and the $\alpha \rightarrow \varepsilon$ transformation.

2) To permit the classification of shock-wave parameters according to the order of their contribution in controlling microstructure, mechanical properties, and hardening.

3) To assess the validity of previous results pertaining to the hardness, microstructure, and mechanical properties of shock-loaded pure iron and low-carbon steel.

4) To evaluate the hardness response of shocked iron to strain aging as a result of shock loading.

5) To improve the mechanistic understanding of the shock strengthening of iron, as it is affected by shock parameters other than peak pressure.

6) Assessment of the advantages of the combined effects of thermal and mechanical treatments.

7) Determination of the combined effects of temperature and the shock-wave parameters (peak pressure, pulse duration, and rarefaction rate) on the recovery of the shock-hardened materials.

8) Correlation of the mechanical and thermal behavior with the dislocation substructure, phase transformation products and grain morphology.

III. EXPERIMENTAL MATERIALS AND PROCEDURES

3.1 Materials

The materials under investigation were Armco Magnetic Ingot Iron and AISI 1008 Steel. Magnetic Ingot Iron sheet, 0.110 in. (2.8 mm) thick was obtained from Armco Steel Corporation in a cold-rolled form. The AISI 1008 sheet of thickness 9.118 in. (3.0 mm) was received in a recrystallized form from the supplier.

The chemical analyses of the Ingot Iron and AISI 1008 Steel as determined by Anamet Laboratories, Inc., Berkeley, California are (weight percent):

Element	Ingot Iron	1008
Al	0.07	0.003
C	0.006	0.074
Cr	0.05	<0.005
Cu	0.11	<0.005
MN	0.14	0.39
Mo	0.04	0.02
Ni	0.07	<0.005
N	0.006	0.002
O	0.004	0.007
P	0.006	0.007
Si	0.08	<0.005
S	0.019	0.010
Ti	0.07	<0.005

The Magnetic Ingot Iron was cut into three inch (8.0 cm) by four inch (10.0 cm) pieces, annealed at 723°C for one-half hour in an Argon atmosphere, and allowed to furnace cool. The average grain diameters were 19.3 μm and 130 μm for the AISI 1008 Steel and Magnetic Ingot Iron, respectively. The microstructures of the AISI 1008 and Magnetic Ingot Iron are shown in Figure 1.

3.2 Shock-Loading Procedure

The explosive-loading conditions to permit a correlation of shock hardening and substructure with differences in shock-wave parameters were generated with a computer program [24]. Orava and Wittman [25] introduced the use of the Gurney model for predicting driver-plate velocity from explosive loading. The computer program supplies a rapid means of utilizing these techniques to generate shot specifications from desired parameters. The shot parameters with explosive and tooling dimensions are listed in Table I.

Shock deformation is achieved by the propagation through the material of a planar shock wave produced by means of a "mouse trap" or parallel-plate generator, illustrated in Figure 2. This accelerates a driver plate to a high velocity impact with the specimen assembly shown in Figure 3. This system is designed to prevent spalling and to minimize internal wave reflections and their effects.

The assembly consists of a 1/16 in. (1.6 mm) thick cold-rolled steel cover plate to protect the specimen surface and a 3/4 in. (1.9 cm) thick spall plate. In between the cover plate and spall plate two 3 in. (8.0 cm) by 4 in. (10.0 cm) specimens are placed with the top one being Magnetic Ingot Iron and the lower 1008 Steel. This composite is surrounded by four 1 in. (2.5 cm) thick momentum traps and rests on a 3/4 in. (1.9 cm) thick steel anvil plate. The various components are adhered together by means of an epoxy resin to ensure transmittal of the shock wave across the metal-metal interface. All of the steel is cold-rolled AISI 1020, the acoustic impedence of which closely matches that of Magnetic Ingot Iron and AISI 1008.

The driver plate, determined by computer program to generate

desired shock-wave parameters, positioned either parallel or inclined to and displaced at the necessary standoff distance from the target, is accelerated by means of an explosive detonated by a plane-wave generator. The plane-wave system, used to detonate this explosive uniformly, is comprised of balsa wood standoffs supporting the driver plate and explosive. The inclined-plate shot setup is used for loads less than 15 GPa. Above 15 GPa the parallel-plate or "mouse trap" assembly is used. In the "mouse trap" assembly, point detonation of the line-wave generator results in the line detonation of the starter charge of Detasheet C-2 placed on the glass plate (Figure 2A). As the two sheets burn, they fracture the glass. The preset angle provides a planar shower of glass fragments onto the main charge. This results in simultaneous detonation over the entire main charge surface.

The assembly is placed on a piece of insulation board set on a reinforced cardboard box filled with water. The water serves both as a quenching media and to slow the shot assembly. The steel anvil experiences spallation, but the spall plate/specimen composite is recovered from a pool formed by some of the water originally in the cardboard box.

The explosive used in the experiments is "Detasheet C-1" and "Detasheet C-2," a DuPont PETN-base plastic explosive with density of 1.55×10^2 kg/m^3 and 3.1×10^2 kg/m^3, respectively. The detonation velocity is given by the manufacturer as 7000m sec^{-1}.

The completed shot assemblies ready for detonation are shown in Figure 4. The explosive shots were detonated at Ellsworth Air Force Base, Rapid City, South Dakota under the supervision of ordnance officers.

3.3 Cold Rolling Procedure

To provide a basis of comparison, samples of ingot iron and AISI 1008 steel were cold rolled to the same maximum shear strain as the shock-strengthened specimens. Since there is a state of uniaxial strain produced in shock loading, the shear strain experienced by the shock-loaded material was taken as [26]:

$$\gamma ms = 2 \ln V/V_0$$

where V and V_0 are the compressed and initial specific volumes, respectively. The factor of two represents the straining at the compressive and tensile parts of the shock wave. When the maximum shear strain for the shocked material is equated to the maximum shear strain for the rolled material, given as:

$$\gamma mr = 2 \ln (1 + \varepsilon_{tr}),$$

the engineering thickness strain, ε_{tr}, can be determined. Hence, the percent reduction in thickness can also be determined.

The values for the relative volumes (V/V_0) were taken from the Hugoniot curve for iron [16]. Table II lists the values from the Hugoniot curve, the calculated engineering thickness strains, and the corresponding percent reduction in thicknesses for the cold-rolled samples. There was approximately 0.5% reduction in thickness per pass.

3.4 Thermal Treatments

The AISI 1008 steel and ingot iron samples, both shocked and cold rolled, were subjected to one-hour isochronal thermal treatments between 100 and 650°C. Control samples of the two materials were also

heat-treated. To insure that all of the samples experienced a constant time at temperature, all of the specimens for each heat treatment, were thermally treated together.

A LINDBERG salt bath furnace, Type 56622, was used for the recovery experiments. The composition of the salt was 50% potassium nitrate - 50% sodium nitrate, or 50% potassium nitrate - 50% sodium nitrite [27]. The temperature of the salt bath was monitored by an external, Type K, themocouple connected to a Leeds-Northrup Millivolt Potentiometer, Type 3690. The accuracy of the temperatures was approximately ±5°C.

Following the recovery treatments, the samples were water quenched and mounted in metallographic mounts with room-temperature-cure epoxy.

3.5 Hardness Testing Procedure

Strain aging was followed using Diamond Pyramid Hardness (DPH) measurements. Measurements were performed on the shot samples immediately upon returning to the lab from the detonation range. The initial readings were made directly on the shot samples at room temperature without surface improvement. After the initial hardness readings were taken, a 1.2-in. (0.013 m) square piece was cut from each 3-in. (0.076 m) by 4-in. (0.102 m) shot sample. These pieces were ambient-temperature mounted in a clear polyester casting resin to enable polishing for better hardness readings during the rest of the room temperature strain aging measurements. The mounted samples, upon curing, were mechanically polished on a Jarrett Precision Polisher to 600 grit. The samples were Nital etched for 20 seconds to remove the deformed surface layer.

The hardness readings were taken on an Avery Visual Hardness Testing Machine, Type 6406, with a 30 kg load. To insure accuracy, the Avery Hardness Tester was checked before each series of measurements with a calibration bar. Approximately ten readings were taken on each sample with no edge effects included. The raw data were converted to Diamond Pyramid Hardness (DPH) numbers by the relationship [28]:

$$DPH = (1.854)\ \frac{\text{load}\ \ (\text{kg})}{\text{diagonal}^2 (\text{mm})^2}$$

All the remaining shock-loaded material was stored at -18°C, in order to retain the as shocked properties.

3.6 Optical Metallography Preparation

After the hardness testing, the samples were ground through 15 μm emery paper. They were then polished with 1 μm diamond paste and with 0.05 μm alumina.

The mechanically-polished specimens were subsequently electropolished. The electrolytic solution consisted of 90% glacial acetic acid and 10% perchloric acid. To obtain the optimal polishing conditions for this electrolyte and the two materials, current-voltage data were obtained as suggested by Thomas [29]. A current density of 0.4 amps/cm^2 and voltages of about 10 and 20 volts were required for the ingot iron and AISI 1008 steel, respectively. The electropolishing times were three minutes for the ingot iron and four minutes for the AISI 1008 Steel.

The optical metallography was done on a Vickers Projection Microscope.

3.7 Quantitative Metallography

Quantitative metallographic techniques were employed to determine the volume fraction of grains that contained twins, and the volume fraction of twins within the twinned grains. The point count method was chosen as the most efficient way to measure volume fraction. A 5 by 5 point grid was employed on the metallograph viewing screen. A minimum of 200 grains in area was used for the volume percent of grains containing twins. The point count was also used to determine the volume percent in each grain.

3.8 Tensile Sample Preparation and Testing Procedure

Tensile samples were machined from each shocked and rolled specimen according to the specifications of ASTM A 370 subsize specimens. The dimensions of the tensile bars are given in Figure 5. One tensile sample from each of the deformed specimens was annealed at 450°C for one hour.

The tensile bars were mechanically ground on 55 μm silicon paper and electropolished in a solution of 90% glacial acetic acid - 10% perchloric acid. A time of 10 minutes at a current density of 0.6 amps/cm^2 removed 2.5 x 10^{-4} m from the gauge thickness. After removing the surface layer, the minimum cross-sectional areas were determined by a micrometer.

All tensile tests were performed on a MTS machine, Model 914.69, at room temperature and at a strain rate of 10^{-3} sec^{-1}. The load/elongation curves were converted to engineering stress/plastic strain curves using the point-intercept method. The 0.2% offset yield strength, ultimate tensile strength (UTS), and the percent elongation

to UTS data were determined from these graphs. The percent reduction in area data were obtained from measurements on a light microscope with a filar eyepiece.

3.9 TEM Specimen Preparation

TEM specimens were cut from the as-shocked and the shocked, plus aged samples using a BUEHLER ISO-MET low speed saw. The average thickness of the cut samples was 6×10^{-4}m. These wafers were mechanically thinned to 10^{-4}m using 30 μm silicon carbide paper. Discs 3 mm in diameter were then punched with a standard Diemens grid punch. The discs were subsequently electrothinned using a FISCHION Twin-Jet Electropolisher. The average thinning time was five minutes at a current density of 0.7 amps/cm^2. The samples were observed on a RCA EMU-3G TEM at 100 kV.

IV. EXPERIMENTAL RESULTS

4.1 Structure and Properties of The As-Shocked Material

4.1.1 Optical Metallography

The microstructures of the shock-loaded Armco Magnetic Ingot Iron and the AISI 1008 Steel both exhibited twinning as the predominant feature. An X-ray diffractometer analysis of the as-shocked specimens revealed the presence of only B.C.C. alpha iron, with no detectable amount of high-pressure epsilon being retained upon unloading.

With duration and rarefaction rate held constant, a variation of peak pressure has a significant effect on the percentage of grains which contain twins after shock loading. The photomicrographs shown in Figures 6 and 7 show that as peak pressure increases the number of grains containing twins plus the volume fraction within twinned grains increases.

Increased peak pressure duration increases the volume fraction of grains exhibiting twins and the number of twins within twinned grains in shock-loaded iron and steel. This result is shown in Figures 8 and 9. Shot pairs where rarefaction rate and pressure are held constant, such as shots 10 and 11, shots 13 and 14, and shots 16 and 17, in particular, show that increased duration increases twin volume fraction. Twin formation in both the materials studied are more influenced by duration between 0.5 and 1.0 μsec than between 1.0 and 2.0 μsec. These data are presented in Table III.

The remaining shock-wave parameter, rarefaction rate, was found to have a less pronounced effect on the shocked microstructure. Figures 10 and 11 both demonstrate that at a given pressure and duration the higher rarefaction rate favors smaller twins than does a

lower rarefaction rate. The effect of rarefaction rate on volume fraction of twins formed is not well pronounced. No systematic trend across all shock pressures was detected. All data related to the role of rarefaction rate are tabulated in Table IV.

4.1.2 Hardness and Room Temperature Strain Aging

When duration and rarefaction are held constant a moderate increase in hardness on the Diamond Pyramid Hardness scale (DPH), was observed for the 8, 10, and 13 GPa pressures. Between 13 and 25 GPa pressure, the hardness jumped more than 100 DPH points for both materials studied. The data showing these results are plotted along with the data of Zukas [31] and Dieter [16] in Figure 12.

Strain aging at room temperature is occurring in the Armco Ingot Iron and 1008 Steel between the time of the explosive event and 48 hours. After 48 hours, no significant change in hardness with time was observed. These results are provided in Figures 13 and 14. The absence of data points in Figures 13 and 14 at 3 to 4 hours after shock loading for several of the tests, is related to the poor condition of the specimen surface, making usable hardness measurement impossible.

When duration is varied with peak pressure and rarefaction rate held constant, a direct correlation is also observed between hardness and microstructure. The hardness data tabulated in Table V for shot pairs 10 and 11, and 13 and 14, could be compared with the photomicrographs in Figures 8 and 9. It appears that in the pressure range of 13 to 33 GPa, where three waves would traverse the

the iron specimens, duration is significant in developing the microstructure and mechanical properties of the material. Duration appears to have had little or no effect on microstructure or hardness between 8-13 GPa and above 33 GPa pressure. A summary of some of the hardness data are given in Table V.

When peak pressure and pressure duration are held constant, it appears that varying rarefaction rate results in no systematic modification of microstructure or hardness, with one exception -- shot pair 11 and 12. Table VI provides a summary of DPH hardness data to show the role of rarefaction rate.

4.1.3 Tensile Properties

Peak pressure is seen to affect the yield strength and ultimate tensile strength (UTS) significantly (Figure 15, A and B). The engineering stress-strain curves with only peak pressure changing demonstrate the marked increase in strength for the 25 and 35 GPa shots over the lower pressure shots. All the stress-strain curves fail to show the typical work-hardening behavior of ordinary steels. Instead, the stress-strain curves show signs of early plastic instability such that the UTS is reached at small tensile elongations. These results are shown in Figures 16 and 17.

The amount of elongation to UTS present for material shocked at or below 13 GPa is similar. The 25 and 35 GPa shots yielded greatly reduced elongations to UTS. The presence of a plastic instability is further exemplified by the data on percent elongation to UTS and for reduction in area. When the materials are shocked to higher pressures, a very low elongation to UTS is observed with considerable

reduction in area still present. (See Tables VII and VIII).

Increased pulse duration is observed to increase the 0.2% offset yield of both materials (Table IX). Figures 18 and 19 show that increased duration increases yield strength, expecially after the 25 and 35 GPa shots.

The amount of reduction in area is slightly lower in the higher duration shots. Uniform elongation to UTS is also slightly affected with the higher duration shots exhibiting increased elongations prior to failure. These trends are shown in Figures 18 and 19.

Rarefaction rate is found to be the least significant shock parameter. Little systematic trend was detectable in the dependence of tensile behavior on rarefaction rate. Out of a total of 24 strength comparisons, (yield and UTS), in 14 cases the higher strength was associated with a lower rarefaction rate. In comparing ductility, 9 of the 24 had a lower ductility associated with a lower rarefaction rate.

4.2 Variation of Hardness with Recovery Anneals

4.2.1 Effects of Peak Pressure

The results of macrohardness measurements on the annealed materials where peak pressure is varied with constant pulse duration (1.0 μsec) and rarefaction rate (-51.5 GPa/μsec) are shown in Figure 20 for the AISI 1008 Steel, and in Figure 21 for the ingot iron. These data are also found in Tables X and XI. Figures 20 and 21 show that as the peak pressure is increased from the undeformed state to 35 GPa, there is a corresponding increase in

hardness. The highest initial hardness values were obtained by the samples shocked at 25 GPa. Up to 450°C, the hardness values remain somewhat constant, with the exception of the 25 GPa specimens which dropped in hardness between 25 and 100°C. Above 450°C, there is a more pronounced softening in the 25 and 35 GPa samples than in the lower peak-pressure samples.

The shock-induced hardness completely recovers in the AISI 1008 steel at 600°C, and in the ingot iron at 650°C. In addition, the higher peak-pressure shots attain slightly lower hardness values at these high annealing temperatures than the samples shocked at the lower pressures.

4.2.2 Effects of Pulse Duration

The effects of pulse duration on the annealing response of shock-hardened AISI 1008 steel are seen in Figures 22-27 and Table XII. Increasing the pulse duration from 1.0 to 2.0 μsec at the lower pressures (8-13 GPa), with constant rarefaction rates, results in similar annealing responses. See Figures 22-24. At higher peak pressures (18 and 25 GPa), and at constant rarefaction rates, an increase in pulse duration from 0.5 to 1.0 μsec drastically alters the recovery responses (Figures 25 and 27). These figures show that the longer pulse duration increases the initial hardness; a more pronounced softening at the higher temperatures is also evident in these samples. At 35 GPa, increasing the pulse duration from 0.5 to 1.0 μsec slightly increases the hardness, but the annealing responses are nearly identical.

4.2.3 Effects of Rarefaction Rate

The effects of varying the rarefaction rate (i.e. the rate of peak pressure release) at constant peak pressures and pulse duration (1.0 μsec) on the annealing response of AISI 1008 steel are shown in Figures 28-33 and Table XIII. In general, there are no unifying trends among the samples at these conditions.

Smaller rarefaction rates increase the hardness of the 8, 10, 25, and 35 GPa specimens at annealing temperatures up to 500°C. Above this temperature, the lower rarefaction rates promote greater softening in the 25 and 35 GPa samples. In contrast, the 13 and 18 GPa samples show that an increase in the rarefaction rate results in higher initial hardness and greater softening at higher temperatures.

4.2.4 Effects of the Mode of Deformation

A comparison was also made between the effects of the two modes of deformation, cold rolling and shocking, on the annealing response of AISI 1008 steel and ingot iron. The shock-strengthened samples in this comparison have a pulse duration of 1.0 μsec and rarefaction rate of approximately -51.5 GPa/μsec. The results of this study are presented in Figures 34-39 and Table XIV and XV. With the exception of the 8 GPa shot, the shocked samples attain higher hardness than the cold-reduced samples. In addition, there is a greater recovery of hardness at the higher annealing temperatures when the materials are shocked.

4.3 Influence of Recovery Anneal on Tensile Properties

4.3.1 Effects of Peak Pressure

When peak pressure is varied at constant pulse duration (1.0 μsec) and rarefaction rate (≈ -51.5 GPa/μsec), the tensile properties of AISI 1008 steel and ingot iron are characterized as follows:

1) Increasing the peak pressure results in higher 0.2% offset yield strength and UTS.

2) The percent elongation to UTS is generally less than 10%, and the percent reduction in area is greater than 50%. As the peak pressure increases, these forms of ductility decrease.

The low percent elongation to UTS with the higher percent reduction in area is usually a sign of plastic instability or "work softening." These phenomena are discussed in greater detail in the section.

At the same shock-loading conditions, a one-hour anneal at 450°C modifies the tensile properties in the following manner:

1) All the samples show a reduction in the 0.2% offset yield strength. The 25 and 35 GPa shots experience greater drops than the other shots.

2) The UTS of the lower-pressure samples is equal to, or greater than the UTS of the as-shocked tensile specimens.

3) The percent elongation to UTS increases from the as-shocked condition. Again, the lower pressure shots exhibit a greater increase in this measure of ductility than the higher-pressure samples.

4) The 450°C anneal increases the percent reduction in area of the shocked material, but usually not more than 5%.

With the exception of the 8 and 25 GPa shots, the shocked and annealed steel exhibits upper and lower yield points similar to conventionally deformed low-carbon steels [30]. There is also a tendency for the lower pressure shots to work harden after the one-hour anneal. However, the 25 and 35 GPa samples still show signs of plastic instability after aging at 450°C. The above results are

presented in Figure 40 and Table XVI for the AISI 1008 steel, and Figure 41 and Table XVII for the ingot iron.

4.3.2 Effects of Pulse Duration

The effects of pulse duration on the tensile properties of AISI 1008 steel are not as clearly defined as the effects of peak pressure. At the lower pressures (8-13 GPa) an increase in pulse duration from 1.0 to 2.0 μsec shows no systematic trends in strength or in ductility. However, at the higher peak pressures (18-35 GPa) an increase in pulse duration from 0.5 to 1.0 μsec leads to an increase in both the 0.2% offset yield strength and UTS. With this increasing strength, there is a corresponding decrease in both the percent elongation to UTS and the percent reduction in area. See Table XVIII for these comparisons.

As seen in Figures 42-47, all of the as-shocked samples show signs of plastic instability. The instability is partially eliminated by the 450°C anneal aging and also tends to lower to 0.2% offset yield strength and increase the UTS of the shocked specimens. In addition, the trend of greater strength and less ductility with increased duration at the higher pressures is also evident in the shocked and annealed specimens.

4.3.3 Effects of Rarefaction Rate

There are no systematic trends in the tensile properties of the AISI 1008 steel by varying the rarefaction rate and holding the other two shock-wave parameters constant. There is also a lack of a unifying trend between the tensile properties of the as-shocked

and the shocked and annealed conditions. The results from these tests are shown in Figures 48-53 and Table XIX.

4.3.4 Effects of the Mode of Deformation

The AISI 1008 steel shocked to 8, 13, and 18 GPa have lower strengths than the samples cold-rolled to equivalent maximum shear strains (Figures 54-56 and Table XX). However, the 25 and 35 GPa samples exhibit a marked increase in strength over the cold-reduced material as seen in Figures 57-59. The percent elongations to UTS for the cold-rolled steel are all less than 10%, and the percent reduction in areas are greater than 70%.

At the lower shear strains, the shocked and rolled steel have similar ductilities, but the 25 and 35 GPa shots are slightly less ductile than the 14 and 16% reduced samples, respectively.

As reported in Section 4.3.1, the effects of aging at 450°C on the samples with constant pulse duration and rarefaction rate are: a decrease in the 0.2% offset yield strength; similar or greater UTS in the lower pressure shots, and a lower UTS in the 25 and 35 GPa samples; and an increase in ductility.

The response of the rolled steel to the 450°C anneal are sporadic. The 4 and 16% reduced tensile samples exhibit an increase in the 0.2% offset yield strength, but in the remaining samples there is a decrease in the 0.2% offset yield strength after the recovery anneal. The UTS of the rolled and aged specimens equals or exceeds the tensile strengths of the same samples in the as-rolled condition with the exception of the 16% reduced specimen.

4.4 Optical Microscopy

4.4.1 Effects of Peak Pressure

The combined effects of peak pressure and aging on the microstructure of AISI 1008 steel are clearly seen in Figure 60. A predominant feature of the as-shocked samples is twin-like markings or Neumann bands. An increase in peak pressure from 13 to 25 GPa results in an increase in the number of grains containing twins. The 25 GPa sample also shows grains containing a high concentration of very fine, indistinguishable markings; the 13 GPa micrograph shows a smaller percentage of these mottled markings.

Aging at 450°C for one hour clears the grains of the fine structure in the 13 GPa sample, and to a lesser extent, in the 25 GPa sample also. However, there is still evidence of the twinned structures in both of the annealed samples.

At 600°C, the micrographs are completely devoid of twins and the fine substructure. In addition, the grain size has increased at this temperature.

4.4.2 Effects of Pulse Duration

An increase in pulse duration from 0.5 to 1.0 μsec at 18 GPa and at a constant rarefaction rate (≈ -63.5 GPa/μsec) has a marked effect on the microstructures. See Figure 61. The longer duration increases the percentage of twins and of fine markings in the grains.

After the 450°C anneal, the 0.5 μsec duration micrograph shows ferritic grains with essentially no markings; the 1.0 μsec duration micrograph reveals a slightly reduced percentage of markings.

Aging at 600°C for one hour produces similar microstructures in the two specimens: there is no evidence of fine substructure, and there is slight grain growth.

4.4.3 Effects of Rarefaction Rate

Rarefaction seems to have less effect on the microstructures than the other two shock-wave parameters. As can be seen from Figure 62, there is little perceptible difference between the pairs of pictures. This is also the case for the other comparisons of this parameter.

4.4.4 Effects of the Mode of Deformation

There is a noticeable difference between the microstructures of the shocked and rolled samples, especially at the higher shear strains (Figure 63). The cold-reduced steel does not contain any twins or fine structure; therefore, there is no visible difference in the microstructure as the aging temperature increases.

In contrast, the shocked sample's microstructure is characterized by a high percentage of twins and fine substructure. At higher aging temperatures, the markings within the grains disappear.

4.5 Transmission Electron Microscopy

4.5.1 Effects of Peak Pressure

The substructure of the AISI 1008 steel is greatly affected by increasing peak pressure as seen in Figures 64 and 65. In the as-

shocked state, the lower pressure shots are characterized by mechanical twins or bands, and a high density of heterogeneously distributed dislocations. The highest density of dislocations occurs at the twin-matrix boundaries. The dislocations tend to form sub cells, especially in the absence of twins. The 450°C recovery anneals rearrange the mobile dislocations to form a more homogeneous morphology. In fact, the recovered 13 GPa samples show elongated dislocation lines with no evidence of dislocation tangles or networks.

At higher peak pressures, Figure 65, the structures are more homogeneous than at the lower pressures. The substructure consists of shear plates and sub-micron subgrains. These shear plates, which are remnants of the $\alpha \rightarrow \varepsilon \rightarrow \alpha$ phase transformation, are actually elongated subgrains. Electron diffraction shows a polycrystalline arrangement of these subgrains. Also, there is a high density of dislocations within the subgrains.

The major difference between the 25 and 35 GPa micrographs is the absence of dislocations in several subgrains in the 35 GPa samples.

After aging at 450°C for one hour, the subgrains of the high pressure shots become well defined, and the density of the dislocations in the subgrains decreases. Selected area diffraction images of these structures reveal a single-crystal orientation.

4.5.2 Effects of Pulse Duration

Figure 66 illustrates typical microstructures showing the effects of increasing the pulse duration from 0.5 to 1.0 μsec at 18 GPa and a constant rarefaction rate in AISI 1008 steel. At both pulse durations, there is a tendency for the high density of dislocations to form sub-

grains. However, there is no evidence of shear plates in the 0.5 μsec sample, as seen in the 1.0 μsec duration sample.

The response of the 1.0 μsec duration specimen to the 450°C recovery anneal is similar to the response of the high peak-pressure shots (i.e., the formation of well defined subgrains). On the other hand, the shorter duration sample responds in a similar manner to the lower pressure samples.

V. DISCUSSION OF RESULTS

5.1 General Discussion of Structure and Mechanical Properties

5.1.1 Substructure Development

The variation of peak pressure greatly modifies the substructure of the as-shocked and shocked plus annealed samples. (See Figures 6, 7, 60, 64). Peak pressures up to 13 GPa produce mechanical twins and a high density of dislocations. The appearance of Neumann bands in shocked iron is very common [16,17,32], and it has been shown [16] that these markings occur on the {211} planes. It has been further shown [32] that twinning is produced by the compressive shock front rather than by the tensile reflection.

The dislocations accompanying the mechanical twins at low shock pressures were generally tangled in ill-defined networks heterogeneously scattered within the grains. The cellular structures were more diffuse than is found in conventionally deformed iron [33] or in shock-loaded f.c.c. materials [34,35]. In the regions where twin markings were not as prominent, the dislocations were more uniformly distributed and straighter. This latter dislocation configuration is similar to those previously obtained for shocked iron [17].

A possible explanation for the lack of a well-defined cell structure follows: The formation of cells is believed to be due to the interaction of dislocations which are able to move on various slip systems. Thus, the resulting cell boundaries are composed of dislocations with several different Burgers vectors [36].

Meyers [37] recently proposed a mechanism for dislocation generation in shock-wave deformation. According to his model, dislocations

are homogeneously nucleated at the shock front and are periodically left behind to account for the deviatoric strains. The rarefaction part of the wave can further accomodate deviatoric strains by moving dislocations and by generating new ones. The stress fields associated with the newly formed dislocations can then interact with the stress fields of the already existing dislocations. Thus, the dislocations are able to move, but at velocities less than the transverse shear wave velocity of the material.

At high velocities ($0.5 \lesssim v \lesssim 0.9c$), where "c" is the transverse shear velocity, and "v" is the velocity of the moving dislocation, the stress field of a screw dislocation shrinks in the direction of motion. Because of this shrinkage, the force between fast moving screw dislocations goes to zero [38]. In contrast, the stress fields of moving edge dislocations of like sign attract rather than repel each other in this velocity range. Also, the force between edge dislocations increases with increasing velocity [38].

The ramifications of these phenomena are the following: (1) the screw components of the dislocations are relatively immobile compared to the edge components; (2) it seems that cross-slip is inhibited for the screw components; (3) the resulting dislocation morphology contains elongated segments of screw dislocations.

The above model pertains to the lower pressure samples ($\lesssim 13$ GPa); at higher pressures, twinning and phase transformations are the predominant deformation mechanisms in iron-base alloys. Therefore, it follows that in the presence of extensive twinning or phase transformations, the dislocation morphology is different [39].

It is well known [40] that iron can transform from b.c.c. α to h.c.p. ε under the application of shock waves. The close-packed phase resulting from this pressure-induced transformation depends upon both the applied pressure and temperature [41]. Although no quantitative data concerning the $\alpha \rightarrow \varepsilon$ transformation were obtained in the present study, it is beneficial to discuss the qualitative results in terms of other investigations.

In general, the martensitic reaction competes with slip as the mode of deformation when external stresses are applied. The shear stress required to activate the martensitic transformation decreases with decreasing temperature, whereas the shear stress required to initiate slip increases with increasing temperature [42].

In addition, it has been found [42] that the Ms temperature should be raised by uniaxial compressive stresses. This is tantamount to saying that as the applied stresses increase with increasing peak pressures, it is more energetically favorable for the α to transform to ε than for slip to occur. The observed increase in the transformation product with increasing pressure (Figures 65 and 66) is consistent with this contention.

Other investigators [43] have found that the $\alpha \rightarrow \varepsilon$ transformation in iron is abaric; i.e., the transformation begins at approximately 13 GPa and completed at approximately 17 GPa.

The martensitic phase transformation is not isotropic; rather, it is a function of orientation. The observation that pressure-induced transformation in iron is associated with markings on {112} α planes suggests this anisotropy. As further evidence, not every grain shown in Figures 6-11 and 60-63 has transformed.

Kelly [44] proposed that an invariant plane strain on {112} α together with a dilatation or approximately 1.5% will complete the transformation from α to ε. At the maximum dilatation a twin-related pair will result since twins can only have exactly the same common habit plane on {112} α. According to Bowden and Kelly [45], in the absence of a dilatation or with values less than 1.5%, the α to ε transformation cannot occur by a single invariant plane strain. However, the transformation could occur by the addition of a small inhomogeneous shear, which they assumed is in the form of slip. In this case, habit planes other than {112} α are probably involved. The resulting substructures from the martensitic transformations are shown in Figures 64-66. It was not determined whether the shear plates are twin-related to the matrix. It is believed, however, that slip was operating in some cases to form the complex cellular structure and could have also assisted to induce the transformations.

The role of pulse duration on the formation of the substructure is twofold: First, increasing the pulse duration allows the dislocations generated by the shock stress more time to migrate and equilibrate [46]. From the TEM work it was found that an increase in pulse duration from 0.5 to 1.0 μsec is more effective altering the dislocation morphology than an increase from 1.0 to 2.0 μsec. This suggests that the structure becomes saturated with dislocations at durations of approximately 1.0 μsec. Second, as the duration increases, there is more time to activate rate-dependent processes such as twinning and phase transformations. Conventional isothermal experiments on 70% Fe - 30% Ni single crystals have shown that martensitic plates form in about 0.3 μsec and that the linear growth

velocity is about 10^5 cm sec^{-1} [47]. This high growth velocity suggests that the rate of nucleation is the limiting factor in the formation of twins and martensite [48,49]. To this author's knowledge, the kinetics of shock-induced transformations in AISI 1008 steel have not been previously determined. It seems, however, that the time of formation of one plate of ε-martensite is on the order of 0.5 μsec. Consequently, longer duration times would favor nucleation and growth of the stress-aided deformation products. A good example of the role of pulse duration on microsctructure development is shown in Figure 8 and 9.

Thermal energy from the isochronal anneals at 450°C was sufficient to alter the substructures of the shocked AISI 1008 steel. By comparing the 25 GPa as-shocked and shocked plus annealed structures in both Figure 60 and Figure 65, it is evident that cell walls are more mobile than large-angle boundaries.

It is postulated that the mechanism by which the diffuse cells of the as-shocked material sharpen and grow with subsequent anneals is a complex form of subgrain recovery. If, as postulated earlier, the cell walls are composed of dislocations with mixed edge and screw orientations, then they cannot be tilt boundaries. Rather, the cell walls are probably a combination of twist and tilt type [50]. Furthermore, it was pointed out that aging at 450°C led to a decrease in the misorientation across the subgrain boundaries. Thus, it is possible that a mechanism similar to Li's [51] is responsible for the subcell refinement.

The emergence of recrystallized grains was not revealed by optical microscopy in the higher temperature range; annihilation of the markings within the grains simply led to grain growth. This lends support

to the adoption of Li's theory [51]. However, since TEM of the higher-temperature specimens was not performed during this investigation, it is not known whether subgrain reorientation is followed by subgrain coalescence and sub-boundary migration as dictated by the proposed model [51].

5.1.2 Mechanical Properties

The hardness and tensile properties of the shock-hardened and subsequently annealed specimens can be explained in terms of the sub-structures. For example, it was noted in the previous section that the hardness and strength of the AISI 1008 steel and ingot iron increases with increasing peak pressure. As discussed in Section 5.1, there is an attendant increase in dislocation density, twin density, and above 13 GPa, an increase in shear plates, with increasing peak pressure. In addition, there is a tendency to form diffuse cell structures. It is observed that increasing twin volume fraction increased the UTS and 0.2% offset yield strength. (Figure 67 and 68). Thus, by decreasing the mean-free-path of the mobile dislocations by forming barriers, the strength and hardness of the samples increase.

The residual strength of shock-loaded AISI 1008 steel also increases with increasing pulse duration at constant peak pressures and rarefaction rates. For example, Figure 25 and Figure 26 show that an increase from 0.5 to 1.0 μsec duration increases the hardness by greater than 50%. There is also an increase in the yield strength and UTS in these samples as seen in Figures 18 and 19. These results show that the effects of pulse duration on the hardness and strength

are similar to the effects of peak pressure. This is consistent with results from previous investigations as reported by Meyers [52] and by Moin and Murr [53].

The increase in hardness and strength in the longer duration samples can probably be attributed to the more intricate dislocation morphologies and the increase in the number of twins and martensite debris. These deformation products act as barriers for further dislocation gliding thereby increasing strength and hardness.

All of the tensile tests of the shock-hardened samples showed plastic instability or work-softening as noted earlier. The explanation of this phenomenon is briefly summarized below. According to Longo and Reed-Hill [54], work-softening occurs in many materials that have been deformed at low temperatures or at high strain rates. The dislocation substructure generated at these conditions is very unstable due to the lack of dislocation annihilation and the formation of the diffuse cell structures. When the shocked sample is unloaded to its yield stress during the tensile test, the unstable dislocation configuration is replaced by a more stable one. This probably occurs by dislocation annihilation and re-arrangement. The resulting substructure is characteristic of the morphology formed at that stress level, temperature and strain rate [55]. The deformation is concentrated in certain regions which leads to premature necking [54]. The increase in stress from the necking further concentrates the softening. Thus, as noted earlier, the tensile samples exhibit small elongations with a large reduction in area.

Annealing noticeably affects the mechanical properties of the shocked and cold-rolled AISI 1008 steel and ingot iron. In the shock-hardened samples, the recovery of hardness above ~450°C is probably

due to the elimination of sub-grain boundaries, deformation twins, transformation debris, and the diffusion of vacancies. The increased softening in the initially harder samples results from the release of a greater amount of stored energy from the defects. The morphology of the substructure of the cold-rolled samples was not determined. However, it is postulated that softening in these samples occurs mainly by the elimination of subgrain boundaries and possibly by the diffusion of vacancies. This would account for the more sluggish recovery observed in the cold-rolled material than in the shocked material (Figures 20-39).

The one-hour, 450°C recovery anneals had several effects on the st. ess/strain curves of the shocked samples. One obvious change is the increase in elongation to UTS in the low-pressure shots. This stabilization is probably a result of the annihilation of mobile dislocations, and the refinement of the subgrain boundaries. The work-softening effects were only partially reduced in the higher pressure samples. See Tables XVII and XVI and Figures 40-58.

Another modification from aging is the appearance of upper and lower yield points prior to strain hardening. The origin of the yield points has been discussed by several authors [56,57,58] and is summarized below: When the samples are aged at 450°C, carbon and nitrogen diffuse to dislocation lines. Diffusion is aided by the attractive forces between the strain field of the dislocation and the strain field associated with the interstitial. The dislocation is thus anchored by the impurity cloud. Additional stress is needed for the dislocation to break free from its atmosphere. This increase in the stress is responsible for the upper yield point.

The lower yield point was explained as the result of dislocations breaking away from their impurity clouds. At the lower yield point, zones or bands of high dislocation density spread through the material. The deformed regions, known as Lüders bands, grow at an almost constant stress level. When the bands have traversed the gauge length, the grains are filled with dislocations. Plastic deformation continues by multiplication of these dislocations, leading to work hardening.

The lack of upper and lower yield points in the undeformed and as-deformed (shocked and rolled) samples is probably due to the dispersion of the impurity atoms when the samples were annealed. None of the ingot iron samples displayed the yield point phenomena, even after the recovery anneals. Thus, it is postulated that carbon in solid solution is absent in the ingot iron.

The higher strength of the cold-reduced (4,6, and 12%) steel compared to the shocked (8,10, and 18 GPa) steel is difficult to explain (see Figure 42-44). In a study of TMP of Inconel 718 by cold rolling (19.1%) and shocking (51 GPa), Meyers and Orava [59] observed similar results. The authors attributed the higher strengths in the cold-reduced samples to a higher dislocation density. They suggest that this is due to the use of effective strain rather than maximum shear strain as a basis of comparison. Although this reasoning is not applicable to the present study, it is possible that the dislocation morphology produced by cold rolling is a more effective strengthening mechanism than the arrangement produced by shock loading.

5.2 Purity and Grain Size

Although no direct comparison between the total properties of

the AISI 1008 and the Magnetic Ingot Iron is possible due to the difference in starting grain size, each shows a similar strain aging trend.

The volume % of grains containing twins is higher in the Magnetic Ingot Iron than the AISI 1008 in 10 out of the 18 shots. Hull [60] determined that twinning stress increases with decreasing grain size in 3% silicon iron. The higher volume fraction of twins in the larger grain size Magnetic Ingot Iron presents data consistent with this theory.

The strain-aging behavior of the Magnetic Ingot Iron and AISI 1008 were found to be very similar. Considering the compositional differences between the two materials this finding is at first difficult to believe. Reed-Hill [30] has determined that 0.04 percent carbon or nitrogen is needed to have sufficient interstitial solute to form dislocation atmospheres. The AISI 1008 with 0.074 percent carbon would be expected to show considerably more strain-aging than the 0.006 percent Magnetic Ingot Iron. However, the Ingot Iron contains 0.006 nitrogen which would add its effect to that of the carbon. Holland [61] has determined that the diffusion of nitrogen to form atmospheres would be expected to be the rate-controlling process for strain-aging in iron when nitrogen and carbon are both present. It is believed that the higher percent of faster nitrogen in the Magnetic Ingot Iron compensates for the lower carbon content making the strain-aging of the two materials similar.

VI. CONCLUSIONS

The conclusions that can be drawn from the experimental results follow:

1) Peak pressure is the most significant shock-strengthening parameter. An increase in peak pressure increases the tensile strength and hardness.

2) For material shocked between 25 GPa and 35 GPa pressure, a two-fold increase in UTS is observed. Residual hardness increases between 13 GPa and 25 GPa and appears to level off.

3) A variation in pulse duration does contribute to minor differences in the shock strengthening of iron. The volume fraction of twins was shown to increase with increased duration. Increasing the pulse duration also leads to increase the 0.2% offset yield. The effects of duration were found to be more pronounced in the 13-33 GPa pressure range.

4) Rarefaction rate is found to be the least significant shock parameter. No systematic modification in mechanical properties or microstructure was observed. Accordingly, in previous work, pulse duration effects can probably be attributed to duration and not to concurrent changes in rarefaction rate.

5) Of the three shock-wave parameters, peak pressure has the most effect on the annealing response of shock-hardened AISI 1008 steel and Armco ingot iron.

   a) The samples shock-loaded below the 13 GPa phase transition experienced limited hardness recovery. There was only gradual softening with increasing temperature.

b) Peak pressures greater than 13 GPa promote increased initial hardness and more dramatic softening with subsequent recovery anneals.

6) Increasing the pulse duration from 1.0 to 2.0 μsec seems to have only minor effects on thermal response. In contrast, as increase from 0.5 to 1.0 μsec leads to a more pronounced softening. This suggests that at constant peak pressure and rarefaction rate, hardness saturates at pulse durations of approximately 1.0 μsec.

7) Varying rarefaction rate shows no unifying trends on the softening of shocked AISI 1008 steel.

8) With small amounts of plastic deformation there is little difference in the hardness or annealing response between cold-reduced (4 and 6%) and shocked (8 and 13 GPa) steel. At high plastic deformation, a more dramatic softening occurs during annealing of the shock-hardened materials than occurs in the samples cold reduced to equivalent maximum shear strain.

9) The elimination of work softening in the lower peak-pressure samples was a major effect of the one hour, 450°C recovery anneals. However, the recovered high pressure shots continued to exhibit work softening. A secondary effect of aging was the appearance of upper and lower yield points in the AISI 1008 steel. This yielding phenomena was not observed in the recovered ingot iron.

(10) The recovery anneals generally improved the mechanical properties of both the cold-rolled and shocked AISI 1008 steel.

The modifications were characterized by drops in the 0.2% offset yield strength, equivalent UTS in the cold-rolled and lower pressure specimens, and increased ductilities. The 25 and 35 GPa shots experienced a decrease in both the yield strength and the UTS, and slight increases in the ductility.

(11) Diffuse cellular structures and mechanical twins were the predominant microstructural features in the lower peak-pressure samples. Above 13 GPa, there was a higher density of dislocations which tended to form subgrains. In addition, there was evidence of the $\alpha \rightarrow \varepsilon \rightarrow \alpha$ phase transformation at the higher pressures.

(12) The phase transition was found to depend on peak pressure, pulse duration and crystallographic orientation of the grains for the 18 GPa samples.

REFERENCES

1. R. N. Orava and R. H. Wittman, "High-Energy-Rate-Deformation Processing and its TMP Applications," Advances in Deformation Processing, eds. J. J. Burke and V. Weiss, Plenum Press, New York, 512 (1978).

2. R. N. Orava and H. E. Otto, "The Effect of High Energy Rate Forming on the Terminal Characteristics of Metal - A Review," Journal of Metals 22, 17-31 (1970).

3. R. N. Orava, "An Investigation of the Influence of Shock-wave Profile on the Mechanical and Thermal Response of Polycrystalline Iron," U. S. Army Research Proposal, South Dakota School of Mines and Technology, Rapid City, South Dakota (1974).

4. S. V. Radcliffe and E. B. Kula, "Deformation, Transformation, and Strength," Fundamentals of Deformation Processing, eds. W. A. Bakofen, J. J. Burke, L. F. Coffin, Jr., N. L. Reed, and V. Weiss, Syracuse University Press, 321-63 (1964).

5. D. J. Bailey and R. Stevenson, "High Strength Low Carbon Sheet Steel by Thermomechanical Treatment: I - Strengthening Mechanisms," submitted to Met Trans. A for publication.

6. J. Y. Koo and G. Thomas, "Design of Duplex Fe/X/0.1C Steels for Improved Mechanical Properties," Met Trans. A. 8, 525-28 (1977).

7. J. Y. Koo and G. Thomas, "Thermal Cycling Treatments and Microstructures for Improved Properties of Fe-0.12%C - 9.5%Mn Steels," Mat. Sci. and Eng. 24, 187-98 (1976).

8. J. Waldman, H. Sulinski and H. Markus, "Thermomechanical Processing of Aluminum Alloy Ingots," source cited in Ref. 1, 301-20.

9. E. B. Kula and M. Azrin, "Thermomechanical Processing of Ferrous Alloys," source cited in Ref. 1, 245-300.

10. V. F. Zackay, "Thermomechanical Processing," Mat. Sci. and Eng. 25, 247-61 (1976).

11. R. N. Orava, "Metallurgical Effects of High Energy Rate Forming," Metallurgical Effects at High Strain Rates, Plenum Press, New York, 129-155 (1973).

12. M. A. Meyers, "Thermomechanical Processing of a Nickel-Base Superalloy by Cold Rolling and Shock-Wave Deformation," Ph.D. Dissertation, University of Denver, 16 (1974).

13. B. A. Stein and P. C. Johnson, "Shock Hardening and Explosive Ausforming of Alloy Steels," Trans. TMS-AIME 227, 1188-92 (1963).

14. L. E. Murr and J. A. Korbonski, "Thermal Recovery in 304 Stainless Steel Following Shock Loading and Explosive Forming," Met. Trans. 1, 333-40 (1970).

15. L. E. Murr and F. I. Grace, "Defect Microstructure and Mechanical Properties in Shock-Hardened Metals," Exp. Mech. 9, 153-64 (1969).

16. G. E. Dieter, "Metallurgical Effects of High-Intensity Shock Waves in Metals," Response of Metals to High Velocity Deformation, eds. P. G. Shewmon and V. F. Zackay, Interscience Publishers, New York, 419-21 (1961).

17. W. C. Leslie, E. Hornbogen, and G. E. Dieter, "The Structure of Shock-Hardened Iron Before and After Annealing," JISI 200, 622-33 (1962).

18. E. G. Zukas and R. G. McQueen, "Shock Loading to Produce Fine Grain Size," Trans. TMS-AIME 221, 412-13 (1961).

19. Z. M. Gelunova, V. P. Lemyakin, P. O. Pashkov, "Effect of Shock Waves on the Structure of Armoc-Iron and Copper at Various Temperatures," Phys. Metals Metallogr. 28, 105-10 (1969).

20. Z. M. Gelunova, V. P. Lemyakin, P. O. Pashkov, "Mechanical Properties of Iron Recrystallized Under Shock Loading in a Hot State," Phys. Metals Metallogr. 30, 104-8 (1970).

21. L. E. Murr and M. F. Rose, "Thermal Recovery of Explosive Shock-Loaded Stainless Steel," Phil. Mag, 18 281-95 (1968).

22. A. Christou, "Recovery of Flow Stress and Electrical Resistivity of Shock-Deformed B.C.C. Fe-MN Alloys," Phil. Mag. 26, 97-111 (1972).

23. D. T. C. Huo and C. H. Ma, "Effects of Shock-Loading on Young's Modulus and Activation Energy of Recovery in 1018 Steel," Acta Met. 23, 285-88 (1975).

24. R. O. Lokken, "An Investigation of the Influence of Shock-Wave Parameters on the Shock Strengthening of Nickel," MS Thesis, South Dakota School of Mines and Technology, Rapid City, SD (1976).

25. R. N. Orava and R. H. Wittman, "Techniques for the Control and Application of Explosive Shock Waves," Proc. 5th Intl. Conf. on High Energy Rate Fabrication held in June, 1975.

26. R. N. Orava, "Response of Nickel-Base Superalloys to Thermomechanical Processing by Shock-Wave Deformation," Denver Research Institute, University of Denver, Final Report No. DRI 2638, Contract No. N62269-73-C-0376, U. S. Naval Air Systems Command, April (1974).

27. "Tempering of Steels," ASM Metals Handbook, vol. 2, 8th ed., 51 (1976).

28. G. L. Kehl, Principles of Metallographic Laboratory Practice, 3rd ed., McGraw-Hill, New York, 228 (1949).

29. G. Thomas, Transmission Electron Microscopy of Metals, John Wiley and Sons, New York, 152 (1966).

30. R. E. Reed-Hill, Physical Metallurgy Principles, D. Van Nostrand Company, New York, 342 (1973).

31. E. G. Zukas, "Shock Wave Strengthening" Metals Engineering Quarterly, Vol. 6, p. 1-20, May, 1966.

32. C. S. Smith, "Metallographic Studies of Metals After Explosive Shock," Trans. AIME, 212, 581 (1958).

33. W. C. Leslie, J. T. Michalak, and F. W. Aul, "The Annealing of Cold-Worked Iron," Iron and Its Dilute Solid Solutions, eds., C. W. Spencer and F. E. Werner, Interscience, New York, 120-21 (1963).

34. W. C. Willan, "The Influence of Shock-Wave Parameters on the Mechanical-Thermal Processing of Polycrystalline Nickel," M.S. Thesis, South Dakota School of Mines and Technology, Rapid City, S.D. (1977).

35. R. L. Nolder and G. Thomas, "The Substructure of Plastically Deformed Nickel," Acta Met. 12, 230-32 (1964).

36. R. W. Cahn, "Recovery and Recrystallization," Physical Metallurgy, ed. R. W. Cahn, American El Sevier Publishing Company, Inc., New York, 1144 (1974).

37. M. A. Meyers, "A Mechanism for Dislocation Generation in Shock-Wave Deformation," Script Met., 12, 21-26 (1978).

38. J. Weertman, "High Velocity Dislocations," source cited in Ref. 16, 244.

39. H. Kressel and N. Brown, "Dislocation Morphology in Shock Deformed B.C.C. and F.C.C. Metals and Alloys," Acta Met. 14, 1861 (1966).

40. R. S. Davis, "Iron Phase Transformations at High Pressures," source cited in Ref. 40, 73.

41. D. Bancroft, E. L. Peterson, and S. Minshall, "Polymorphism of Iron at High Pressures," JAP 27, 557 (1956).

42. J. R. Patel and M. Cohen, "Criterion for the Action of Applied Stress in the Martensitic Transformation," Acta Met. 1, 531-38 (1953).

43. P. C. Johnson, B. A. Stein, and R. S. Davis, "Temperature of Shock-Induced Phase Transformations in Iron," JAP 33, 557-61 (1962).

44. P. M. Kelly, "The Martensitic Transformation in Steels with Low Stacking Fault Energy," Acta Met., 13, 635 (1965).

45. H. G. Bowden and P. M. Kelly, "The Crystallography of the Pressure Induced Phase Transformations in Iron Alloys," Acta Met., 15, 1499 (1967).

46. L. E. Murr and D. Kuhlmann-Wilsdorf, "Experimental and Theoretical Observations on the Relationship Between Dislocation Cell Size, Dislocation Density, Residual Hardness, Peak Pressure and Pulse Duration in Shock-Loaded Nickel," Acta Met. 26, 847 (1978).

47. R. r. Bunshah and R. F. Mehl, "Rate of Propagation of Martensite," Trans. AIME, 197, 1251 (1953).

48. J. D. Verhoeven, Fundamentals of Physical Metallurgy, John Wiley and Sons, New York, 497 (1975).

49. R. E. Reed-Hill, source cited in Ref. 36, 629.

50. W. C. Leslie, et al., source cited in Ref. 40, 153.

51. J. C. M. Li, "Possibility of Subgrain Rotation During Recrystallization," JAP, 33, 2958-65 (1962).

52. M. A. Meyers, "Discussion of Residual Strength of Shock Loaded RMI 38644," Met. Trans. 8A, 1641-44 (1977).

53. E. Moin and L. E. Murr, "Summary of Pulse Duration Effects on the Shock-Hardening of Metals and Alloys," Scripta Met. 12, 575-76 (1978).

54. W. P. Longo and R. E. Reed-Hill, "Work Softening in Polycrystalline Metals," Scripta Met., 4, 769 (1970).

55. M. A. Meyers, "Work Softening in Shock-Loaded Nickel," Met. Trans. 8A, 1582 (1977).

56. J. Weertman and J. R. Weertman, "Mechanical Properties I," source cited in Ref. 43, 955-59.

57. E. Hornbogen, "Physical Metallurgy of Steels," source cited in Ref. 43, 620-21.

58. R. E. Reed-Hill, source cited in Ref. 36, 344-46.

59. M. A. Meyers and R. N. Orava, "Thermomechanical Processing of Inconel 718 by Shock-Wave Deformation," Met. Trans., 7A, 179-90 (1976).

60. D. Hull, "Effect of Grain Size and Temperature on Size, Twinning and Fracture in 3% Silicon Iron," Acta Met, 9, 191 (1961).

61. J. R. Holland, "Strain Aging Effects and Stress Relations In Iron During Shock Loading," Acta Met, 15, 696 (1967).

TABLE I
PARAMETRIC, TOOLING, AND EXPLOSIVE REQUIREMENTS
FOR 18 SHOCK-LOADING EXPERIMENTS

SHOT #	PEAK PRESSURE (GPa)	PRESSURE DURATION (μsec)	RAREFACTION RATE (GPa/μsec)	DRIVER PLATE	DRIVER VELOCITY (m/sec)	DRIVER THICKNESS (mm)	EXPLOSIVE NEEDED (# sheets) C1	C2
1	8.0	1.0	-51.55	nickel	437.23	2.674	0	2
2	8.0	1.0	-34.90	1018-ST	502.92	1.925	1	1
3	8.0	2.0	-35.00	304-SS	459.14	4.970	1	3
4	10.0	1.0	-51.40	304-SS	562.20	2.793	1	2
5	10.0	1.0	-36.50	1018-ST	612.71	2.531	1	2
6	10.0	2.0	-36.40	304-SS	562.20	5.028	1	4
7	13.0	1.0	-51.00	copper	713.07	2.577	1	3
8	13.0	1.0	-38.80	1018-ST	768.81	2.282	0	3
9	13.0	2.0	-38.50	304-SS	710.15	5.441	1	6

TABLE I CONT.
PARAMETRIC, TOOLING, AND EXPLOSIVE REQUIREMENTS
FOR 18 SHOCK-LOADING EXPERIMENTS

SHOT #	PEAK PRESSURE (GPa)	PRESSURE DURATION (μsec)	RAREFACTION RATE (GPa/μsec)	DRIVER PLATE	DRIVER VELOCITY (m/sec)	DRIVER THICKNESS (mm)	EXPLOSIVE NEEDED (# sheets) C1	C2
10	18.0	0.5	-63.80	2024-AL	1479.40	1.926	1	1
11	18.0	1.0	-63.30	nickel	898.46	2.766	1	3
12	18.0	1.0	-42.50	1018-ST	1010.18	2.693	1	3
13	25.0	0.5	-71.80	2024-AL	1934.38	2.105	1	2
14	25.0	1.0	-70.50	nickel	1185.18	3.031	1	5
15	25.0	1.0	-51.10	2024-AL	1934.38	4.211	0	5
16	35.0	0.5	-78.00	921T-AL	2522.91	2.524	0	5
17	35.0	1.0	-79.90	nickel	1558.49	3.356	0	9
18	35.0	1.0	-53.30	1018-ST	1710.78	3.286	0	9

TABLE II

VALUES OF RELATIVE VOLUMES FROM HUGONIOT CURVE FOR IRON [16]
CALCULATED ENGINEERING THICKNESS STRAINS, AND PERCENT REDUCTION IN THICKNESS

PEAK PRESSURE (GPa)	RELATIVE VOLUME	ENGINEERING THICKNESS STRAIN	REDUCTION IN THICKNESS (%)
8	0.96	-0.04	4
13	0.94	-0.06	6
18	0.88	-0.12	12
25	0.86	-0.14	14
35	0.84	-0.16	16

TABLE III
EFFECT OF PULSE DURATION ON THE VOLUME FRACTION OF TWINNED GRAINS AND % VOLUME OF TWINS WITHIN GRAINS

SHOT	PEAK PRESSURE (GPa)	PRESSURE DURATION (μsec)	RAREFACTION RATE (GPa/μsec)	VOLUME % OF GRAINS WITH TWINS		VOLUME % TWINS WITHIN TWINNED GRAINS	
				MAG FE	1008	MAG FE	1008
2	8.0	1.0	-34.90	3	0	20	0
3	8.0	2.0	-35.00	2	2	15	7
5	10.0	1.0	-36.50	10	5	75	10
6	10.0	2.0	-36.40	12	5	77	5
8	13.0	1.0	-38.80	55	12	22	8
9	13.0	2.0	-38.50	42	21	25	53
10	18.0	0.5	-63.80	31	10	12	30
11	18.0	1.0	-63.30	61	32	75	9
13	25.0	0.5	-71.80	5	2	11	3
14	25.0	1.0	-70.50	42	60	68	10
16	35.0	0.5	-78.00	73	45	85	46
17	35.0	1.0	-79.90	77	87	95	96

TABLE IV
EFFECT OF RAREFACTION RATE ON THE VOLUME FRACTION OF TWINNED GRAINS AND % VOLUME OF TWINS WITHIN GRAINS

SHOT	PEAK PRESSURE (GPa)	PRESSURE DURATION (μsec)	RAREFACTION RATE (GPa/μsec)	VOLUME % OF GRAINS WITH TWINS		VOLUME % TWINS WITHIN TWINNED GRAINS	
				MAG FE	1008	MAG FE	1008
1	8.0	1.0	-51.55	0	0	0	0
2	8.0	1.0	-34.90	3	0	20	0
4	10.0	1.0	-51.40	1	8	17	28
5	10.0	1.0	-36.50	10	5	75	10
7	13.0	1.0	-51.00	13	15	63	10
8	13.0	1.0	-38.80	55	12	22	8
11	18.0	1.0	-63.30	61	32	75	9
12	18.0	1.0	-42.50	61	76	12	10
14	25.0	1.0	-70.50	42	60	68	10
15	25.0	1.0	-51.10	57	66	62	57
17	35.0	1.0	-79.90	77	87	95	96
18	35.0	1.0	-53.30	62	88	84	95

TABLE V
EFFECT OF PULSE DURATION ON THE ROOM TEMPERATURE
STRAIN AGING OF MAGNETIC INGOT IRON AND AISI 1008

SHOT	PEAK PRESSURE (GPa)	PRESSURE DURATION (μsec)	RAREFACTION RATE (GPa/μsec)	DPH MAG FE 2 DAYS AFTER SHOT	DPH MAG FE 24 DAYS AFTER SHOT	DPH 1008 2 DAYS AFTER SHOT	DPH 1008 24 DAYS AFTER SHOT
2	8.0	1.0	-34.90	116±3	112±2	129±5	137±4
3	8.0	2.0	-35.00	109±3	106±2	121±3	131±4
5	10.0	1.0	-36.50	125±4	123±4	126±4	132±2
6	10.0	2.0	-36.40	122±1	120±2	124±2	127±4
8	13.0	1.0	-38.80	145±8	154±4	130±4	137±3
9	13.0	2.0	-38.50	120±4	125±3	144±4	147±5
10	18.0	0.5	-63.80	125±2	129±9	138±7	136±2
11	18.0	1.0	-63.30	195±6	188±6	234±9	213±24
13	25.0	0.5	-71.80	119±2	124±4	126±6	132±4
14	25.0	1.0	-70.50	230±11	256±10	248±12	251±30
16	35.0	0.5	-78.00	239±8	263±8	251±7	270±6
17	35.0	1.0	-79.90	237±8	246±10	262±7	275±6

TABLE VI
EFFECT OF RAREFACTION RATE ON THE ROOM TEMPERATURE
STRAIN AGING OF MAGNETIC INGOT IRON AND AISI 1008

SHOT	PEAK PRESSURE (GPa)	PRESSURE DURATION (μsec)	RAREFACTION RATE (GPa/μsec)	DPH MAG FE 2 DAYS AFTER SHOT	DPH MAG FE 24 DAYS AFTER SHOT	DPH 1008 2 DAYS AFTER SHOT	DPH 1008 24 DAYS AFTER SHOT
1	8.0	1.0	-51.55	109±4	106±3	122±2	127±2
2	8.0	1.0	-34.90	116±3	112±2	129±5	137±4
4	10.0	1.0	-51.40	120±3	124±3	131±7	131±5
5	10.0	1.0	-36.50	125±4	123±4	126±4	132±2
7	13.0	1.0	-51.00	130±3	124±4	138±4	146±5
8	13.0	1.0	-38.80	145±8	154±4	130±4	137±3
11	18.0	1.0	-63.30	195±6	188±6	234±9	213±24
12	18.0	1.0	-42.50	159±3	168±10	142±14	146±8
14	25.0	1.0	-70.50	230±11	256±10	248±12	251±30
15	25.0	1.0	-51.10	242±10	262±6	248±10	262±4
17	35.0	1.0	-79.90	237±8	246±10	242±7	275±6
18	35.0	1.0	-53.30	214±7	220±1	233±5	246±7

TABLE VII

TENSILE PROPERTIES OF MAGNETIC INGOT IRON

SHOT	UTS (MN/m^2)	% ELONGATION TO UTS	% REDUCTION IN AREA
–	285.8	26.6	81.52
1	295.2	11.5	79.08
2	296.2	17.5	73.18
3	280.8	26.9	80.56
4	301.1	12.3	77.95
5	288.8	23.1	81.37
6	292.0	14.8	82.24
7	303.7	13.2	76.28
8	339.0	7.4	80.81
9	298.6	21.5	77.04
10	306.0	6.5	77.36
11	421.6	1.5	68.67
12	392.0	3.2	71.56
13	327.0	0.45	79.16
14	328.6	6.25	73.60
15	629.0	1.5	60.58
16	494.4	1.0	72.60
17	618.5	2.1	59.94
18	593.9	1.7	54.02

TABLE VIII

TENSILE PROPERTIES OF AISI 1008 STEEL

SHOT	UTS (MN/m^2)	% ELONGATION TO UTS	% REDUCTION IN AREA
-	305.6	24.4	74.67
1	318.8	12.4	69.52
2	326.2	11.9	66.92
3	360.9	19.5	67.80
4	330.7	18.3	74.02
5	348.0	6.6	68.99
6	334.0	15.3	65.86
7	345.0	3.6	68.93
8	326.5	13.8	74.35
9	325.1	25.7	75.61
10	351.0	28.4	69.76
11	361.9	11.0	67.75
12	367.9	4.3	69.65
13	340.4	25.1	70.39
14	347.6	7.9	72.90
15	680.6	5.8	44.45
16	559.2	1.4	57.08
17	705.1	5.6	53.98
18	718.8	5.6	52.05

TABLE IX
YIELD STRENGTH 0.2 % OFFSET DATA FOR
MAGNETIC INGOT IRON AND AISI 1008 STEEL

SHOT	PRESSURE (GPa)	DURATION (μsec)	RAREFACTION RATE (GPa/μsec)	YIELD STRENGTH (MN/m^2) MAG FE	1008
-	-	-	-	125.4	210.2
1	8.0	1.0	-51.5	292.5	265.0
2	8.0	1.0	-34.9	291.3	311.5
3	8.0	2.0	-35.0	214.5	297.4
4	10.0	1.0	-51.4	294.0	309.4
5	10.0	1.0	-36.5	261.9	304.9
6	10.0	2.0	-36.4	272.1	323.8
7	13.0	1.0	-51.0	279.1	325.4
8	13.0	1.0	-38.8	324.7	307.0
9	13.0	2.0	-38.5	284.8	307.4
10	18.0	0.5	-63.8	296.2	291.5
11	18.0	1.0	-63.3	318.3	306.9
12	18.0	1.0	-42.5	338.8	338.3
13	25.0	0.5	-71.8	319.6	304.4
14	25.0	1.0	-70.5	328.6	329.2
15	25.0	1.0	-51.1	433.1	364.7
16	35.0	0.5	-78.0	399.6	407.2
17	35.0	1.0	-79.9	424.5	478.4
18	35.0	1.0	-53.3	475.3	420.8

TABLE X

EFFECTS OF PEAK PRESSURE AND ISOCHRONAL (1 hr) ANNEALING TEMPERATURE ON THE HARDNESS OF AISI 1008 STEEL

Pulse Duration = 1.0 μsec
Rarefaction Rate ≈ -51.5 GPa/μsec

TEMPERATURE (°C)	PEAK PRESSURE (GPa)					
	UNSHOCKED	8	10	13	25	35
	HARDNESS (DPH)					
25	104±2	126±10	133±9	141±7	247±13	236±8
100	106±2	123±5	134±3	144±2	234±4	239±3
325	105±2	100±4	129±4	141±3	217±6	241±5
450	103±1	103±2	115±1	127±3	211±2	232±4
500	106±1	105±1	118±2	119±2	201±6	213±2
550	102±1	99±1	120±2	133±7	124±6	155±19
600	111±1	110±1	117±3	118±2	98±1	105±1

TABLE XI

EFFECTS OF PEAK PRESSURE AND ISOCHRONAL (1 hr) ANNEALING TEMPERATURE ON THE HARDNESS OF ARMCO INGOT IRON

Pulse Duration = 1.0 μsec
Rarefaction Rate ≈ -51.5 GPa/μsec

TEMPERATURE (°C)	PEAK PRESSURE (GPa)					
	UNSHOCKED	8	10	13	25	35
	HARDNESS (DPH)					
25	84±2	105±6	123±8	126±8	242±15	214±7
100	86±1	118±4	118±3	126±6	206±15	213±2
325	83±2	112±2	113±2	118±2	213±9	221±2
450	83±2	83±2	106±2	109±5	171±10	197±6
500	83±1	80±3	104±4	111±15	180±8	185±4
550	75±1	93±4	93±2	96±6	151±4	207±7
600	82±1	88±3	99±3	83±2	133±6	155±3
650	85±2	88±2	89±3	93±2	78±1	80±1

TABLE XII

EFFECTS OF PULSE DURATION AND ISOCHRONAL (1 hr) ANNEALING TEMPERATURES ON THE HARDNESS OF AISI 1008 STEEL

PULSE DURATION (μsec)	HARDNESS (DPH) TEMPERATURES (°C) 25	100	325	450	500	550	600
PEAK PRESSURE = 8 GPa; RAREFACTION RATE = -35.0 GPa/μsec							
1.0	133±10	120±2	121±1	129±1	123±3	116±2	124±2
2.0	128±5	119±1	117±0	125±2	119±0	120±1	126±1
PEAK PRESSURE = 10 GPa; RAREFACTION RATE = .36.5 GPa/μsec							
1.0	132±7	137±1	141±4	143±11	140±8	119±3	132±1
2.0	130±5	129±1	130±2	121±3	117±3	115±1	133±1
PEAK PRESSURE = 13 GPa; RAREFACTION RATE = -38.7 GPa/μsec							
1.0	134±5	129±2	136±4	135±8	115±3	121±2	136±2
2.0	145±3	139±6	147±3	147±8	127±2	141±18	139±10
PEAK PRESSURE = 18 GPa; RAREFACTION RATE = -63.5 GPa/μsec							
0.5	134±5	140±3	134±4	121±2	118±2	115±3	130±1
1.0	213±33	175±4	176±6	183±7	165±9	123±20	132±2
PEAK PRESSURE = 25 GPa; RAREFACTION RATE = -71.0 GPa/μsec							
0.5	125±6	127±4	146±4	137±3	120±4	117±2	127±2
1.0	245±17	220±4	215±7	190±9	155±17	165±9	132±5
PEAK PRESSURE = 35 GPa; RAREFACTION RATE = -78.5 GPa/μsec							
0.5	252±13	223±9	214±7	177±20	190±10	176±5	122±2
1.0	264±8	227±6	227±5	208±1	196±2	194±1	97±1

TABLE XIII

EFFECTS OF RAREFACTION RATE AND ISOCHRONAL (1 hr) ANNEALING TEMPERATURES ON THE HARDNESS OF AISI 1008 STEEL

RAREFACTION RATE (GPa/μsec)	HARDNESS (DPH) TEMPERATURES (°C) 25	100	325	450	500	550	600
PEAK PRESSURE = 8 GPa; PULSE DURATION = 1.0μsec							
-51.55	126±10	123±5	100±4	103±2	105±1	99±1	110±1
-34.90	133±10	120±2	121±1	129±1	123±3	116±2	124±2
PEAK PRESSURE = 10 GPa; PULSE DURATION = 1.0μsec							
-51.40	133±9	134±3	129±4	115±1	118±2	120±2	117±3
-36.50	132±7	137±1	141±4	143±11	140±8	119±3	132±1
PEAK PRESSURE = 13 GPa; PULSE DURATION = 1.0μsec							
-51.00	141±7	144±2	141±3	127±3	119±2	133±7	118±2
-38.80	134±5	129±2	136±4	135±8	115±3	121±2	136±2
PEAK PRESSURE = 18 GPa; PULSE DURATION = 1.0μsec							
-63.30	213±33	175±4	176±6	183±7	165±9	123±20	132±2
-42.50	141±8	151±8	153±3	167±16	144±11	123±6	149±12
PEAK PRESSURE = 25 GPa; PULSE DURATION = 1.0μsec							
-70.70	245±17	220±4	215±7	190±9	155±17	165±9	132±5
-51.10	247±13	234±4	217±6	211±2	201±6	124±6	98±1
PEAK PRESSURE = 35 GPa; PULSE DURATION = 1.0μsec							
-79.90	264±8	227±6	227±5	208±1	196±2	194±1	97±1
-53.30	236±8	239±3	241±5	232±4	213±2	155±19	105±1

TABLE XIV

EFFECTS OF SHOCK LOADING, COLD ROLLING, AND ISOCHRONAL (1 hr) ANNEALING TEMPERATURE ON THE HARDNESS OF AISI 1008 STEEL

SAMPLE	HARDNESS (DPH) TEMPERATURES (°C)						
	25	100	325	450	500	550	600
Unshocked	104±2	106±2	105±2	103±1	106±1	102±1	111±1
Shocked 8 GPa	126±10	123±5	100±4	103±2	105±1	99±1	110±1
Rolled 4 %	128±2	129±1	133±2	122±5	123±1	121±1	114±4
Shocked 13 GPa	141±7	144±2	141±3	127±3	119±2	133±7	118±2
Rolled 6 %	127±2	133±2	132±1	128±1	124±1	129±1	130±2
Shocked 18 GPa	213±33	175±4	176±6	183±7	165±9	123±20	132±2
Rolled 12 %	137±4	147±2	152±3	144±5	142±1	141±1	142±2
Shocked 25 GPa	247±13	234±4	217±6	211±2	201±6	124±6	98±1
Rolled 14 %	148±4	155±2	155±1	149±2	146±1	147±1	145±5
Shocked 35 Gpa	236±8	239±3	241±5	232±4	213±2	155±19	105±1
Rolled 16 %	144±3	155±2	155±3	148±1	144±1	137±1	132±1

TABLE XV

EFFECTS OF SHOCK LOADING, COLD ROLLING, AND ISOCHRONAL (1 hr) ANNEALING TEMPERATURE ON THE HARDNESS OF ARMCO INGOT IRON

	HARDNESS VALUES (DPH) TEMPERATURES (°C)							
SAMPLE	25	100	325	450	500	550	600	650
Unshocked	84±2	86±2	83±2	83±2	83±1	75±1	82±1	85±2
Shocked 35 GPa	214±7	213±2	221±2	197±6	185±4	207±7	155±3	80±1
Rolled 16 %	120±2	-	-	115±1	120±6	110±2	105±2	-

TABLE XVI

EFFECTS OF PEAK PRESSURE AND ISOCHRONAL (1 hr)
ANNEALING TEMPERATURE ON THE TENSILE PROPERTIES OF AISI 1008 STEEL

Pulse Duration = 1.0μsec
Rarefaction Rate ≈ -51.5 GPa/μsec

PEAK PRESSURE (GPa)	0.2 % YIELD STRENGTH (MN/m^2)		UTS (MN/m^2)		% ELONGATION TO UTS		% REDUCTION IN AREA	
	Shocked	Shocked + 450°C/1hr	Shocked	Shocked + 450°C/1hr	Shocked	Shocked + 450°C/1hr	Shocked	Shocked + 450°C/1hr
Unshocked	215	-	354	-	27	-	79	-
8	265	293	319	331	10	13	77	76
10	310	300	331	347	6	16	78	78
13	325	307	345	350	2	9	72	77
25	372	503	681	579	2	3	52	55
35	414	675	719	690	2	2	59	60

TABLE XVII

EFFECTS OF PEAK PRESSURE AND ISCHRONAL (1 hr)
ANNEALING TEMPERATURE ON THE TESILE PROPERTIES OF ARMCO INGOT IRON

Pulse Duration = 1.0μsec
Rarefaction Rate ≈ -51.5 GPa/μsec

PEAK PRESSURE (GPa)	0.2 % YIELD STRENGTH (MN/m^2)		UTS (MN/m^2)		% ELONGATION TO UTS		% REDUCTION IN AREA	
	Shocked	Shocked + 450°C/1hr	Shocked	Shocked + 450°C/1hr	Shocked	Shocked + 450°C/1hr	Shocked	Shocked + 450°C/1hr
Unshocked	125	-	286	-	35	-	90	-
8	290	243	295	284	2	27	89	89
10	294	253	301	295	8	18	85	89
13	279	247	304	284	12	18	79	90
25	433	525	629	539	1	1	76	80
35	455	567	594	600	2	1	75	77

TABLE XVIII

EFFECTS OF PULSE DURATION AND ISOCHRONAL (1 hr) ANNEALING TEMPERATURE ON THE TENSILE PROPERTIES OF AISI 1008 STEEL

PULSE DURATION (μsec)	0.2 % YIELD STRENGTH (MN/m^2)		UTS (MN/m^2)		% ELONGATION TO UTS		% REDUCTION IN AREA	
	Shocked	Shocked + 450°C/1hr	Shocked	Shocked + 450°C/1hr	Shocked	Shocked + 450°C/1hr	Shocked	Shocked + 450°C/1hr
PEAK PRESSURE = 8 GPa; RAREFACTION RATE = -35.5 GPa/μsec								
1.0	312	292	326	337	7	12	77	76
2.0	297	268	361	354	18	20	76	75
PEAK PRESSURE = 10 GPa; RAREFACTION RATE = -36.5 GPa/μsec								
1.0	305	275	348	367	1	5	78	76
2.0	324	257	334	355	1	12	77	77
PEAK PRESSURE = 13 GPa; RAREFACTION RATE = -38.7 GPa/μsec								
1.0	309	283	327	342	10	8	78	74
2.0	307	314	325	342	21	11	77	75
PEAK PRESSURE = 18 GPa; RAREFACTION RATE = -63.5 GPa/μsec								
0.5	291	283	351	361	7	9	74	75
1.0	320	359	362	428	3	6	77	73
PEAK PRESSURE = 25 GPa; RAREFACTION RATE = -71.0 GPa/μsec								
0.5	304	280	340	386	22	8	74	74
1.0	329	335	348	435	<1	3	77	72
PEAK PRESSURE = 35 GPa; RAREFACTION RATE = -78.5 GPa/μsec								
0.5	394	444	559	486	14	2	66	66
1.0	479	634	705	674	2	1	63	62

TABLE XIX
EFFECTS OF RAREFACTION RATE AND ISOCHRONAL (1 hr)
ANNEALING TEMPERATURE ON THE TENSILE PROPERTIES OF AISI 1008 STEEL

RAREFACTION RATE (GPa/μsec)	0.2 % YIELD STRENGTH (MN/m^2)		UTS (MN/m^2)		% ELONGATION TO UTS		% REDUCTION IN AREA	
	Shocked	Shocked + 450°C/1hr	Shocked	Shocked + 450°C/1hr	Shocked	Shocked + 450°C/1hr	Shocked	Shocked + 450°C/1hr
PEAK PRESSURE = 8 GPa; PULSE DURATION = 1.0μsec								
-51.5	265	293	319	331	10	13	77	76
-34.9	312	292	326	337	7	12	77	76
PEAK PRESSURE = 10 GPa; PULSE DURATION = 1.0μsec								
-51.4	310	300	331	347	6	16	78	78
-36.5	305	275	348	367	1	5	78	76
PEAK PRESSURE = 13 GPa; PULSE DURATION = 1.0μsec								
-51.0	325	307	345	350	2	9	72	77
-38.8	309	283	327	342	10	8	78	74
PEAK PRESSURE = 18 GPa; PULSE DURATION = 1.0μsec								
-63.3	320	359	362	428	7	6	74	73
-42.5	338	297	368	381	3	3	77	73
PEAK PRESSURE = 25 GPa; PULSE DURATION = 1.0μsec								
-70.5	329	335	348	435	<1	3	77	72
-51.0	372	503	681	579	2	3	52	55
PEAK PRESSURE = 35 GPa; PULSE DURATION = 1.0μsec								
-79.9	479	634	705	674	2	1	63	62
-53.3	414	675	719	690	2	2	59	60

TABLE XX

EFFECTS OF SHOCK LOADING, COLD ROLLING, AND ISOCHRONAL (1 hr) ANNEALING TEMPERATURE ON THE TENSILE PROPERTIES OF AISI 1008 STEEL

SAMPLE	0.2 % YIELD STRENGTH (MN/m^2)		UTS (MN/m^2)		% ELONGATION TO UTS		% REDUCTION IN AREA	
	Deformed	Deformed + 450°C/1hr	Deformed	Deformed + 450°C/1hr	Deformed	Deformed + 450°C/1hr	Deformed	Deformed + 450°C/1hr
Undeformed	215	--	354	-	27	-	79	-
Shocked 8 GPa Rolled 4 %	215 328	293 353	354 384	331 395	27 8	13 17	79 76	76 72
Shocked 13 GPa Rolled 6 %	325 309	307 251	345 389	350 403	2 8	9 15	72 77	77 75
Shocked 18 GPa Rolled 12 %	320 441	359 397	362 454	428 454	7 2	6 9	74 72	73 70
Shocked 25 GPa Rolled 14 %	372 444	503 375	681 459	579 458	2 2	3 7	52 72	55 69
Shocked 35 GPa Rolled 16 %	414 283	675 308	719 450	690 443	2 3	2 7	59 72	60 71

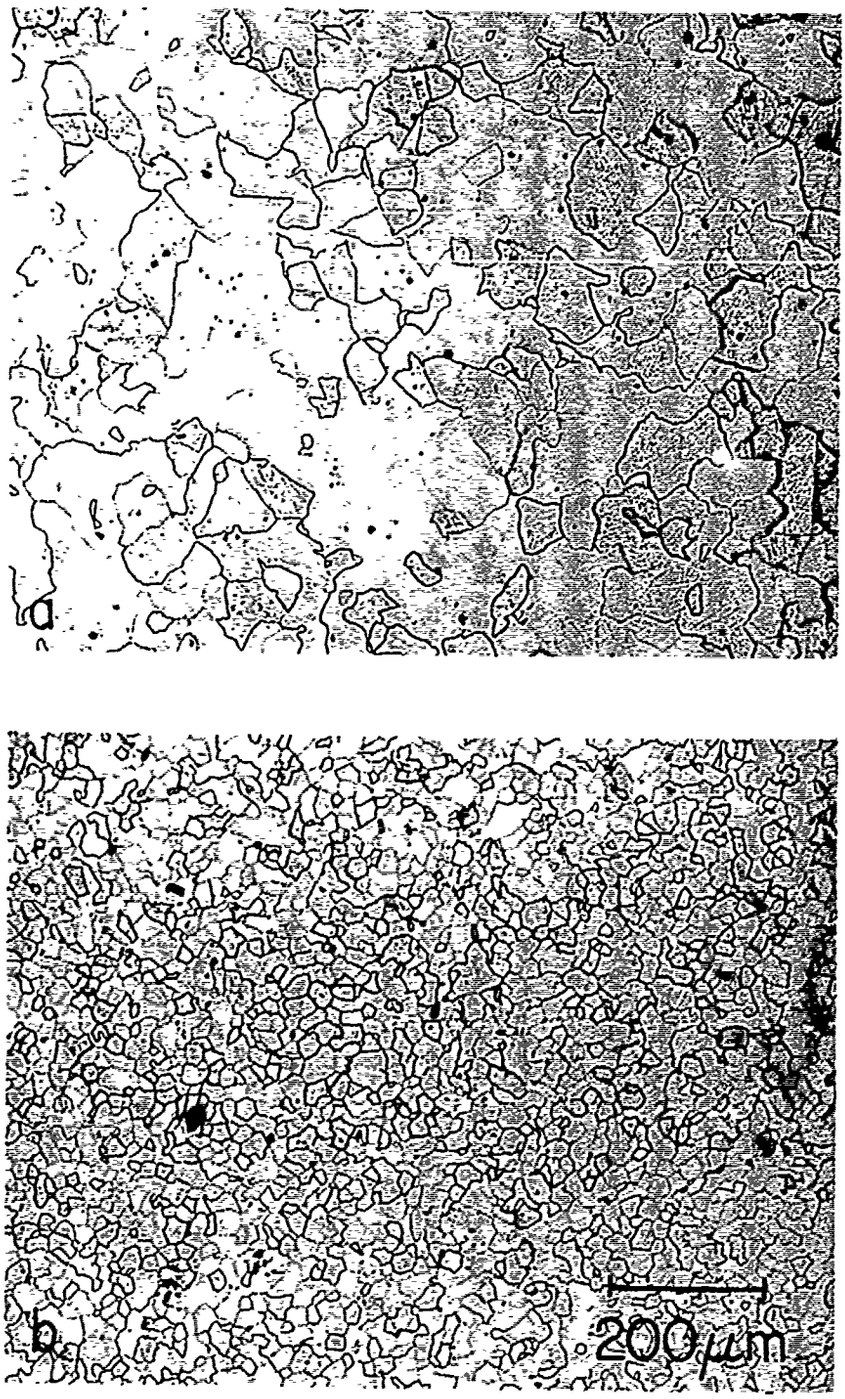

FIGURE 1. Light Micrograph of Preshocked Structure of (a) Armco Magnetic Ingot Iron After Annealing at 723 C for One-Half Hour With Furnace Cool, (b) AISI 1008, As Received.

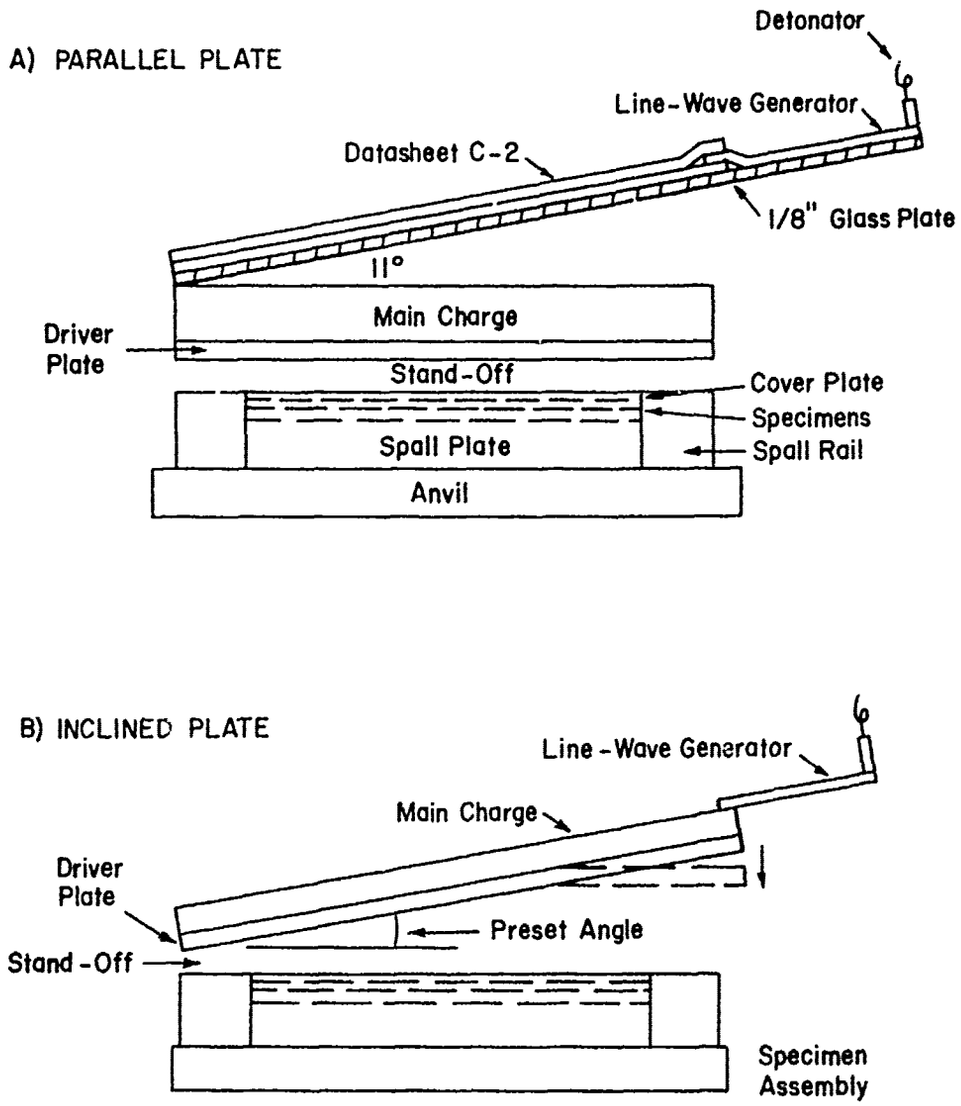

FIGURE 2. Plate Impact Plane-Wave Generators

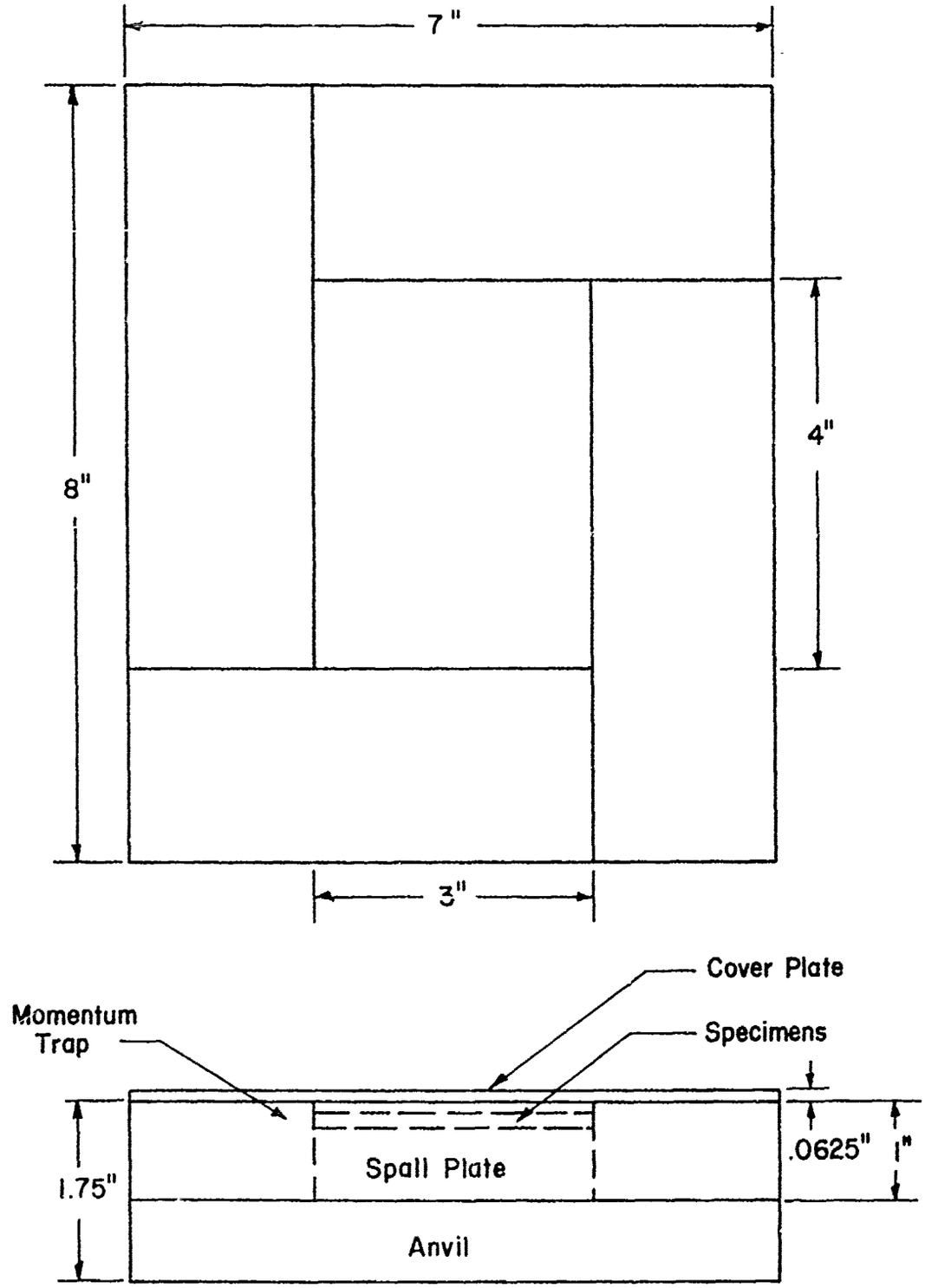

FIGURE 3. Specimen Assembly.

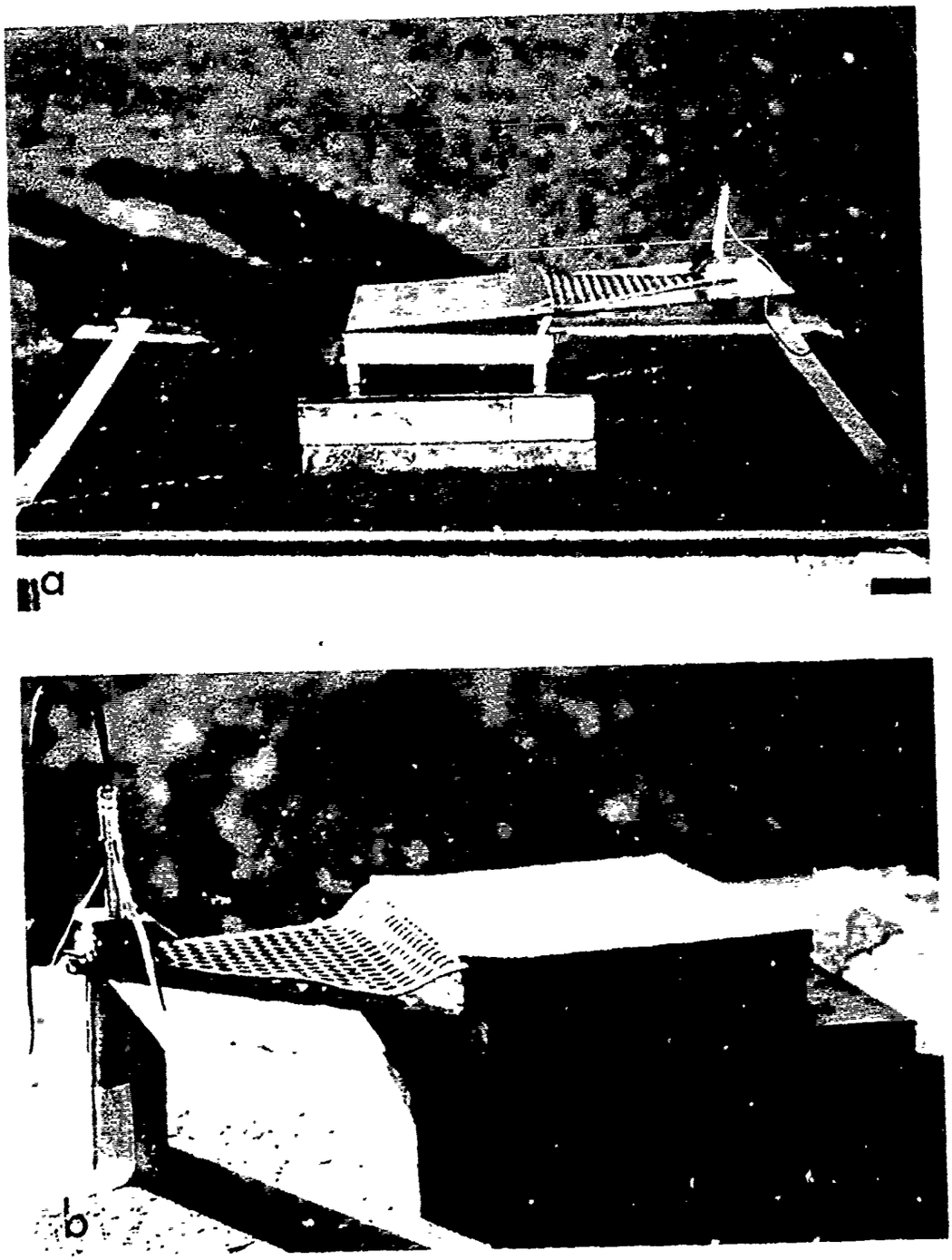

FIGURE 4. Photographic Mock-up of Shot Assemblies Ready for Detonation: (a) Parallel-Plate Assembly, (b) Inclined-Plate Assembly

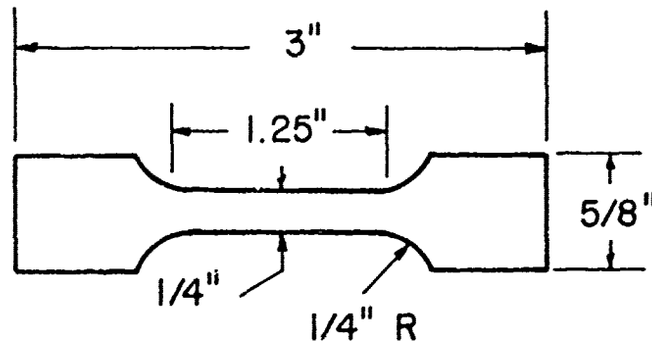

ASTM A 370 SUBSIZE SPECIMEN

FIGURE 5. Sketch of ASTM A 370 Subsize Tensile Specimen

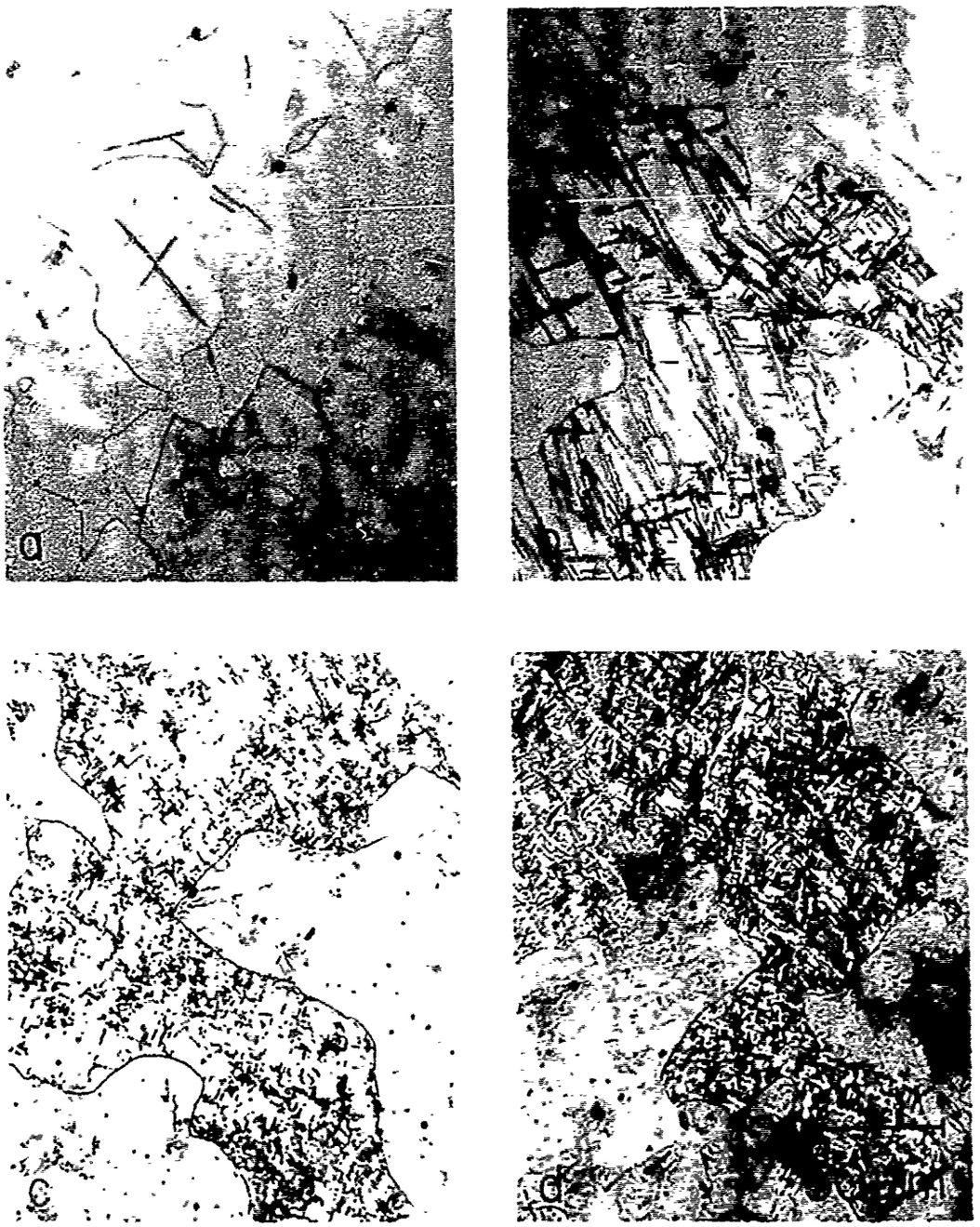

FIGURE 6. Microstructure of Shock-Hardened Armco Magnetic Ingot Iron as a Function of Shock Pressure at Constant Pressure Duration and Rarefaction Rate: (a) 10 GPa, (b) 13 GPa, (c) 25 GPa, (d) 35 GPa.

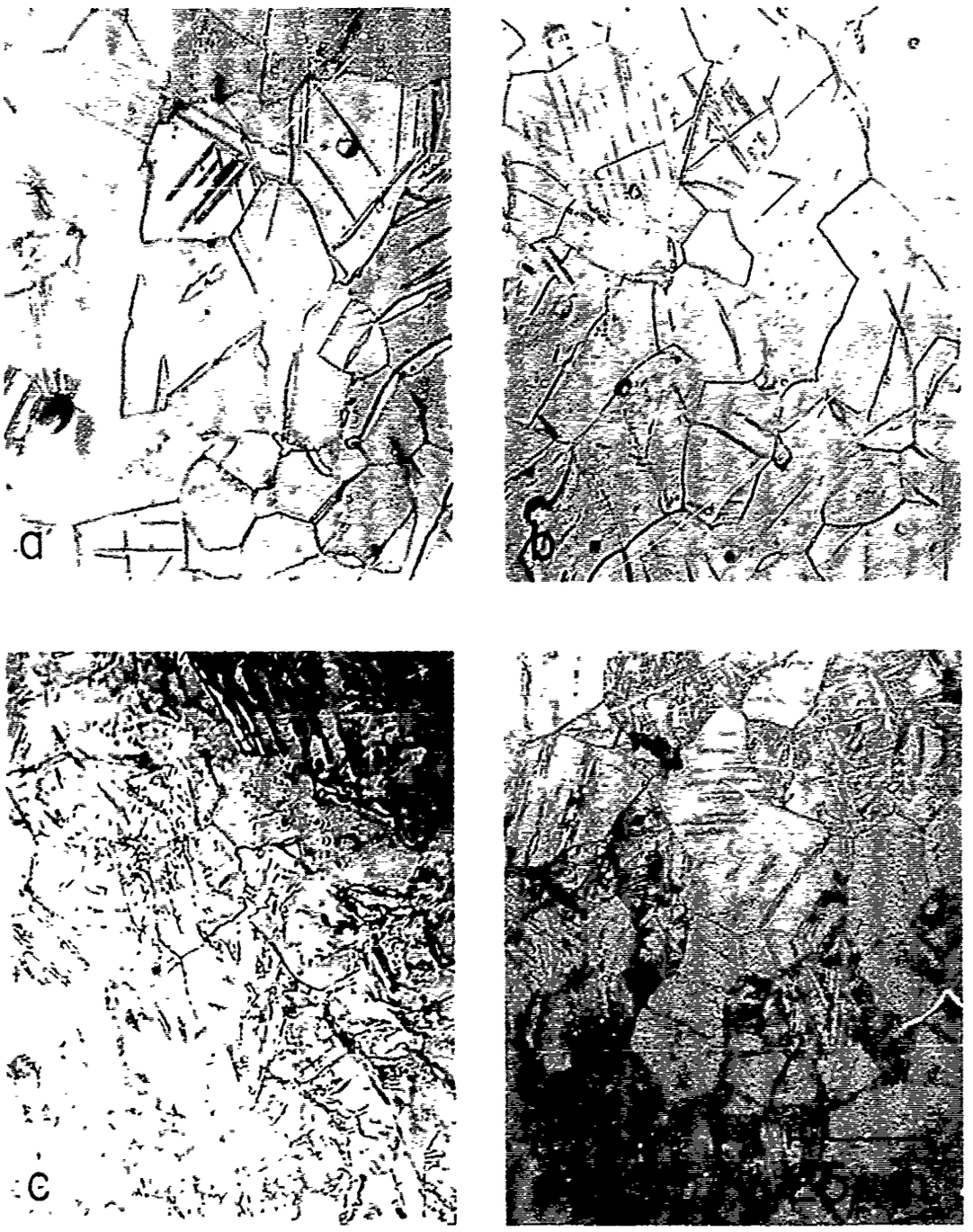

FIGURE 7. Microstructure of Shock Hardened AISI 1008 Steel as a Function of Shock Pressure at Constant Pressure Duration and Rarefaction Rate (a) 10 GPa, (b) 13 GPa, (c) 25 GPa, (d) 35 GPa.

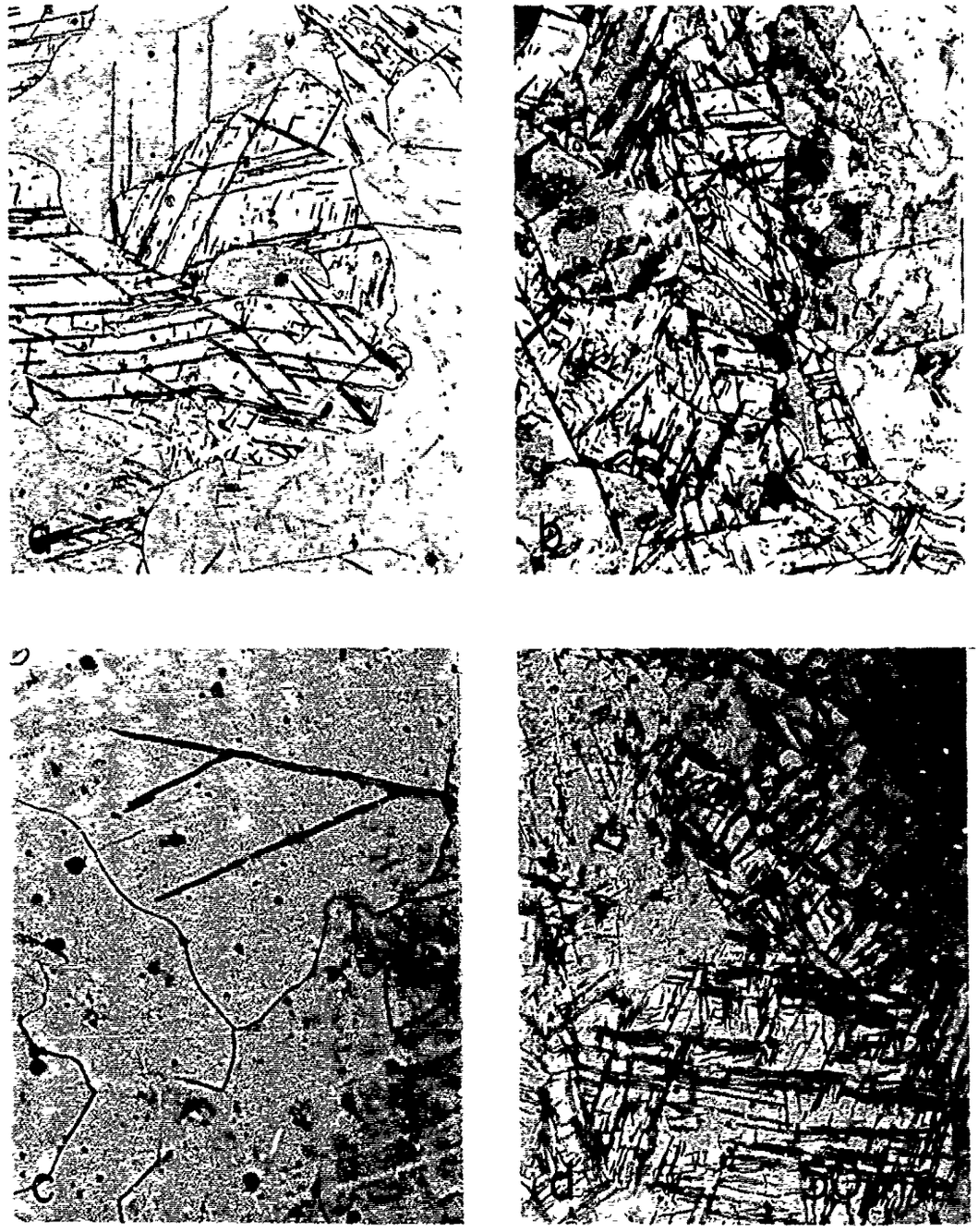

FIGURE 8. Microstructure of Shock-Hardened Armco Magnetic Ingot Iron as a Function of Peak Pressure Duration. (a) 18 GPa pressure, -63.8 GPa/μsec rarefaction, 0.5 μsec duration, (b) same as (a) except 1.0 μsec duration, (c) 25 GPa pressure, -71.0 GPa/μsec rarefaction, 0.5 μsec duration, (d) same as (c) except 1.0 μsec duration.

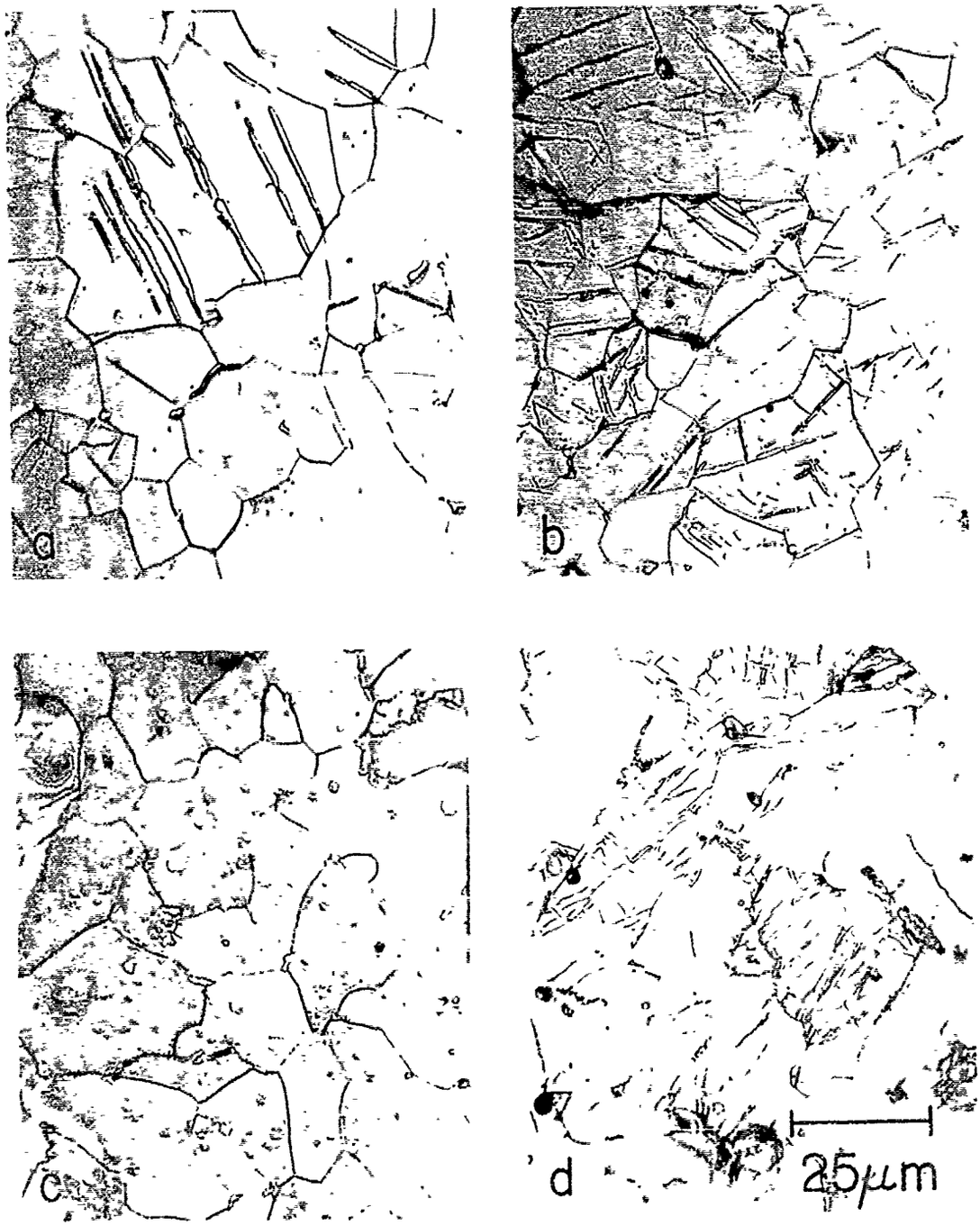

FIGURE 9. Microstructure of Shock-Hardened AISI 1008 Steel as a Function of Peak Pressure Duration. (a) 18 GPa pressure, -63.8 GPa/μsec rarefaction, 0.5 μsec duration, (b) same as (a) except 1.0 μsec duration, (c) 25 GPa pressure, -71.0 GPa/μsec rarefaction, 0.5 μsec duration, (d) same as (c) except 1.0 μsec duration.

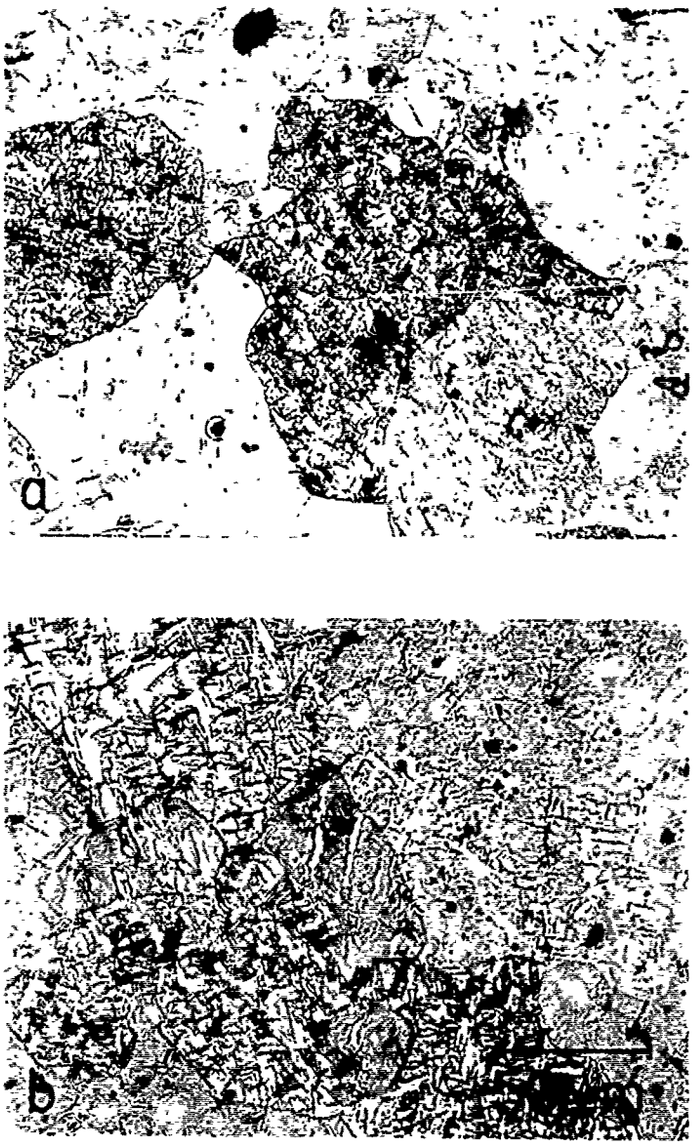

FIGURE 10. Microstructure of Shock-Hardened Armco Magnetic Ingot Iron as a Function of Rarefaction Rate. (a) 35 GPa pressure, 1.0 μsec duration, -79.9 GPa/μsec rarefaction rate, (b) same as (a) except -53.3 GPa/μsec rarefaction rate.

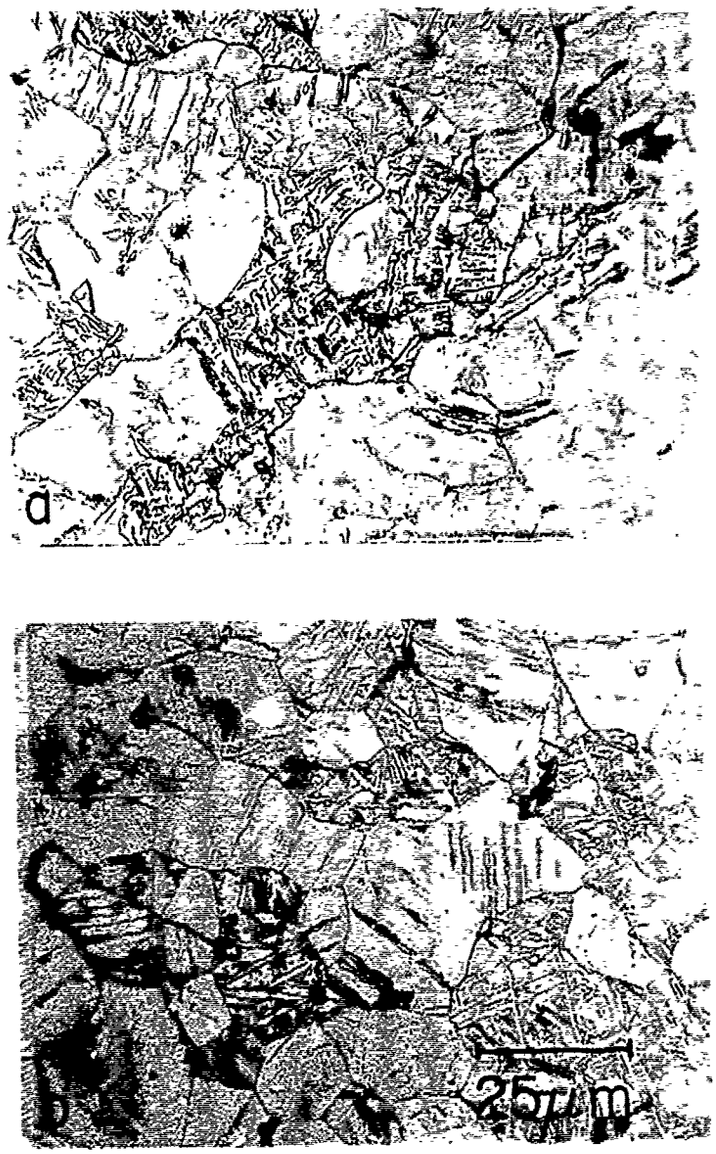

FIGURE 11. Microstructure of Shock-Hardened AISI 1008 Steel as a Function of Rarefaction Rate. (a) 35 GPa pressure, 1.0 μsec duration, -79.9 GPa/μsec rarefaction rate, (b) same as (a) except -53.3 GPa/μsec rarefaction rate.

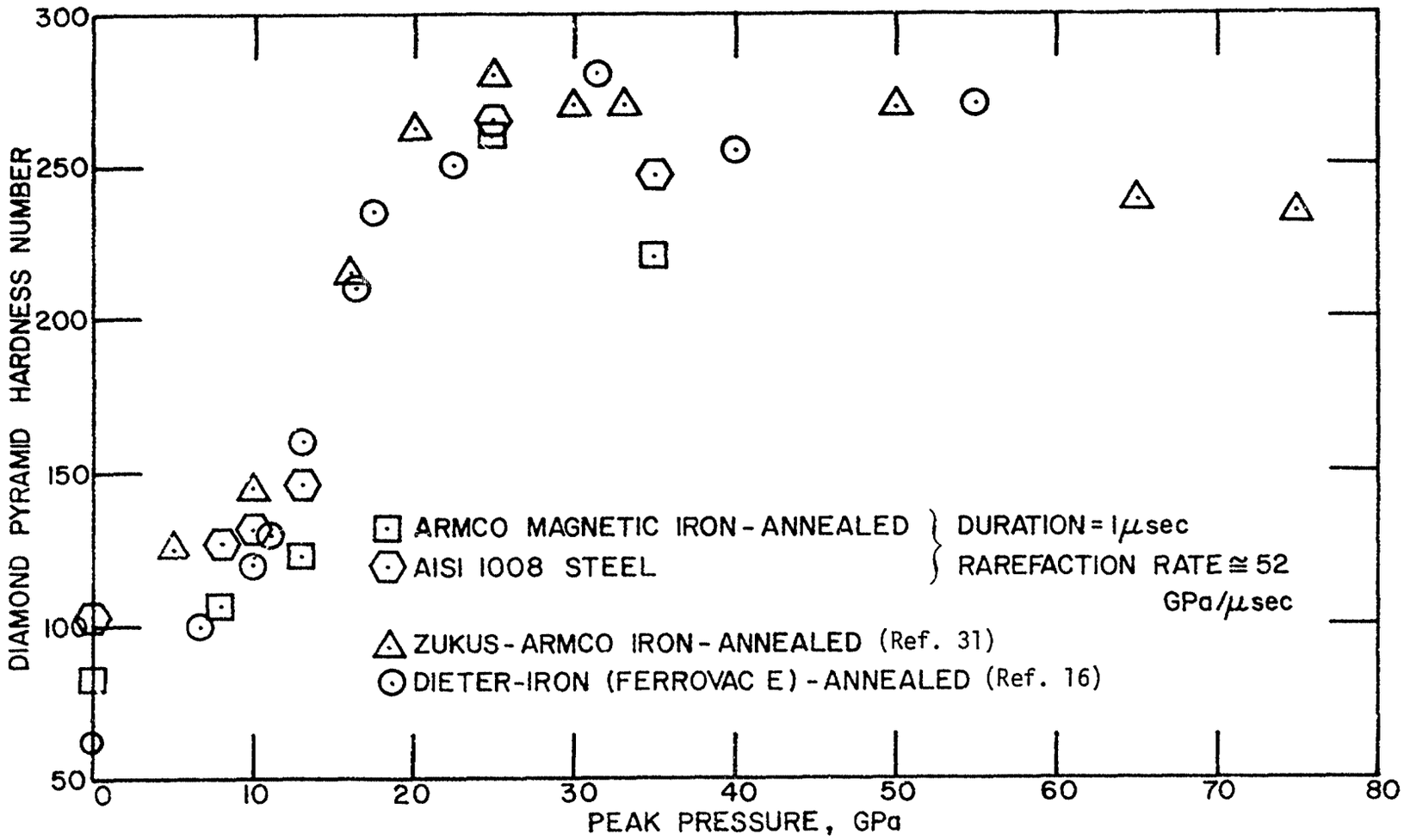

Figure 12. Available Data Showing DPH Hardness vs. Peak Pressure for Iron and Steel.

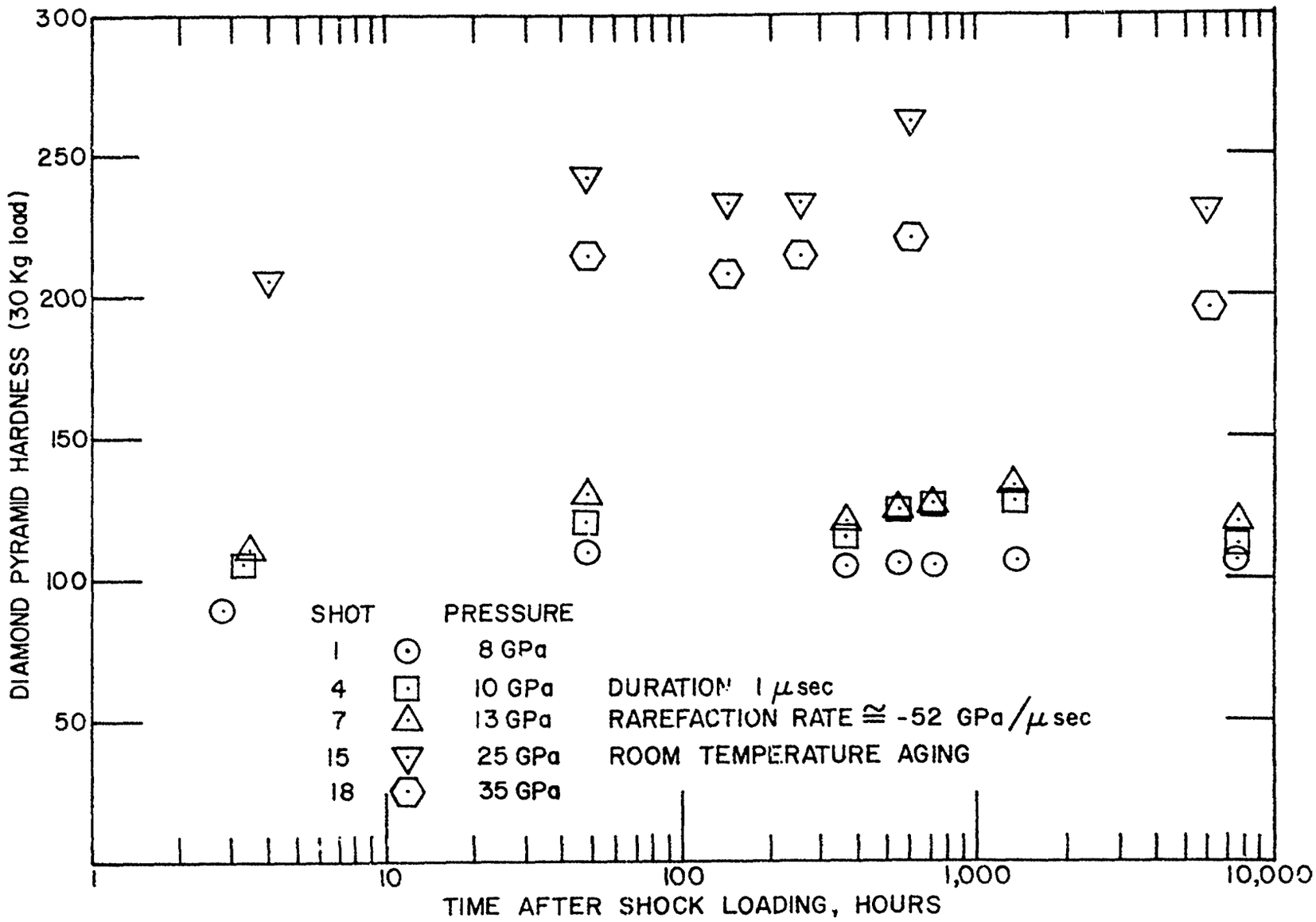

Figure 13. Room Temperature Aging of Armco Magnetic Ingot Iron.

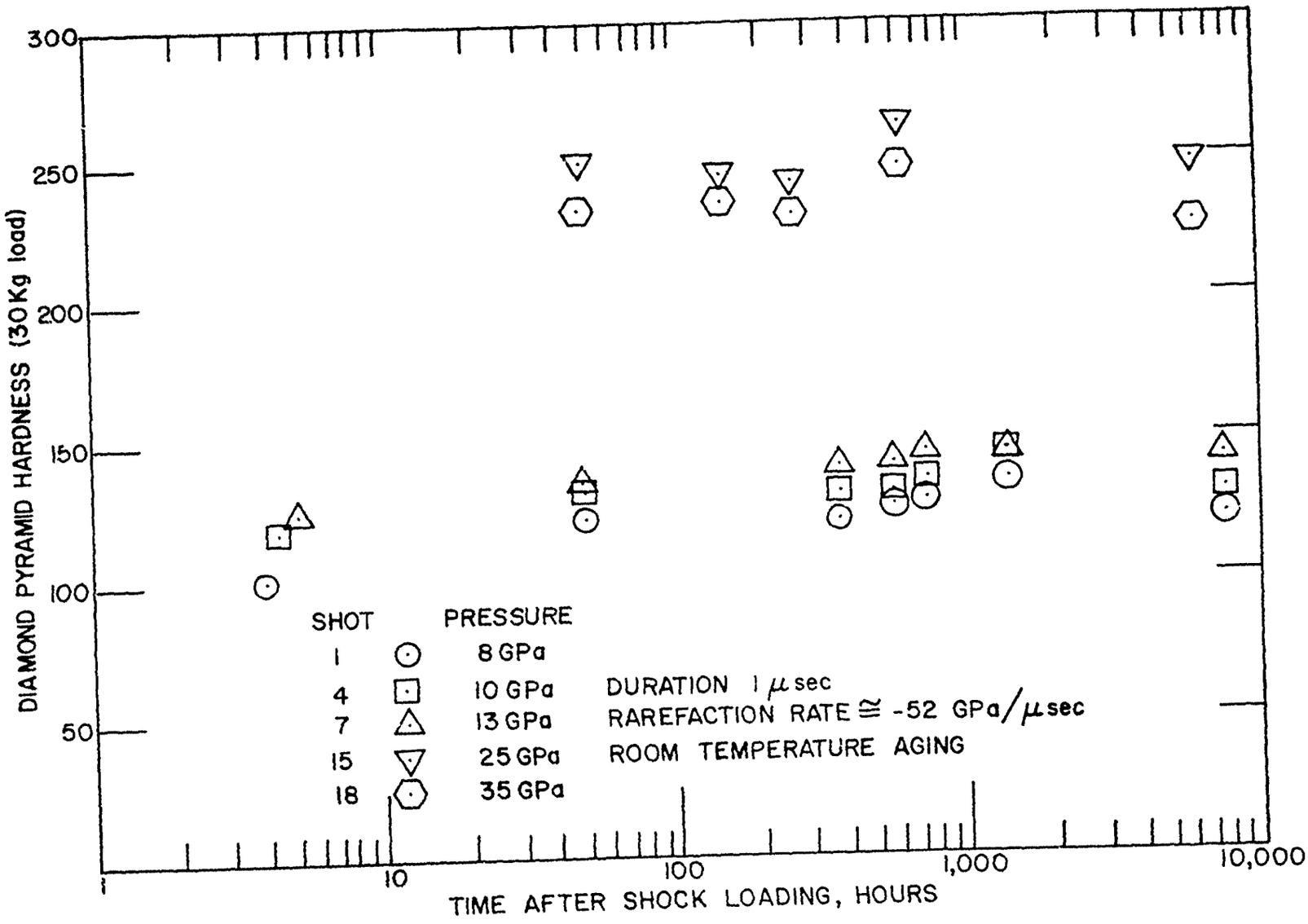

Figure 14. Room Temperature Aging of AISI 1008 Steel.

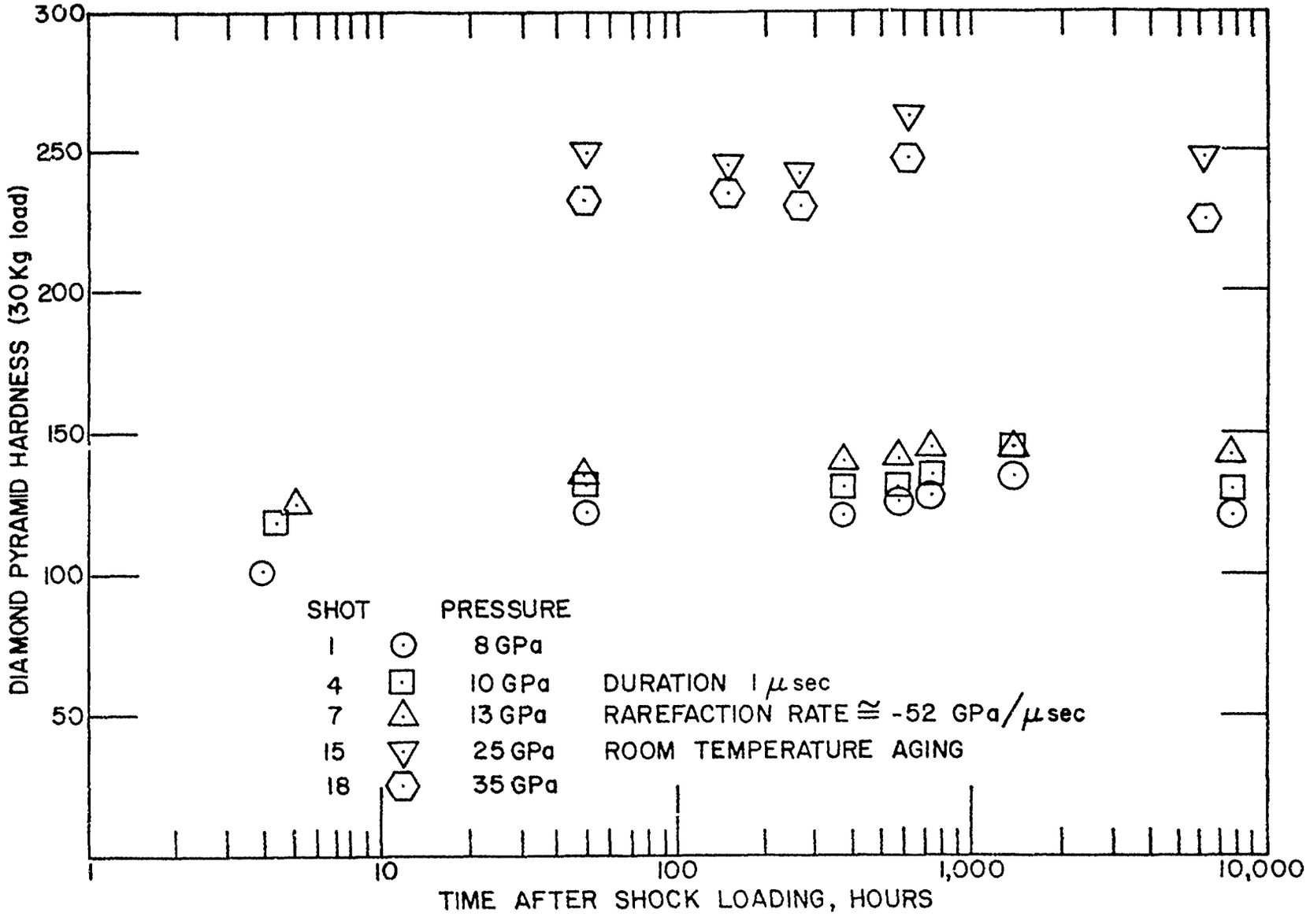

Figure 14. Room Temperature Aging of AISI 1008 Steel.

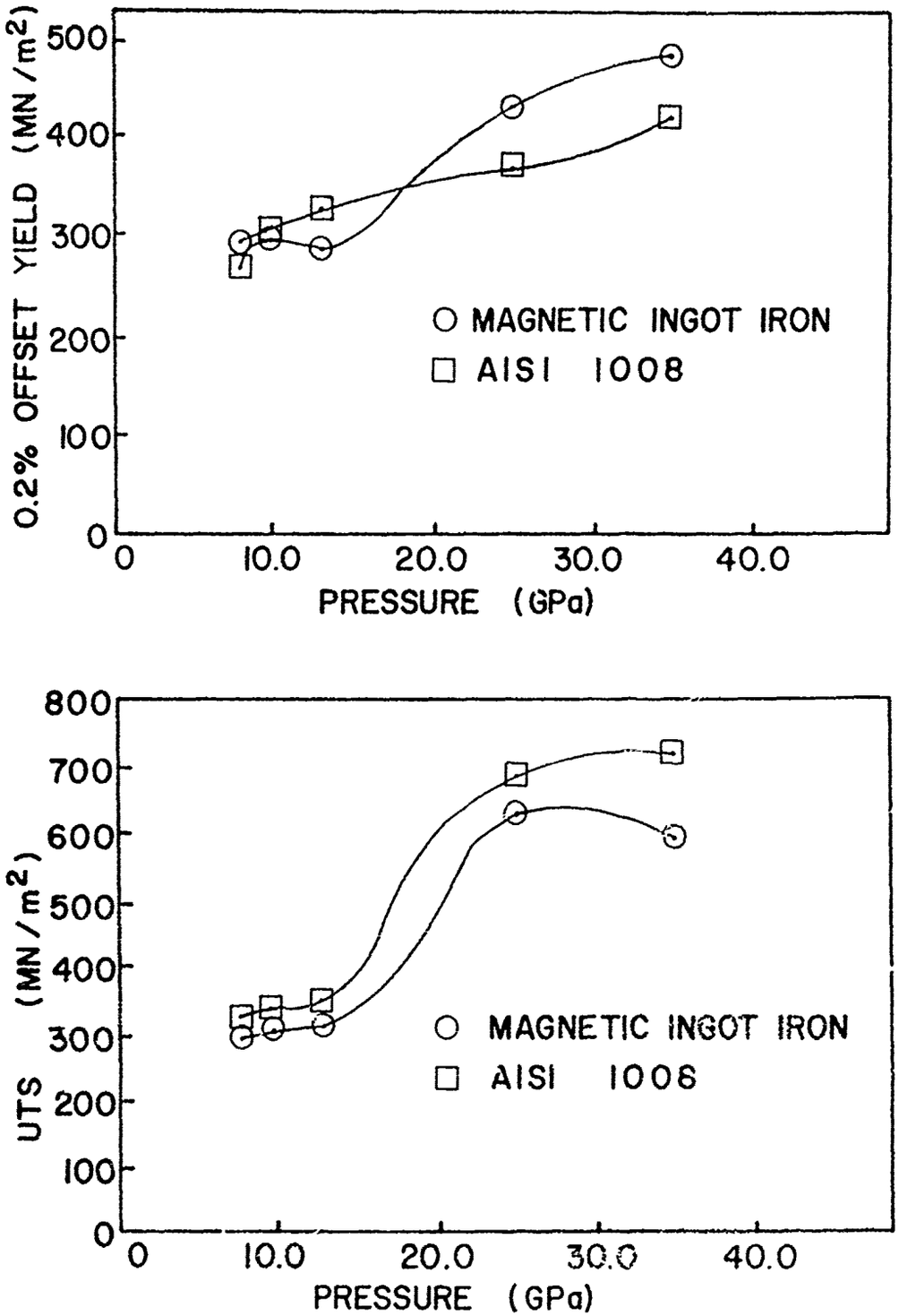

Figure 15. The Effect of Peak Pressure on the (a) 0.2% Offset Yield, (b) UTS, with Constant Duration and Rarefaction Rate.

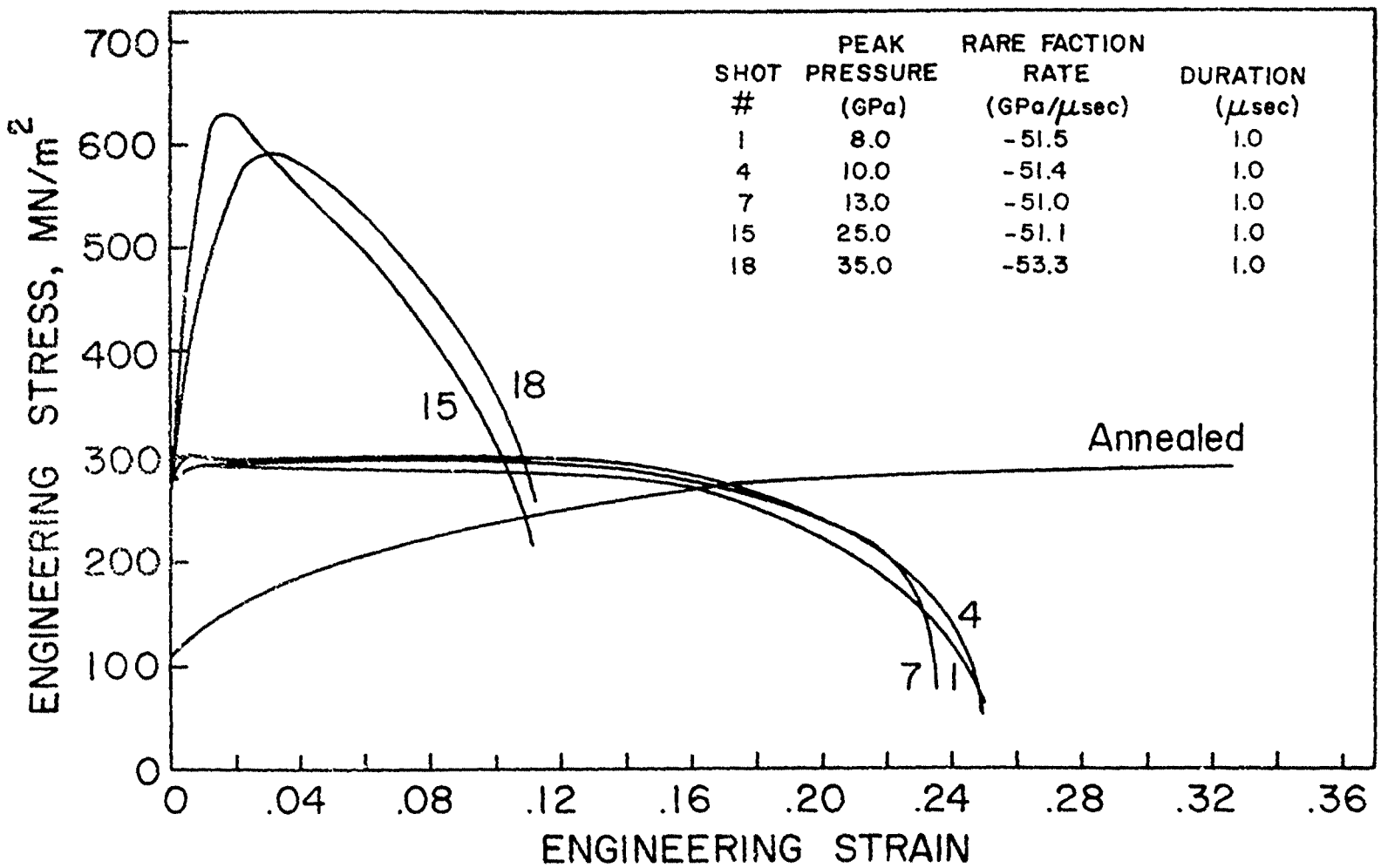

Figure 16. Engineering Stress-Strain Curves Showing the Effect of Peak Pressure on the Tensile Behavior of Armco Magnetic Ingot Iron.

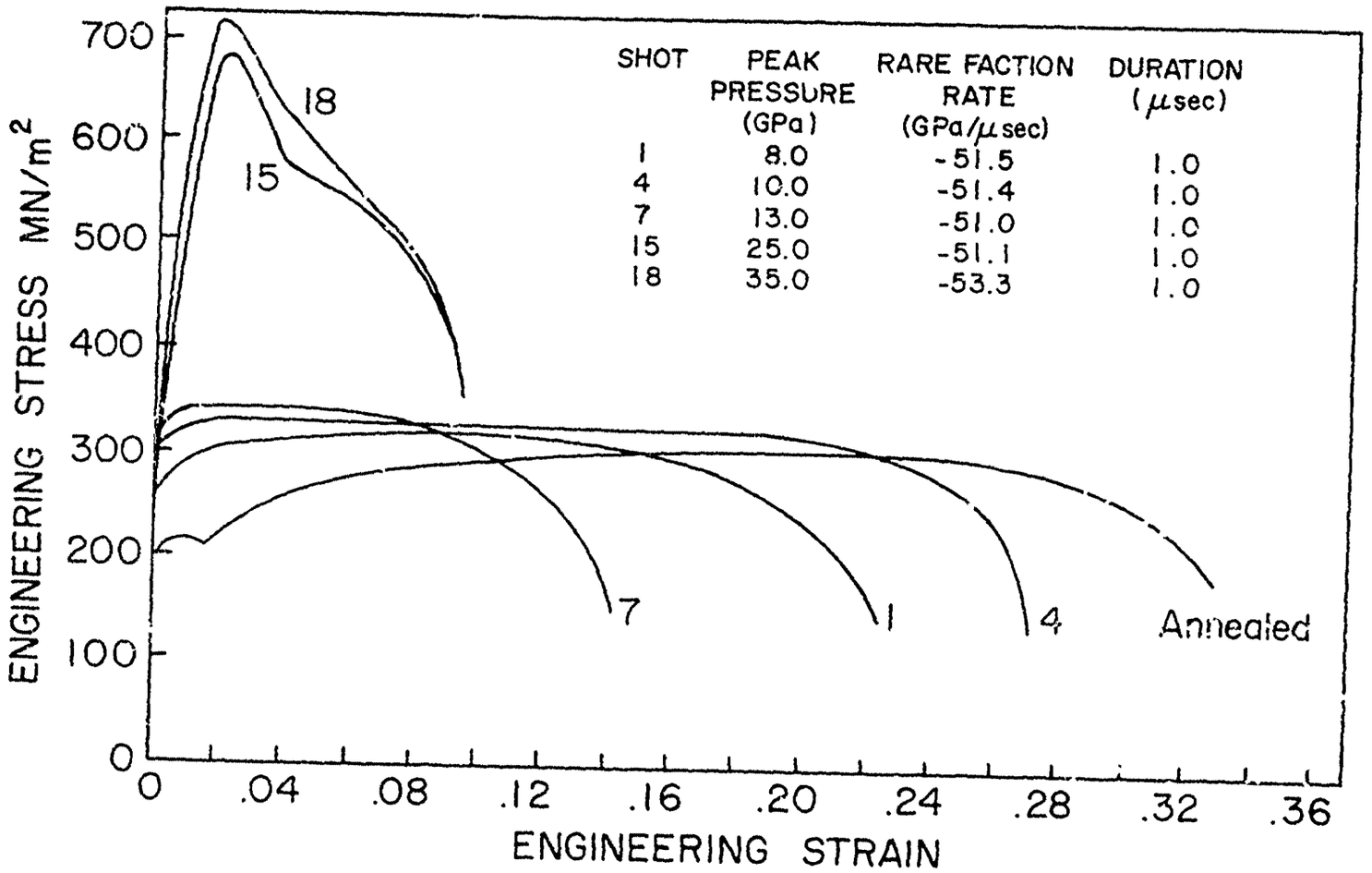

Figure 17. Engineering Stress-Strain Curves Showing the Effect of Peak Pressure on the Tensile Behavior of AISI 1008 Steel.

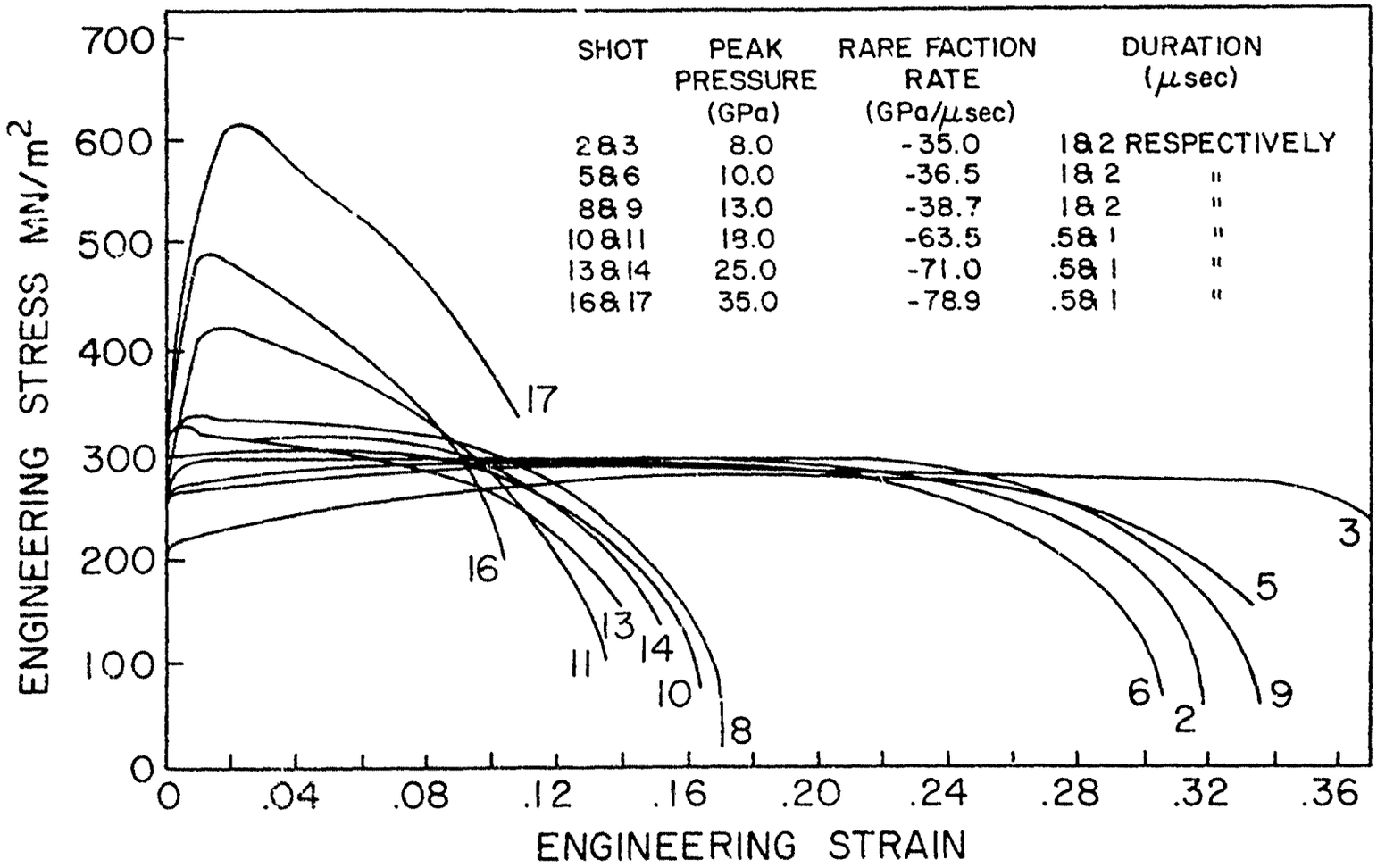

Figure 18. Engineering Stress-Strain Curves Showing the Effect of Pulse Duration on the Tensile Behavior of Magnetic Ingot Iron.

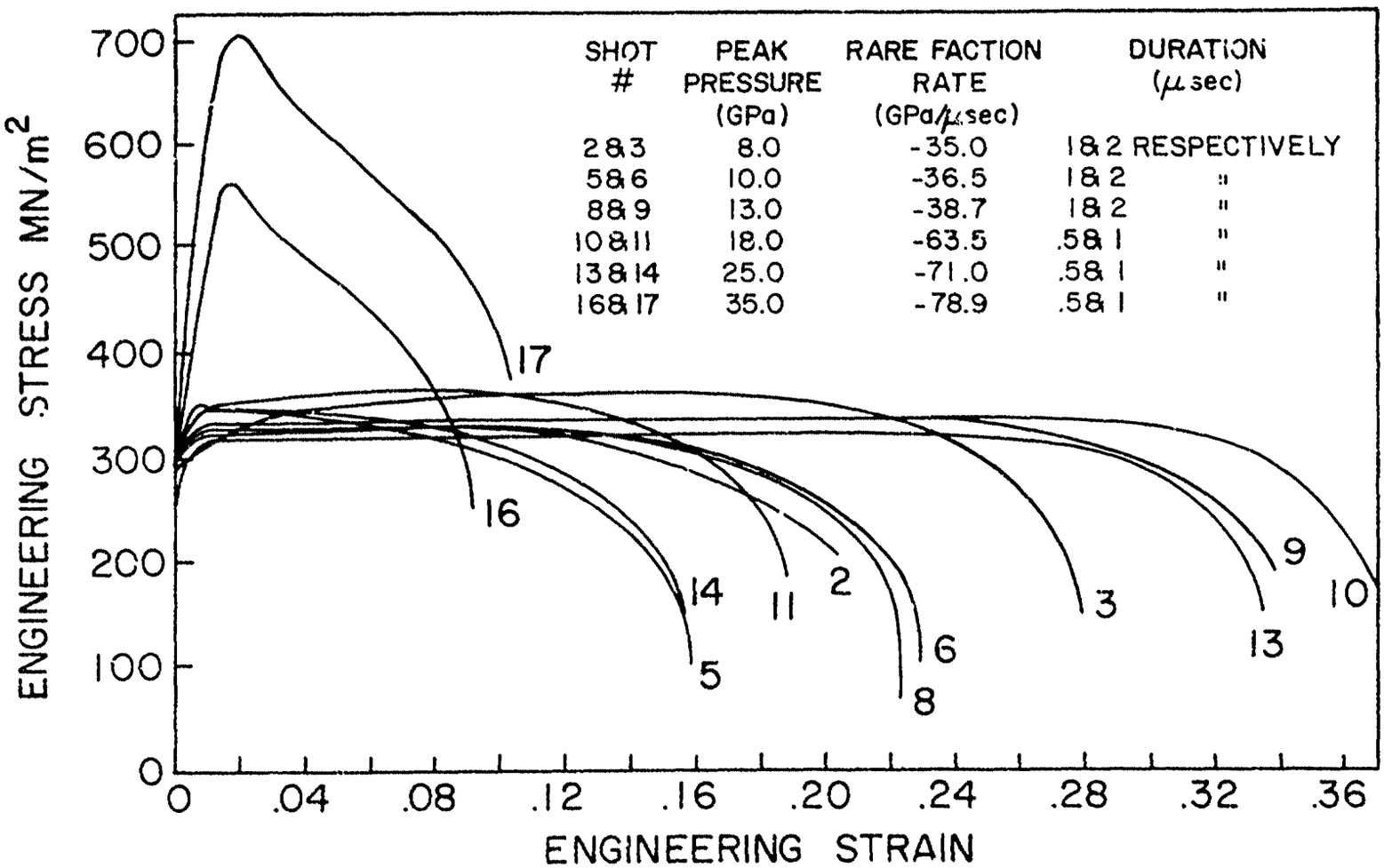

Figure 19. Engineering Stress-Strain Curves Showing the Effect of Pulse Duration on the Tensile Behavior of AISI 1008 Steel.

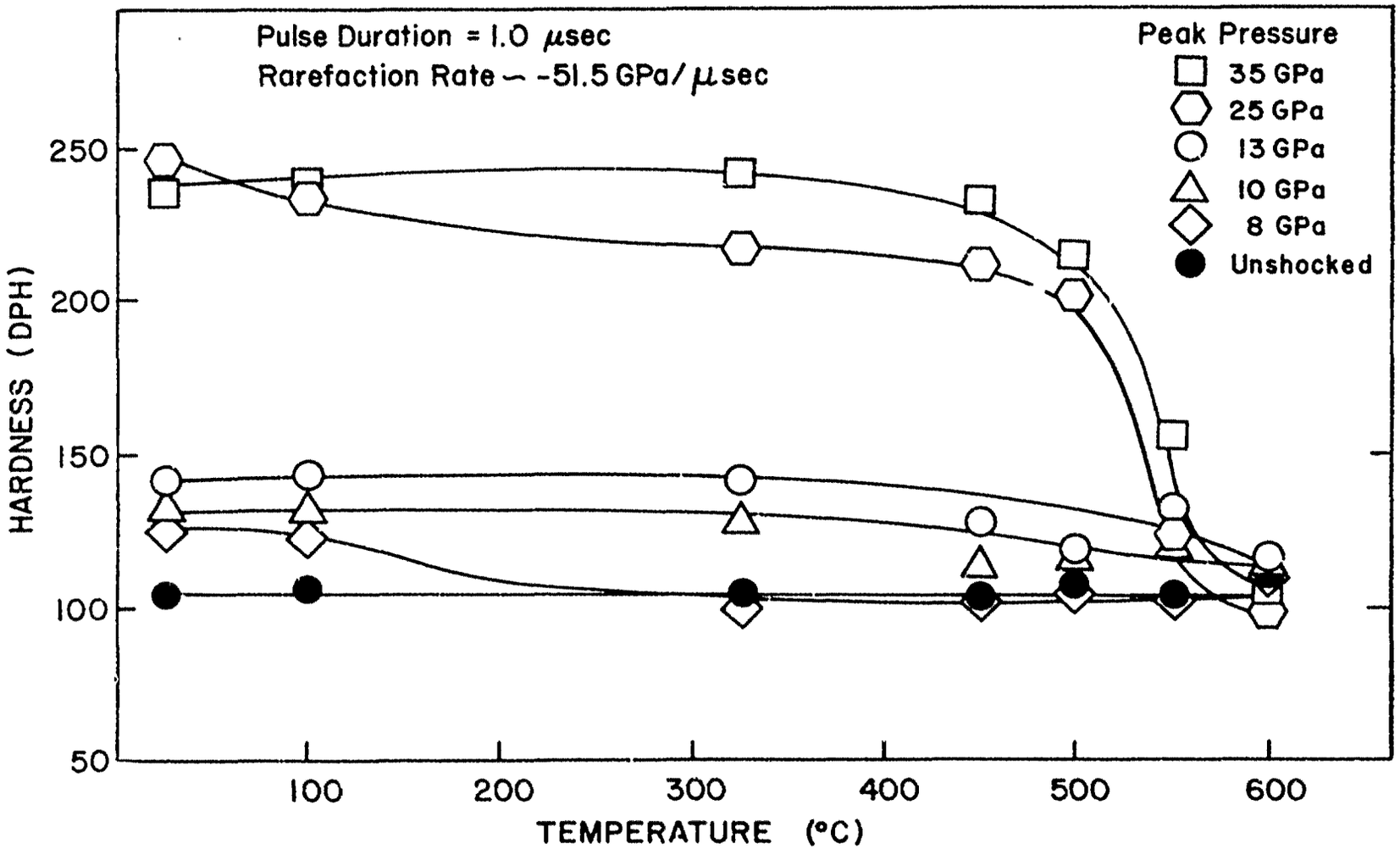

FIGURE 20. The Effects of Peak Pressure and Isochronal (1 hr) Annealing Temperature on the Hardness of AISI 1008 Steel.

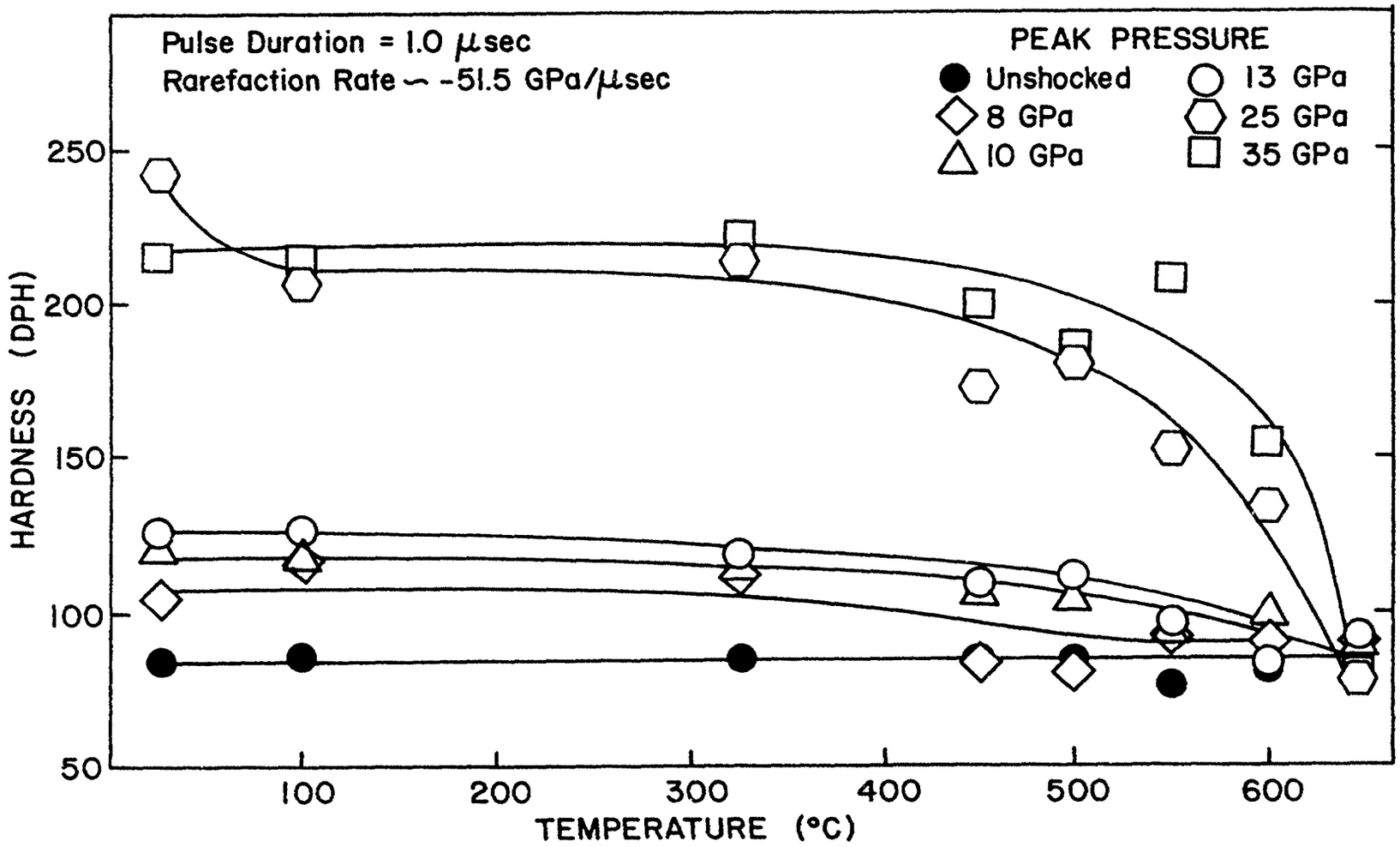

FIGURE 21. The Effects of Peak Pressure and Isochronal (1 hr) Annealing Temperature on the Hardness of ARMCO Ingot Iron.

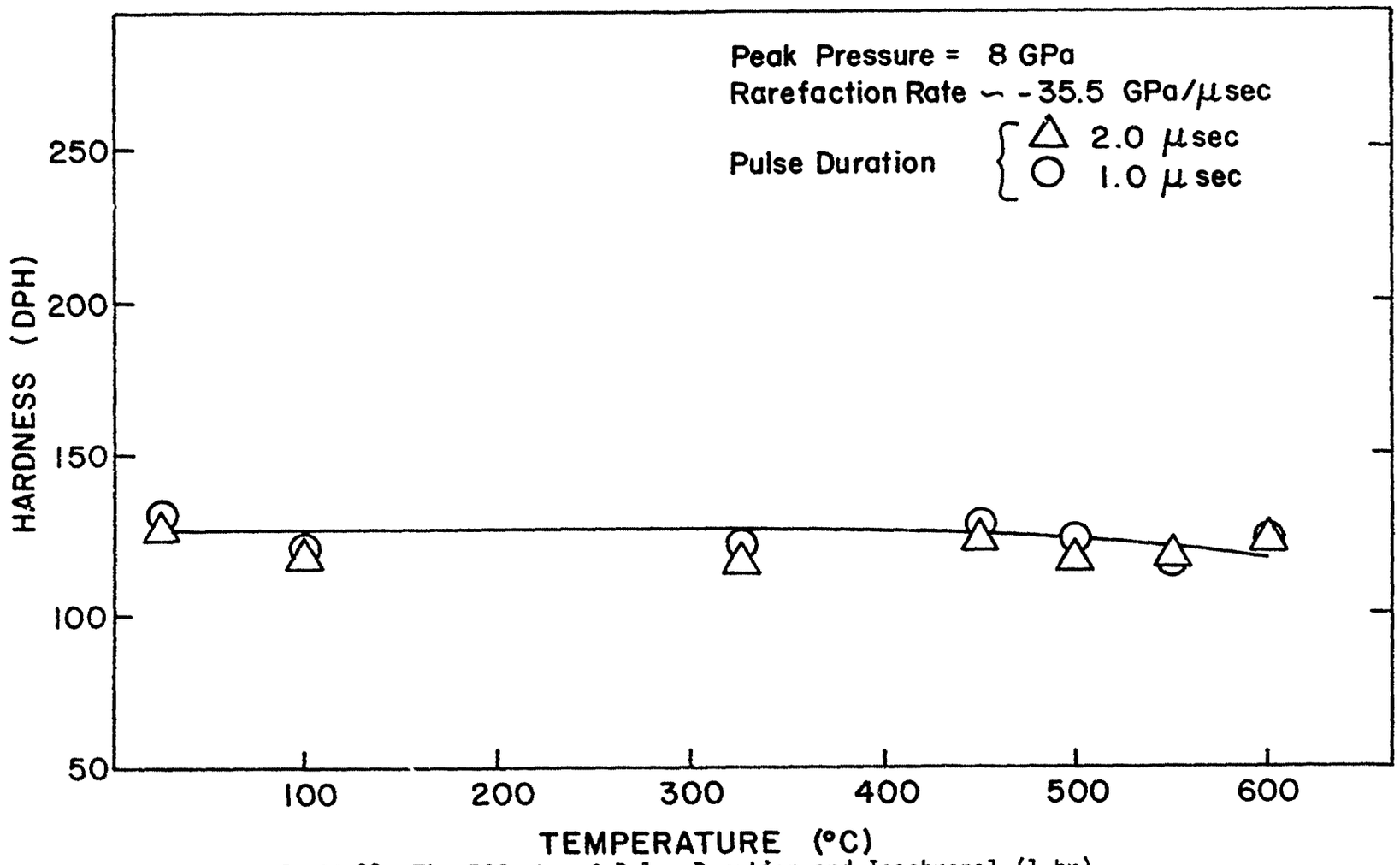

FIGURE 22. The Effects of Pulse Duration and Isochronal (1 hr) Annealing Temperature on the Hardness of AISI 1008 Steel Shocked at 8 GPa.

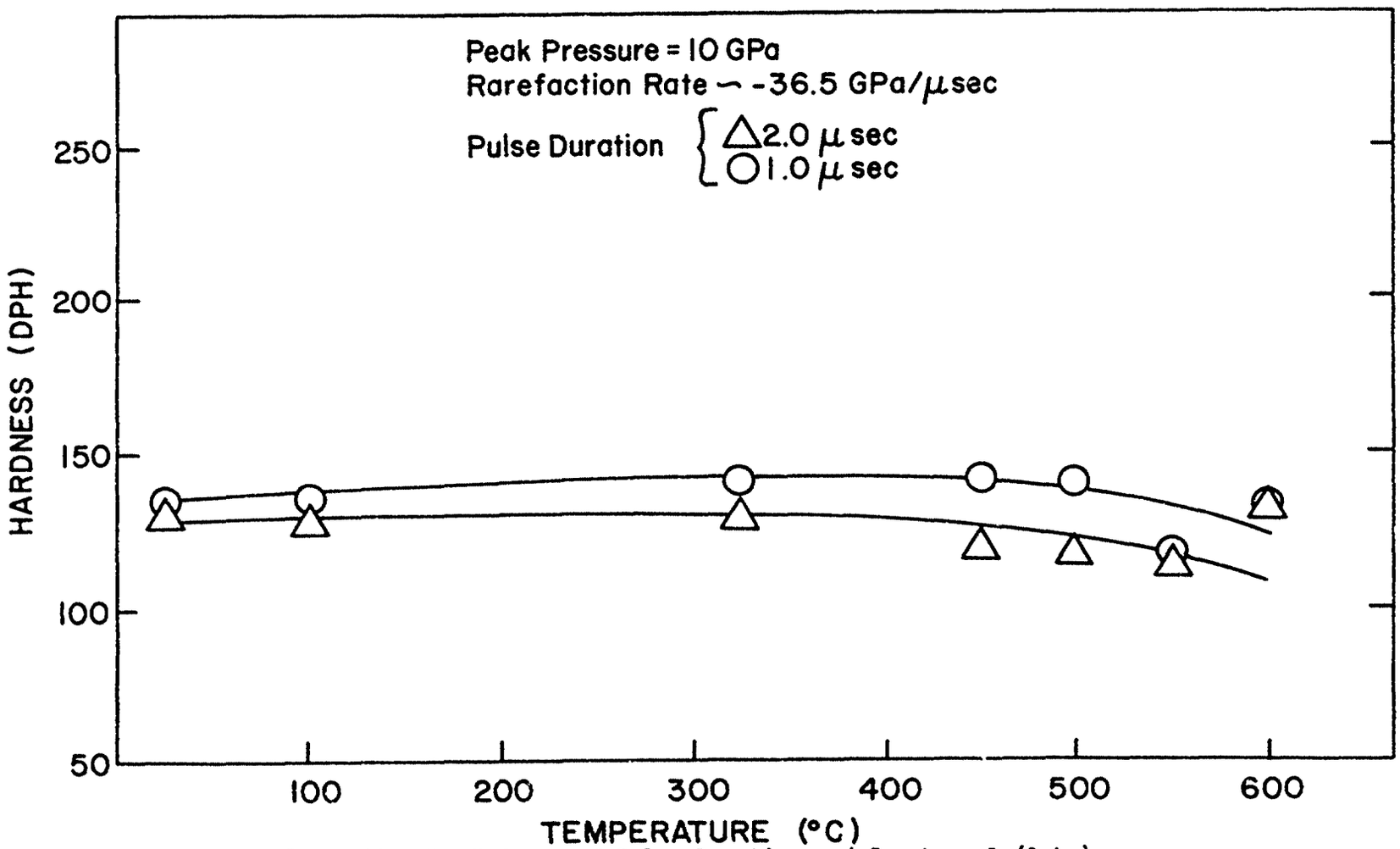

FIGURE 23. The Effects of Pulse Duration and Isochronal (1 hr) Annealing Temperature on the Hardness of AISI 1008 Steel Shocked at 10 GPa.

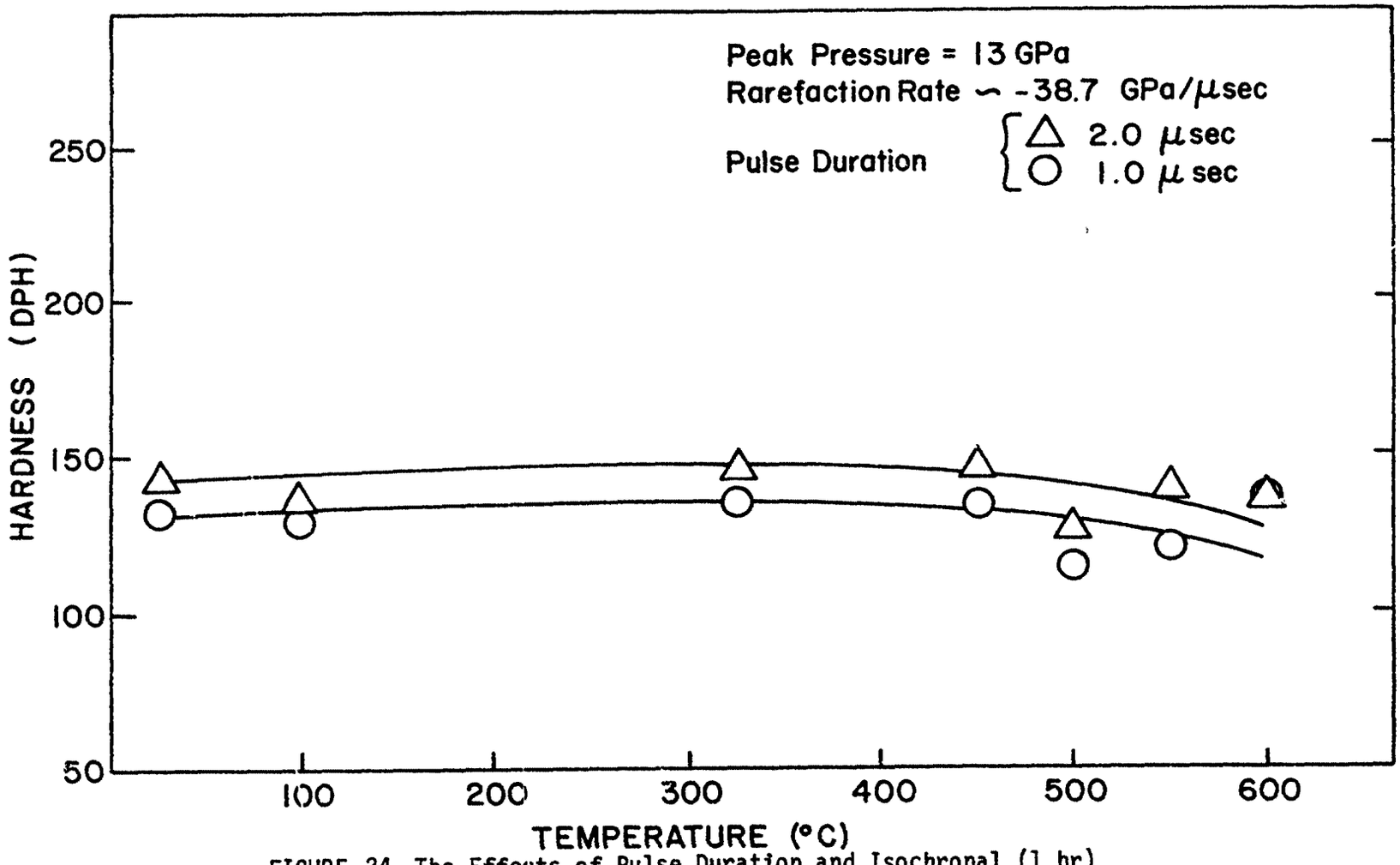

FIGURE 24. The Effects of Pulse Duration and Isochronal (1 hr) Annealing Temperature on the Hardness of AISI 1008 Steel Shocked at 13 GPa.

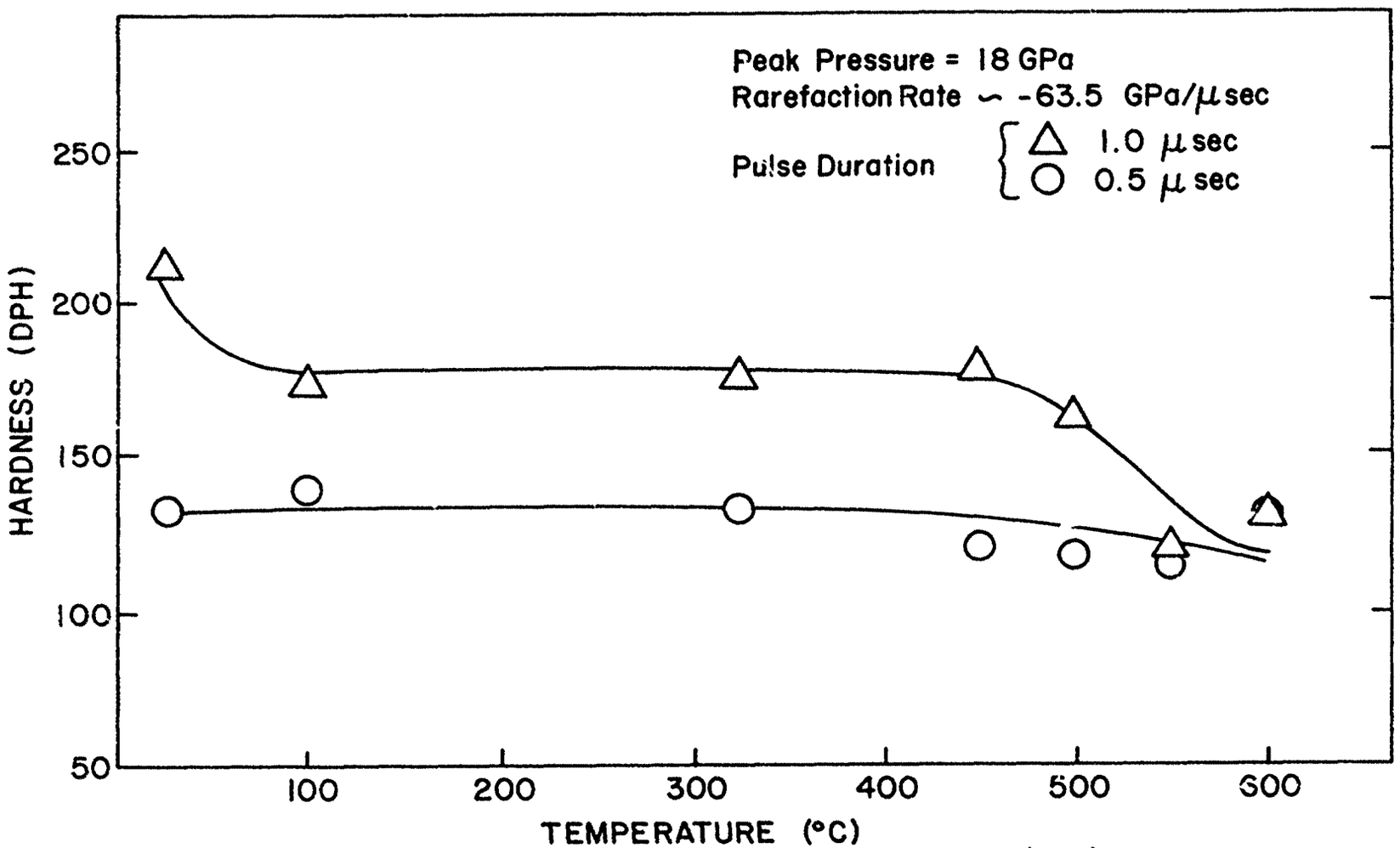

FIGURE 25. The Effects of Pulse Duration and Isochronal (1 hr) Annealing Temperature on the Hardness of AISI 1008 Steel Shocked at 18 GPa.

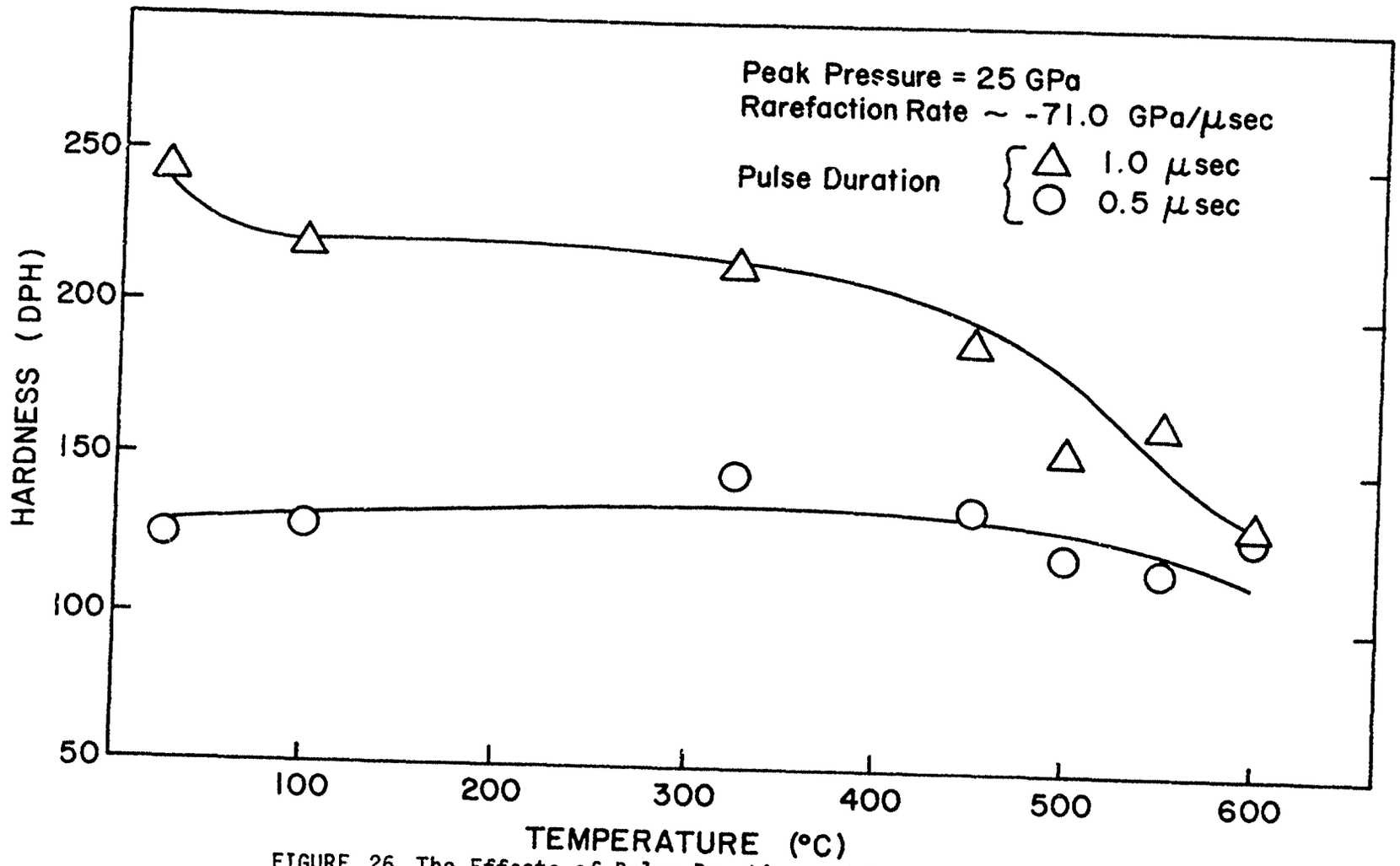

FIGURE 26. The Effects of Pulse Duration and Isochronal (1 hr) Annealing Temperature on the Hardness of AISI 1008 Steel Shocked at 25 GPa.

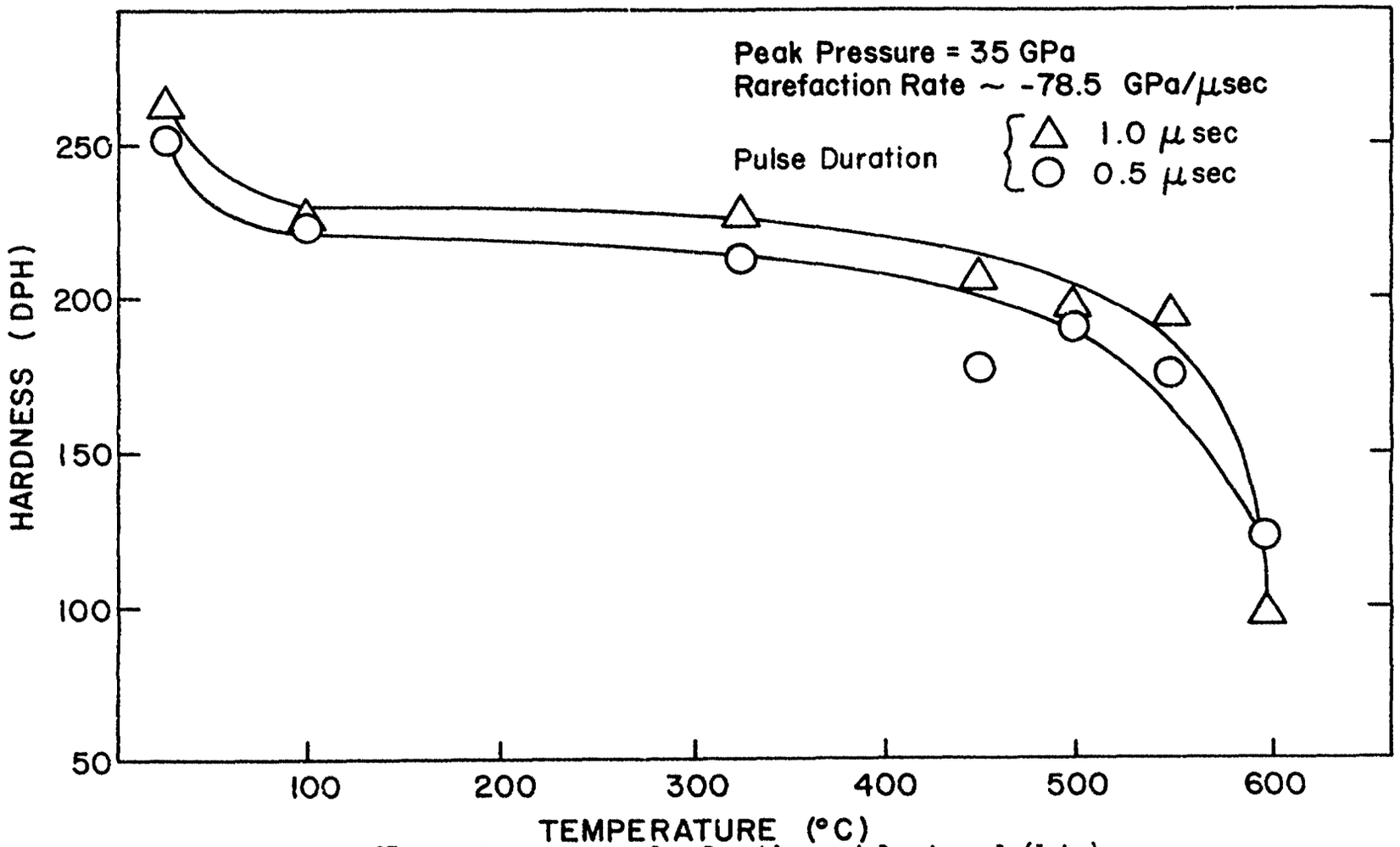

FIGURE 27. The Effects of Pulse Duration and Isochronal (1 hr) Annealing Temperature on the Hardness of AISI 1008 Steel Shocked at 35 GPa.

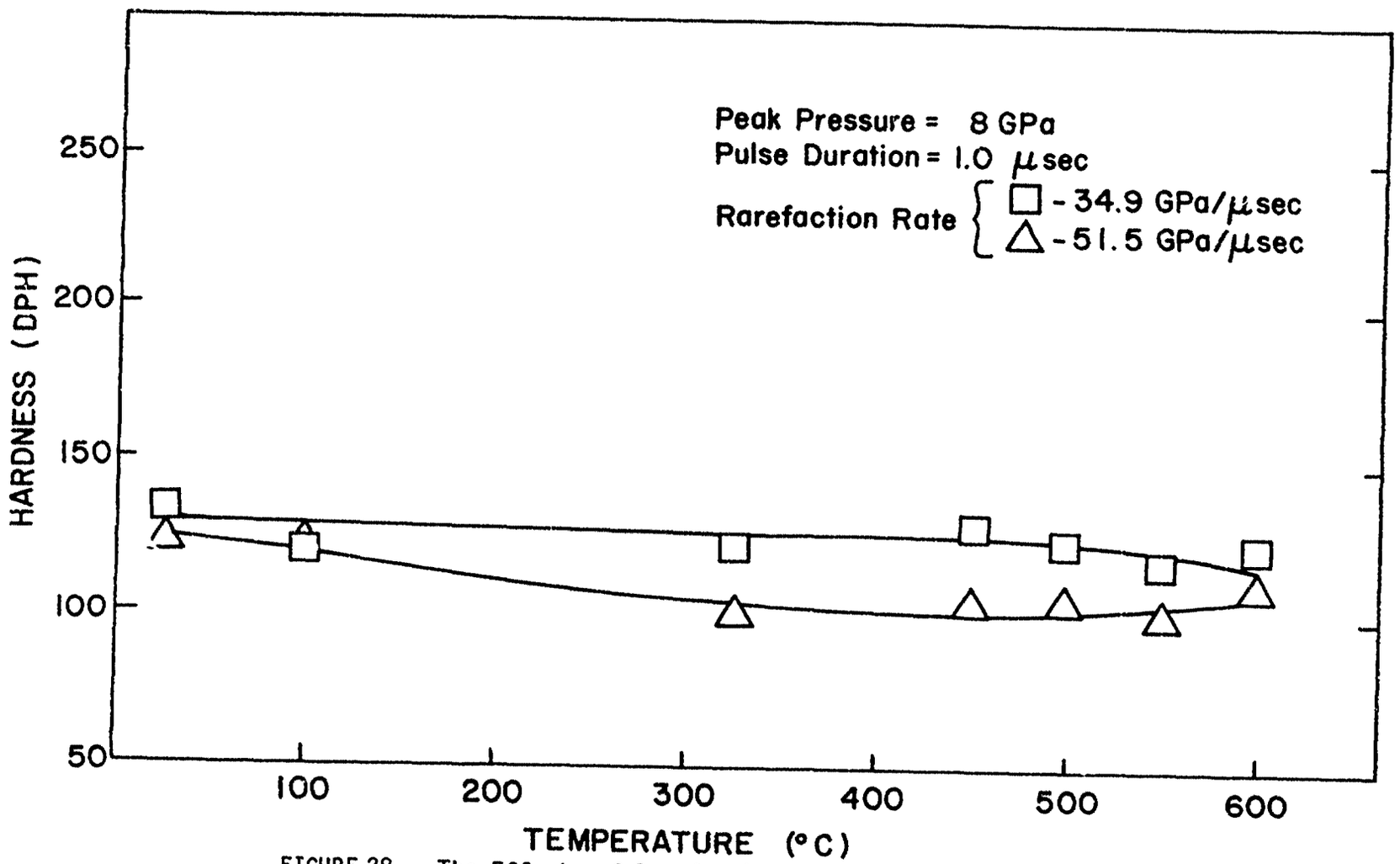

FIGURE 28. The Effects of Rarefaction Rate and Isochronal (1 hr) Annealing Temperature on the Hardness of AISI 1008 Steel Shocked at 8 GPa.

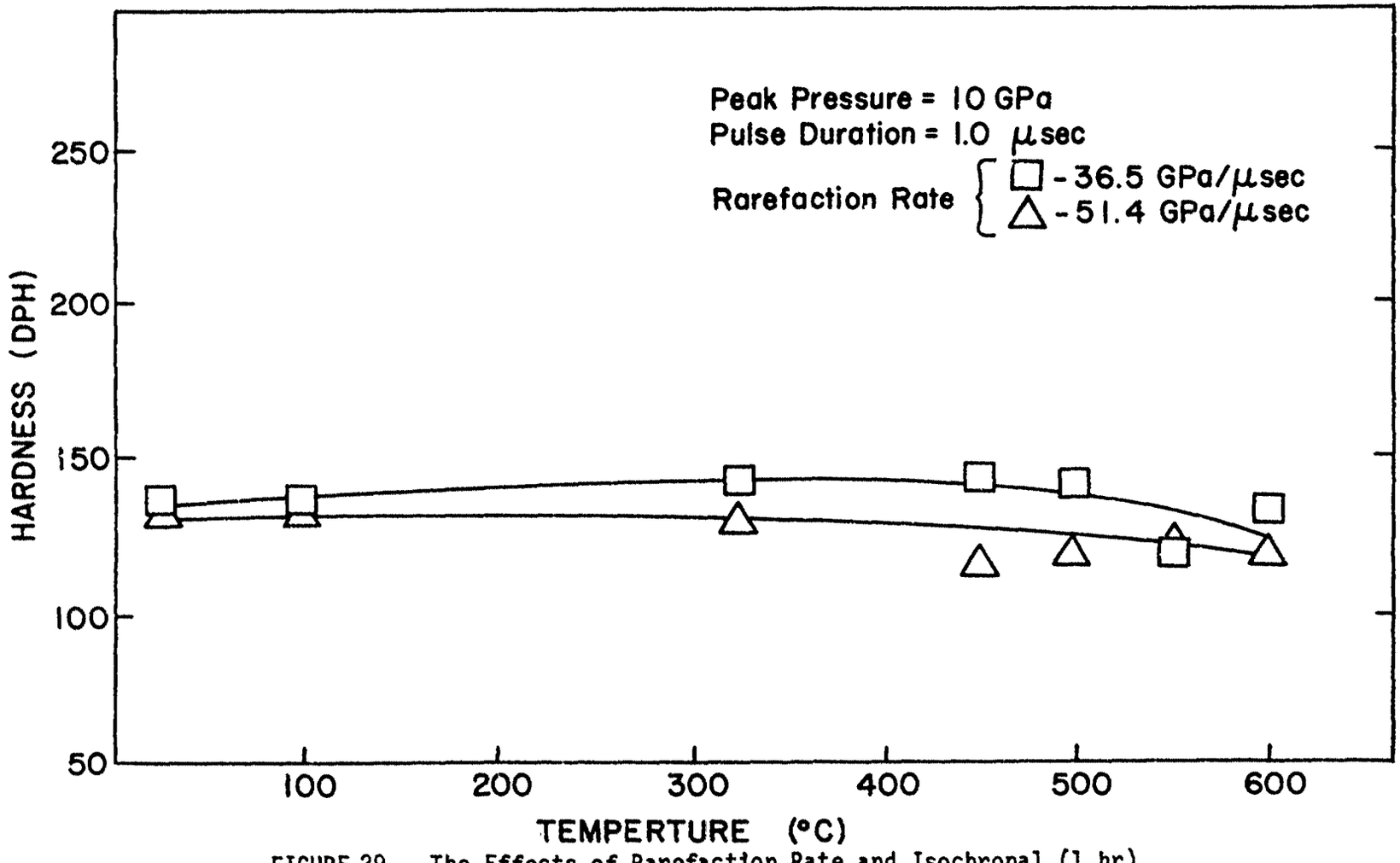

FIGURE 29. The Effects of Rarefaction Rate and Isochronal (1 hr) Annealing Temperature on the Hardness of AISI 1008 Steel Shocked at 10 GPa.

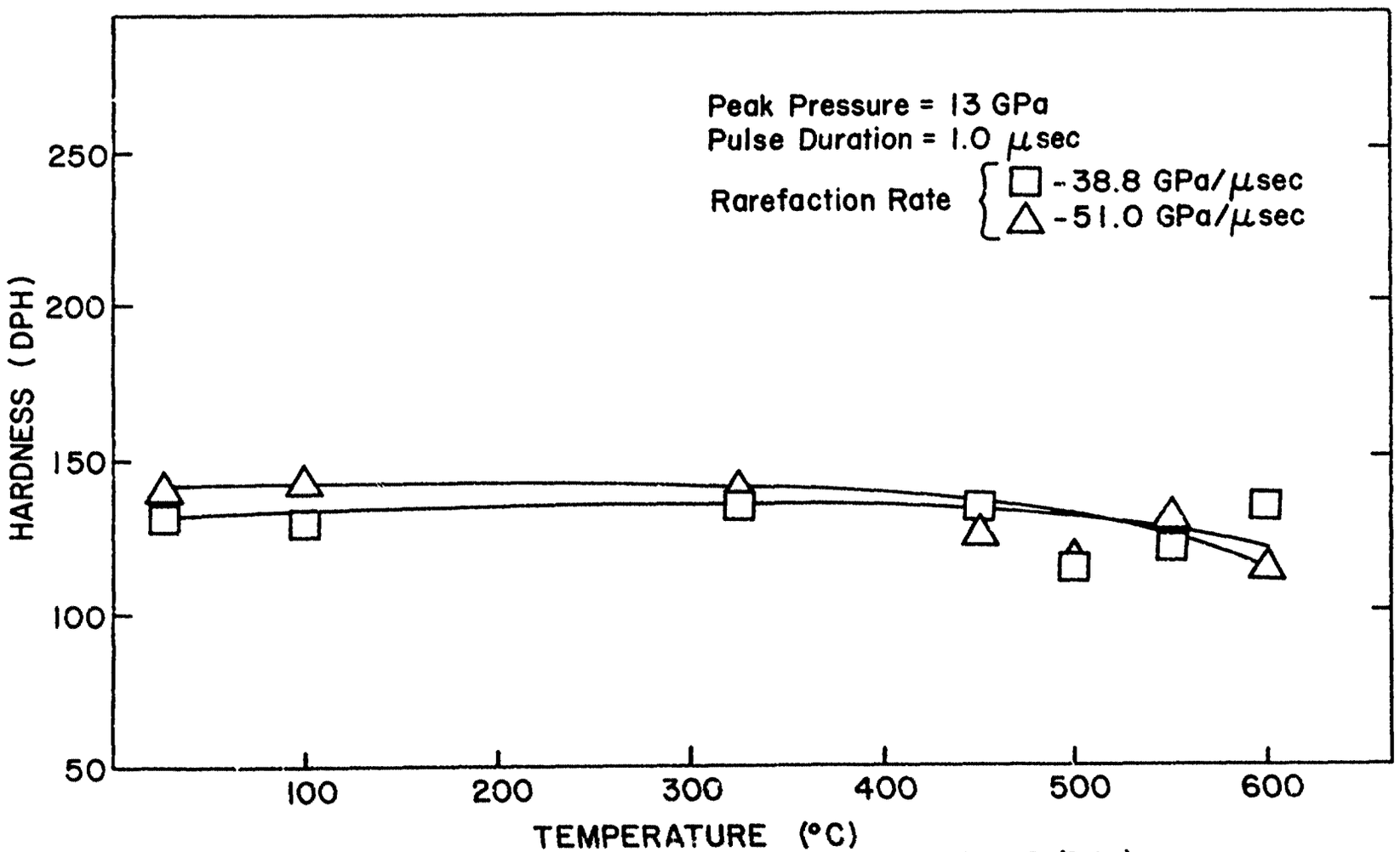

FIGURE 30. The Effects of Rarefaction Rate and Isochronal (1 hr) Annealing Temperature on the Hardness of AISI 1008 Steel Shocked at 13 GPa.

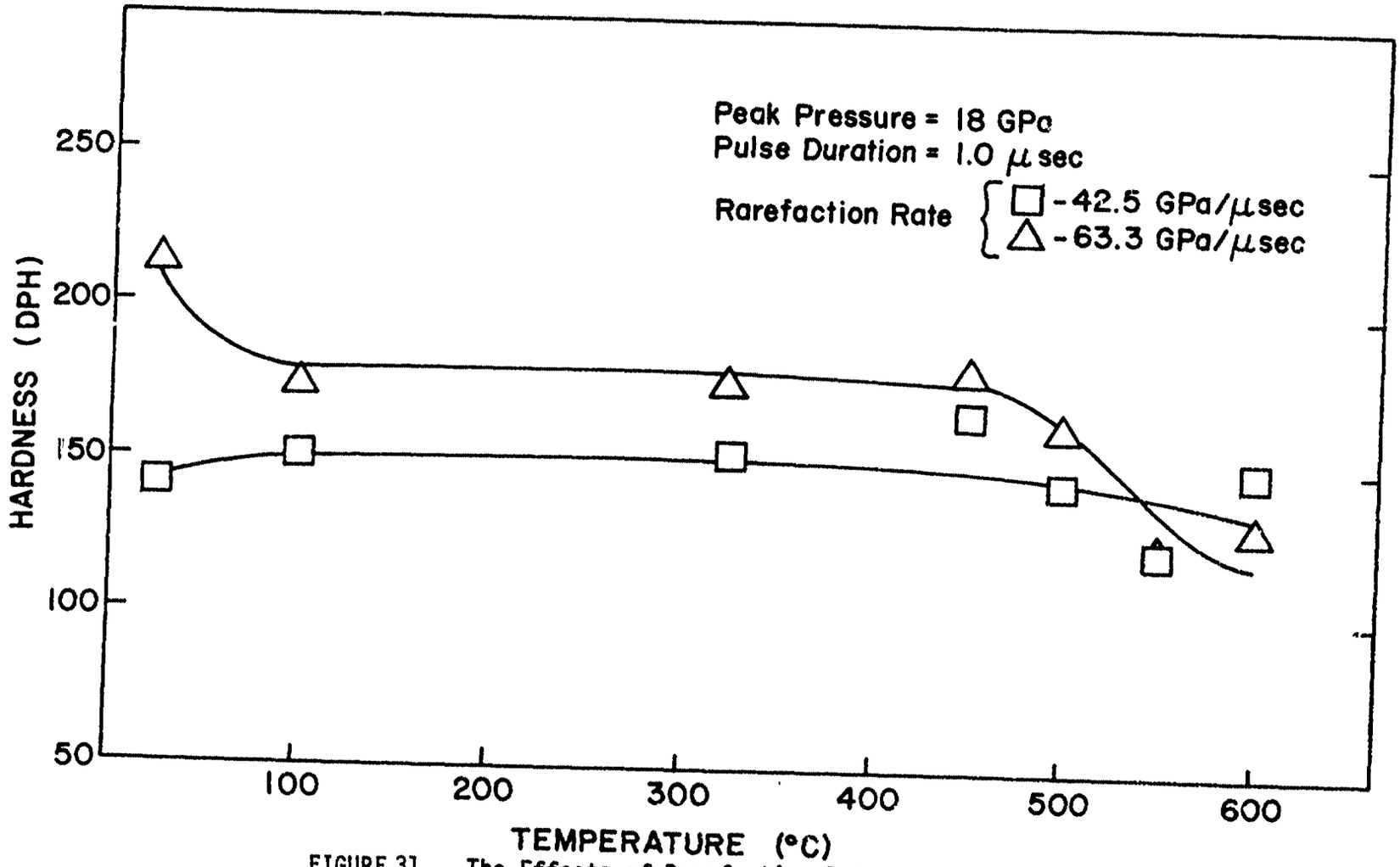

FIGURE 31. The Effects of Rarefaction Rate and Isochronal (1 hr) Annealing Temperature on the Hardness of AISI 1008 Steel Shocked at 18 GPa

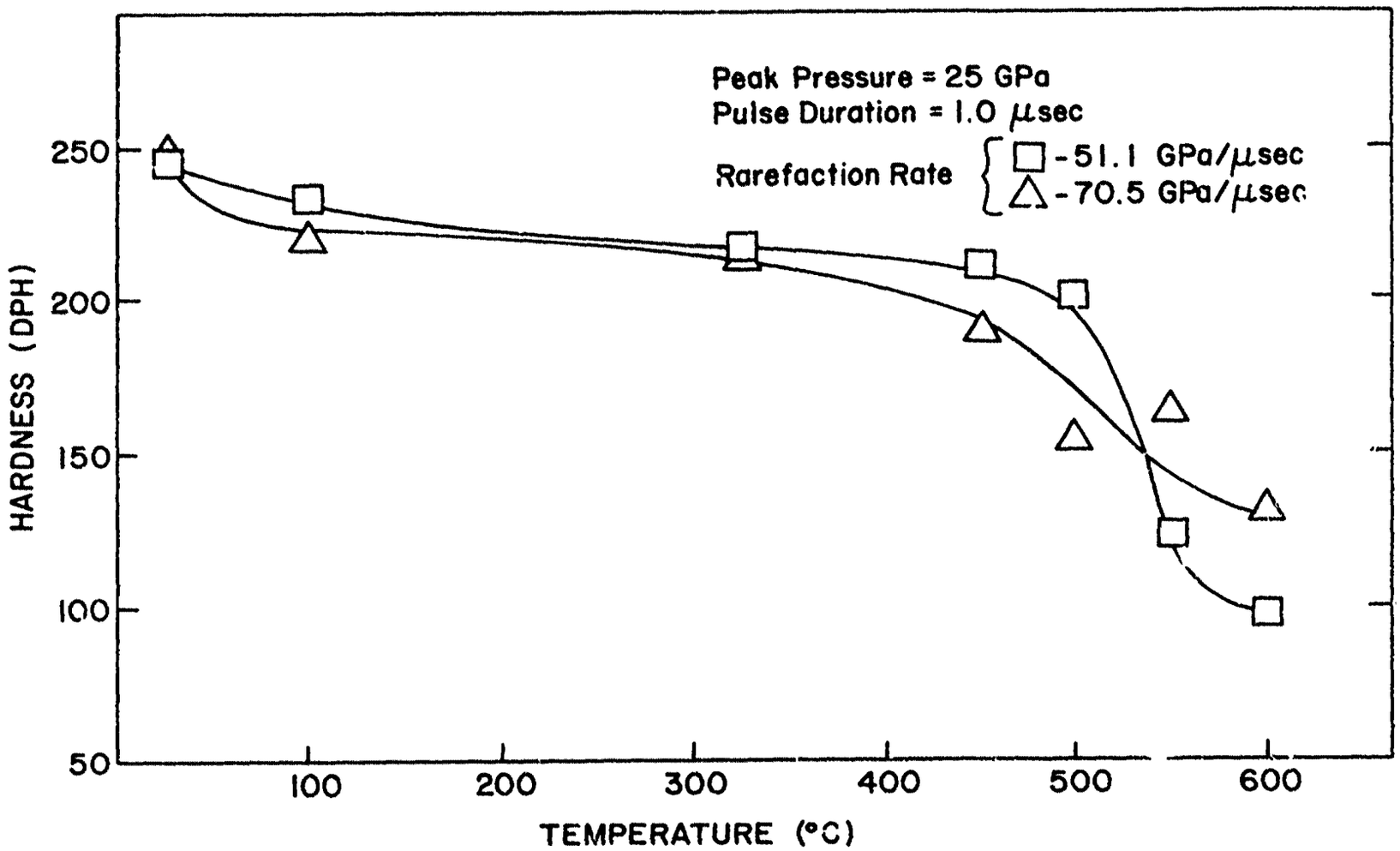

FIGURE 32. The Effects of Rarefaction Rate and Isochronal (1 hr) Annealing Temperature on the Hardness of AISI 1008 Steel Shocked at 25 GPa.

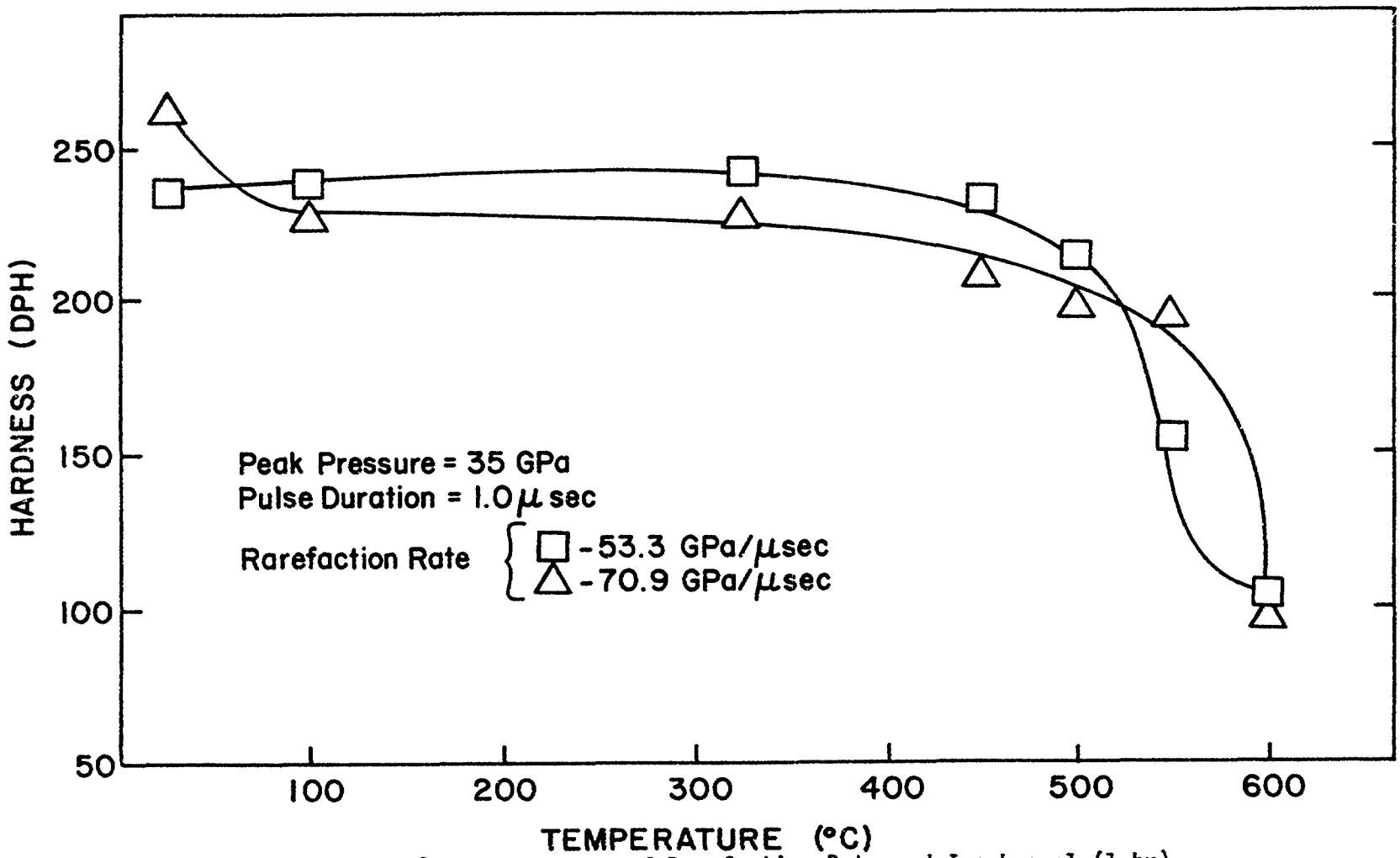

FIGURE 33. The Effects of Rarefaction Rate and Isochronal (1 hr) Annealing Temperature on the Hardness of AISI 1008 Steel shocked at 35 GPa.

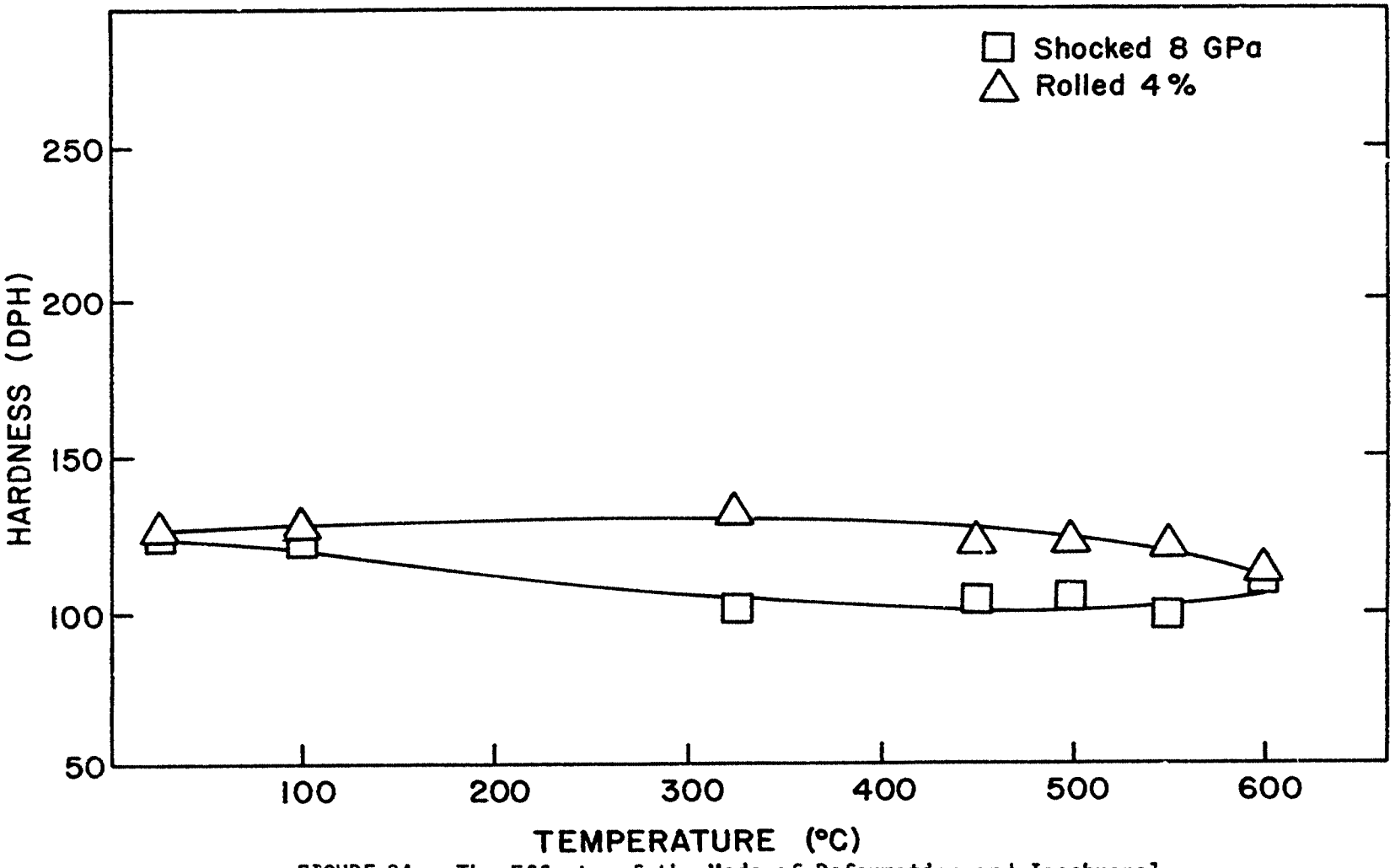

FIGURE 34. The Effects of the Mode of Deformation and Isochronal (1 hr) Annealing Temperature on the Hardness of AISI 1008 Steel Shocked at 8 GPa and Cold-rolled 4%.

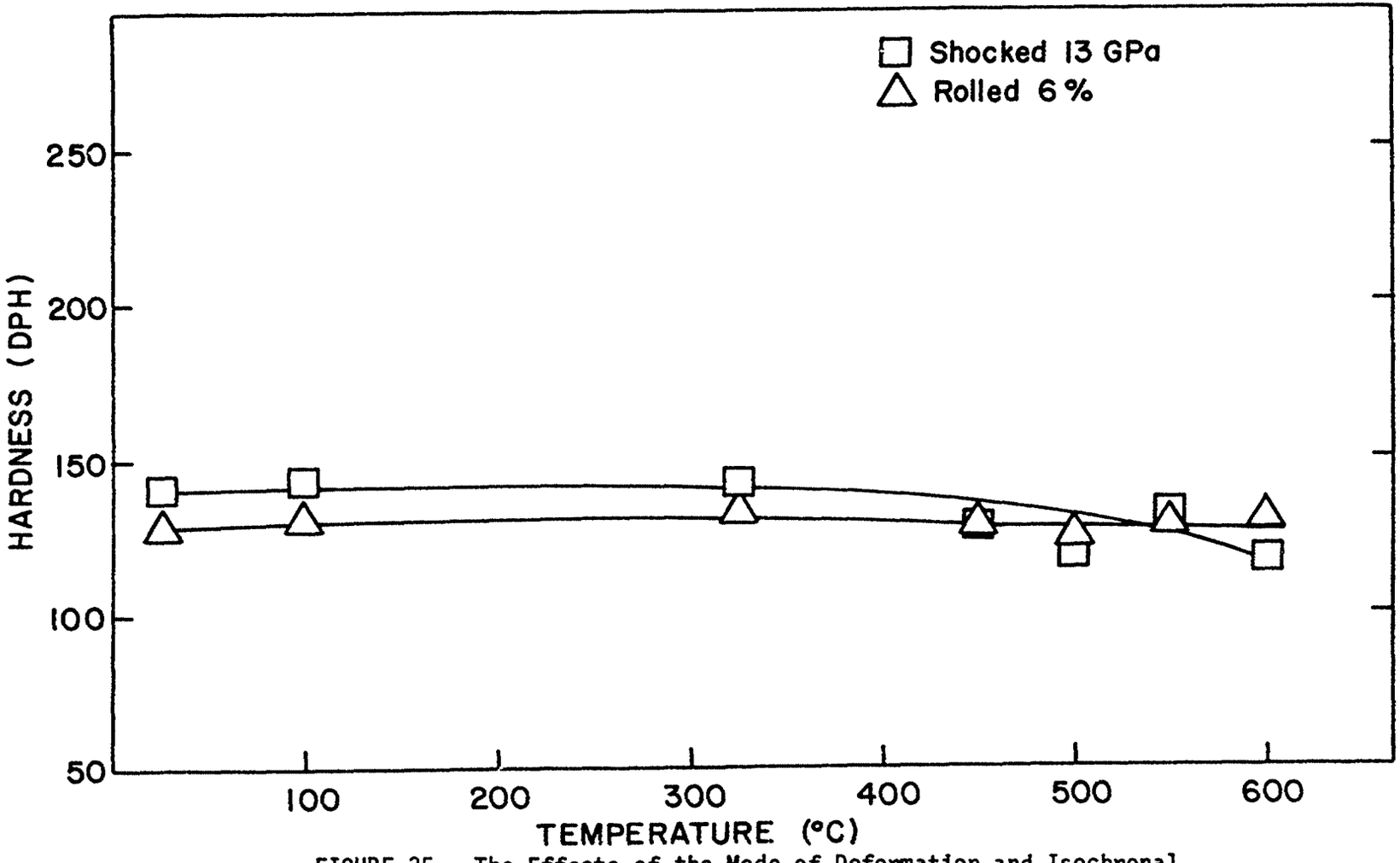

FIGURE 35. The Effects of the Mode of Deformation and Isochronal (1 hr) Annealing Temperature on the Hardness of AISI 1008 Steel Shocked at 13 GPa and Cold-rolled 6%.

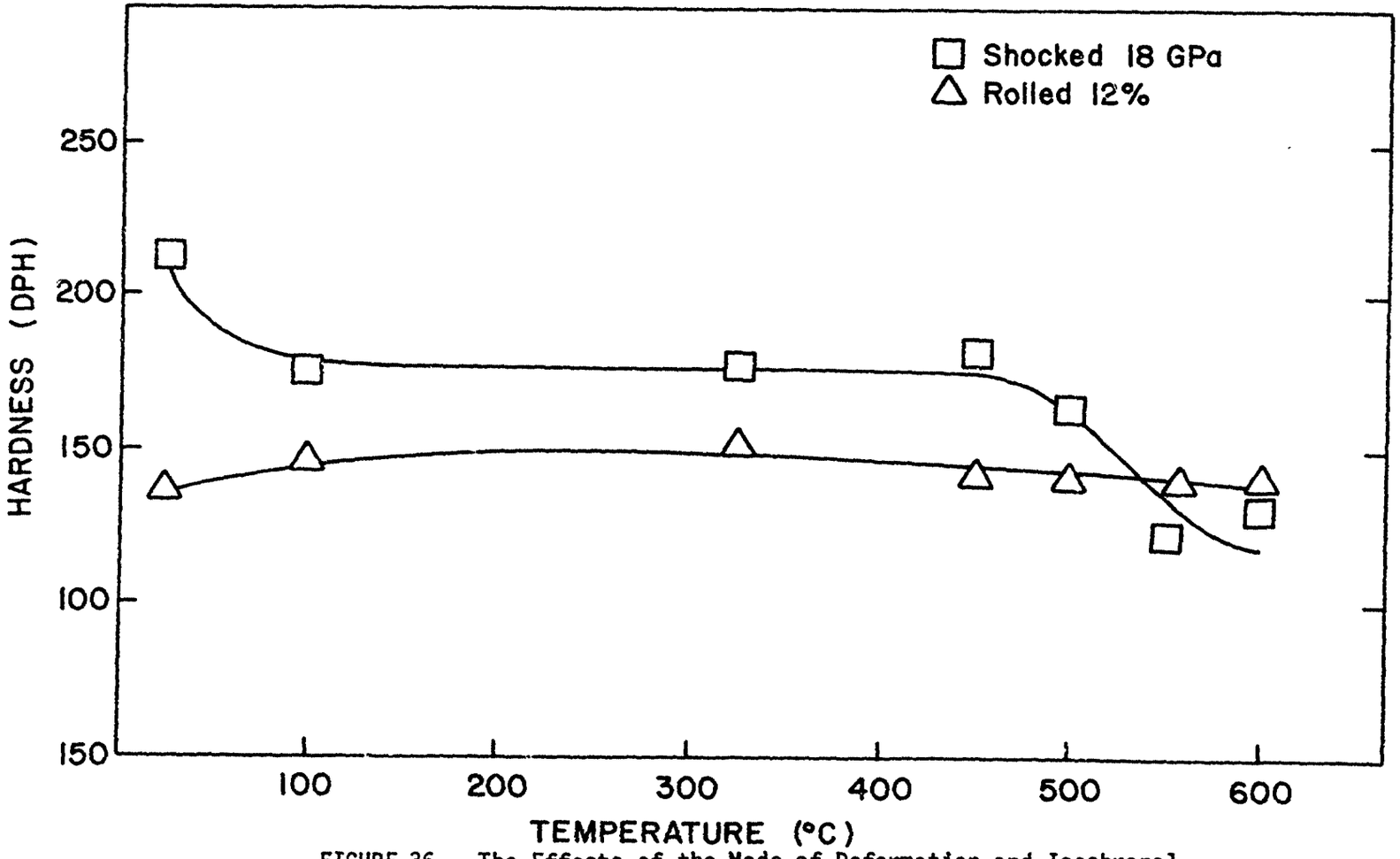

FIGURE 36. The Effects of the Mode of Deformation and Isochronal (1 hr) Annealing Temperature on the Hardness of AISI 1008 Steel Shocked at 18 GPa and Cold-rolled 12%.

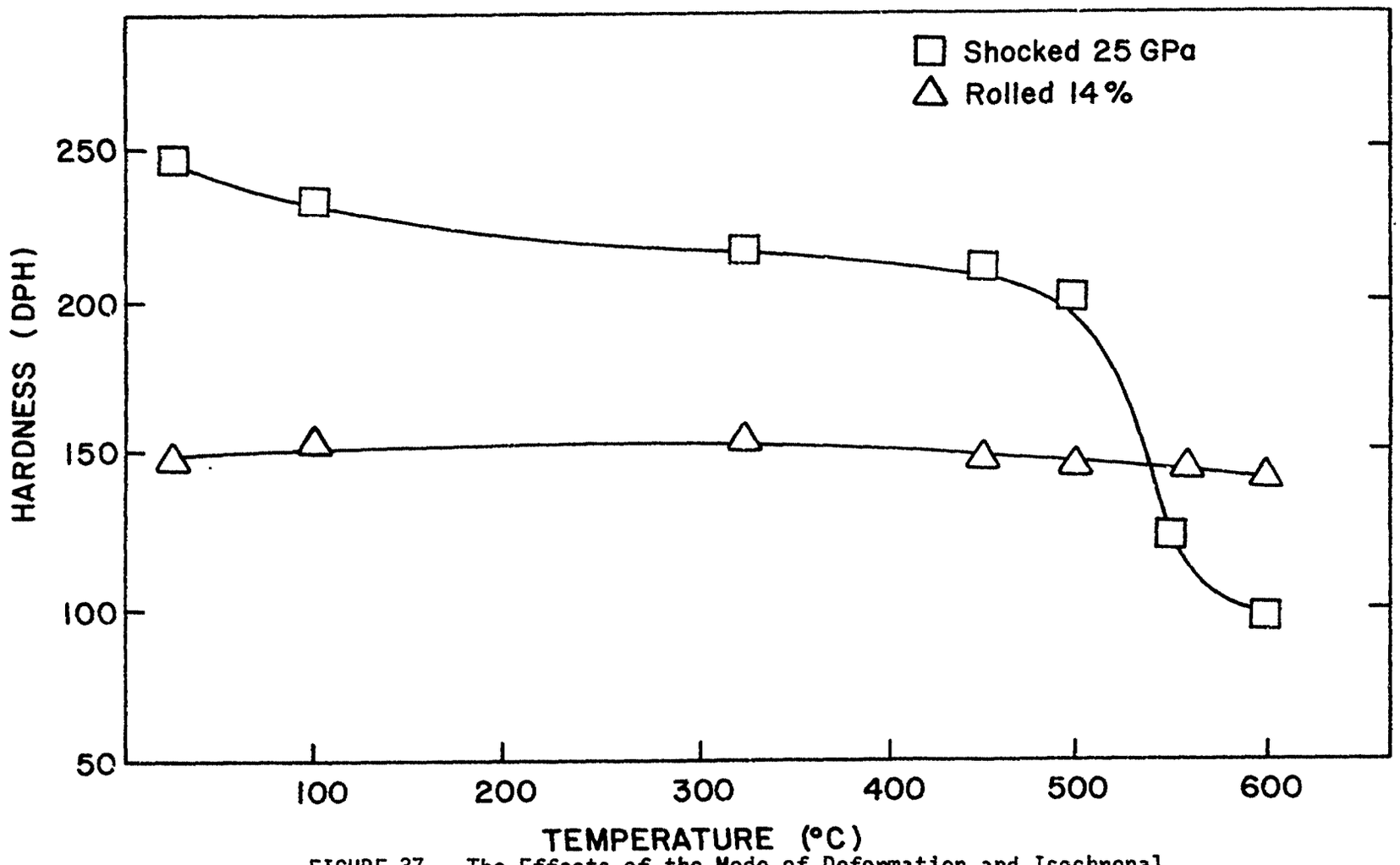

FIGURE 37. The Effects of the Mode of Deformation and Isochronal (1 hr) Annealing Temperature on the Hardness of AISI 1008 Steel Shocked at 25 GPa and Cold-rolled 14%.

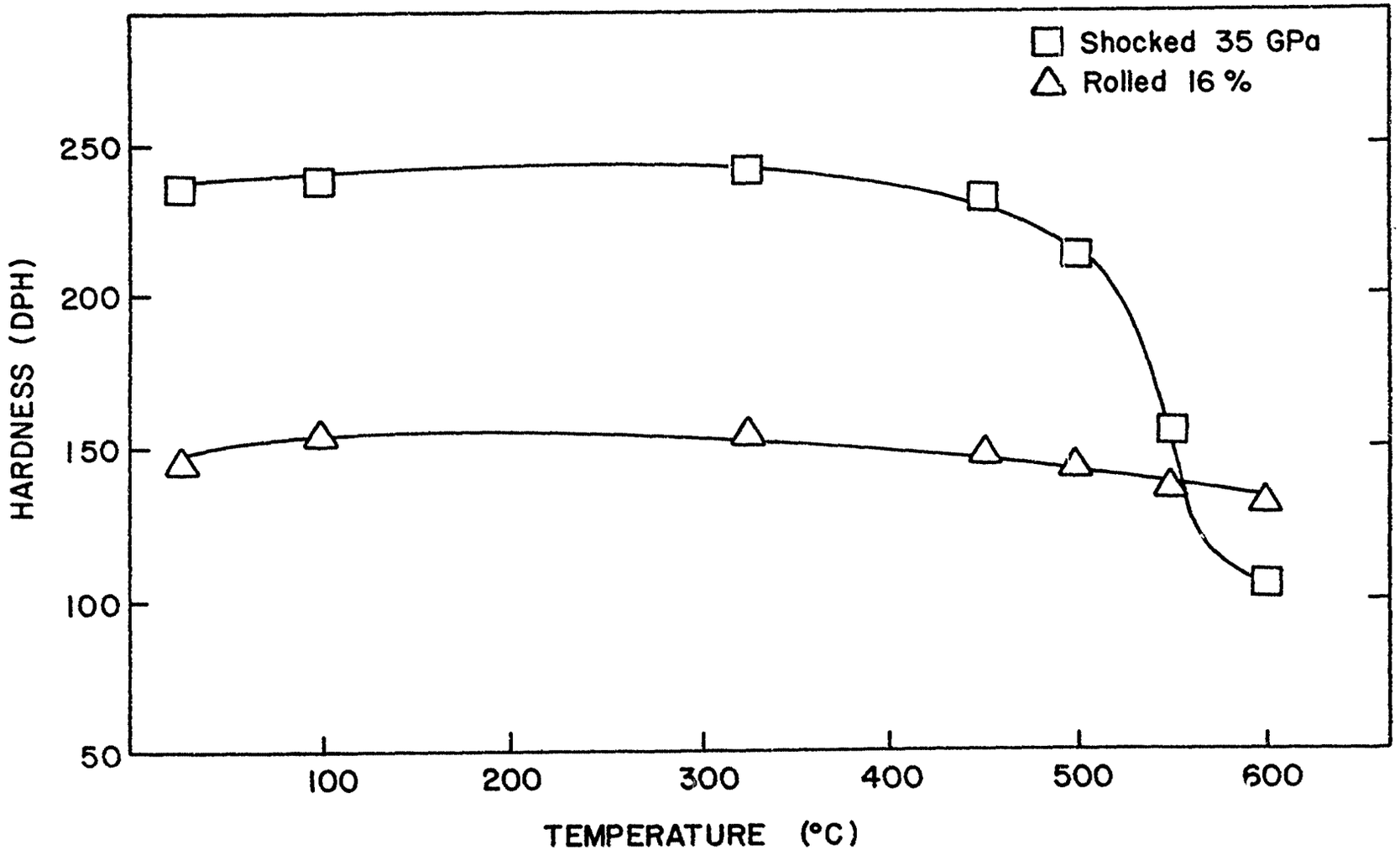

FIGURE 38. The Effects of the Mode of Deformation and Isochronal (1 hr) Annealing Temperature on the Hardness of AISI 1008 Steel Shocked at 35 GPa and Cold-rolled 16%.

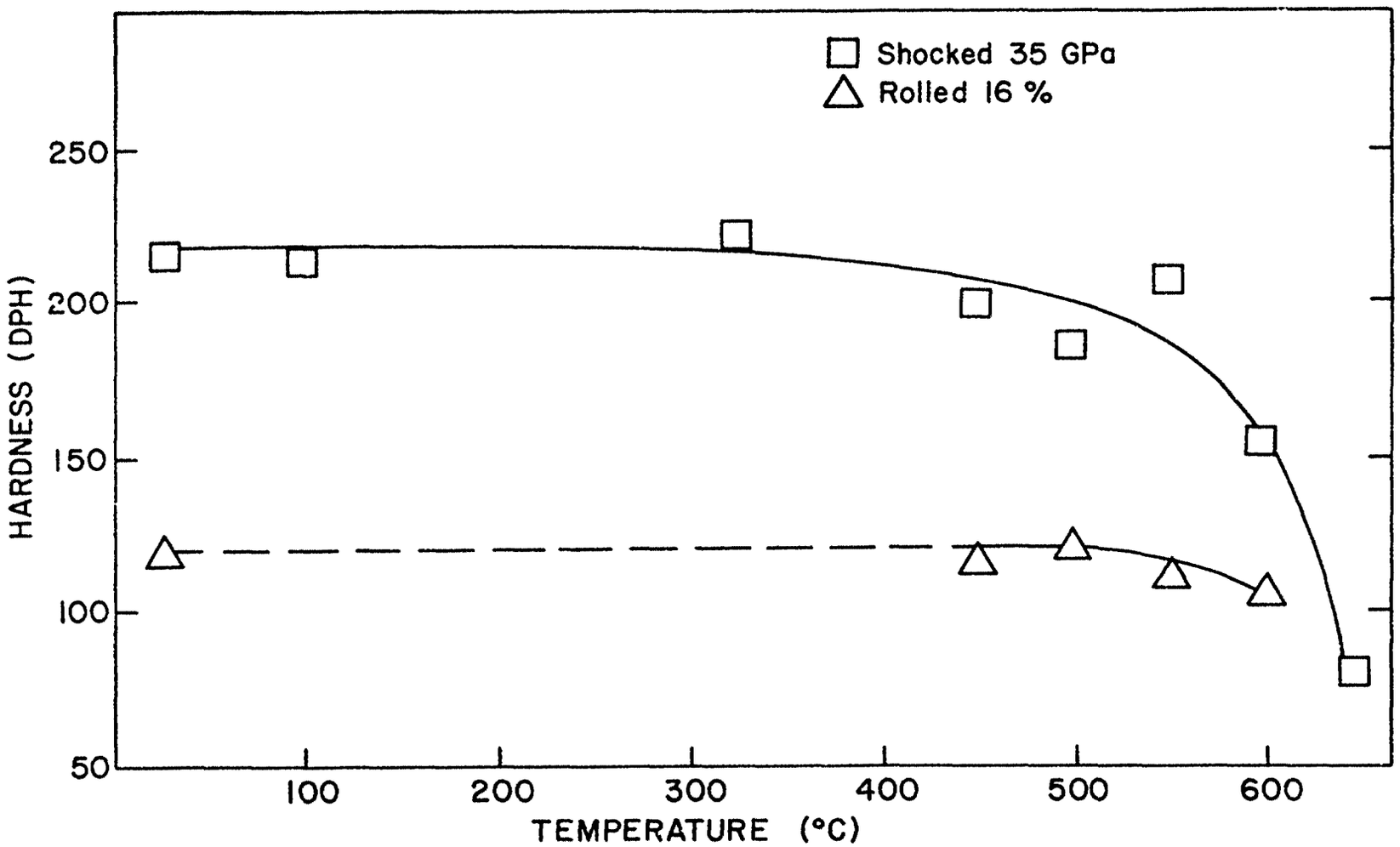

FIGURE 39. The Effects of the Mode of Deformation and Isochronal (1 hr) Annealing Temperature on the Hardness of ARMCO Ingot Iron Shocked at 35 GPa and Cold-rolled 16%.

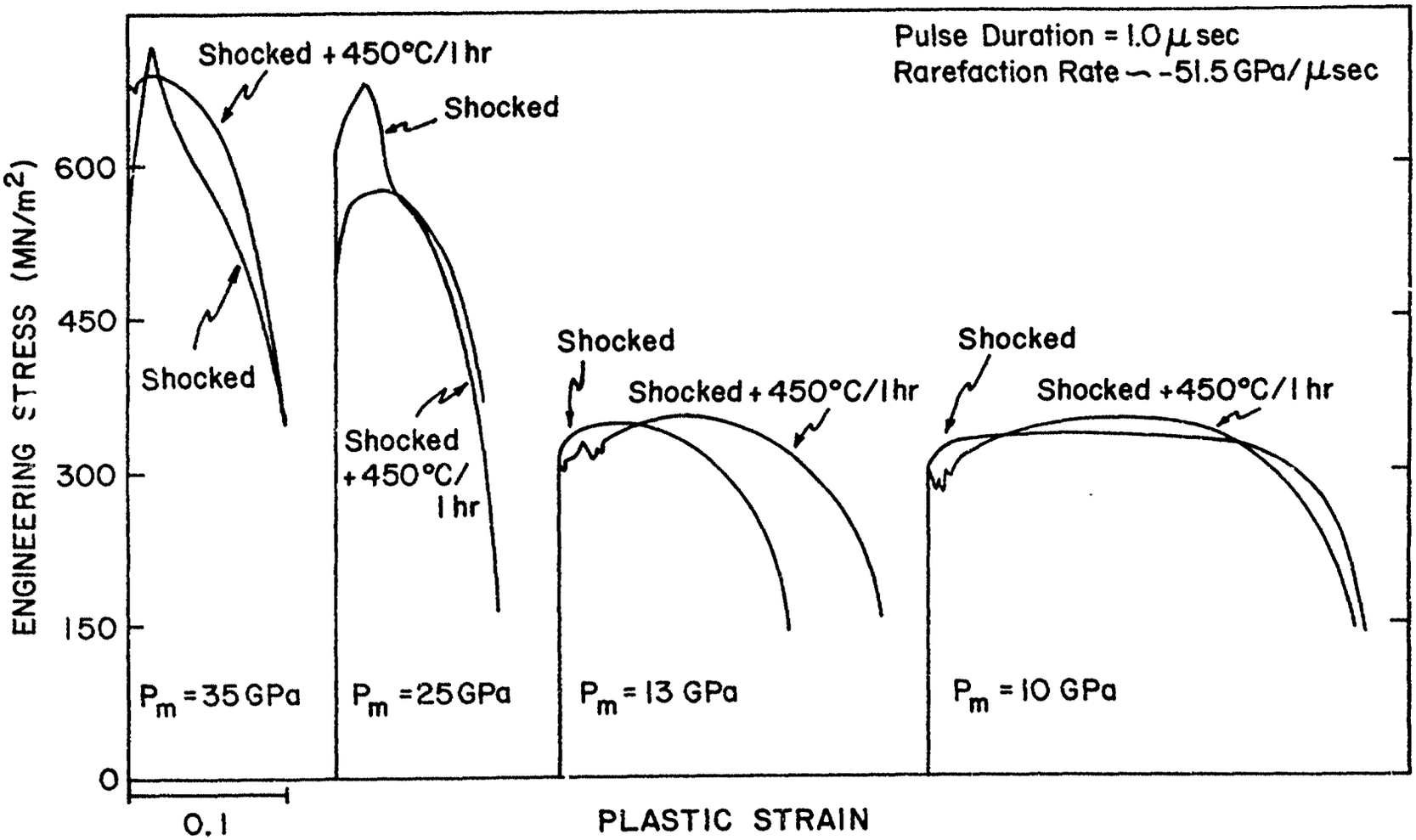

FIGURE 40. The Effects of Peak Pressure and Isochronal (1 hr) Annealing Temperature on the Tensile Properties of AISI 1008 Steel.

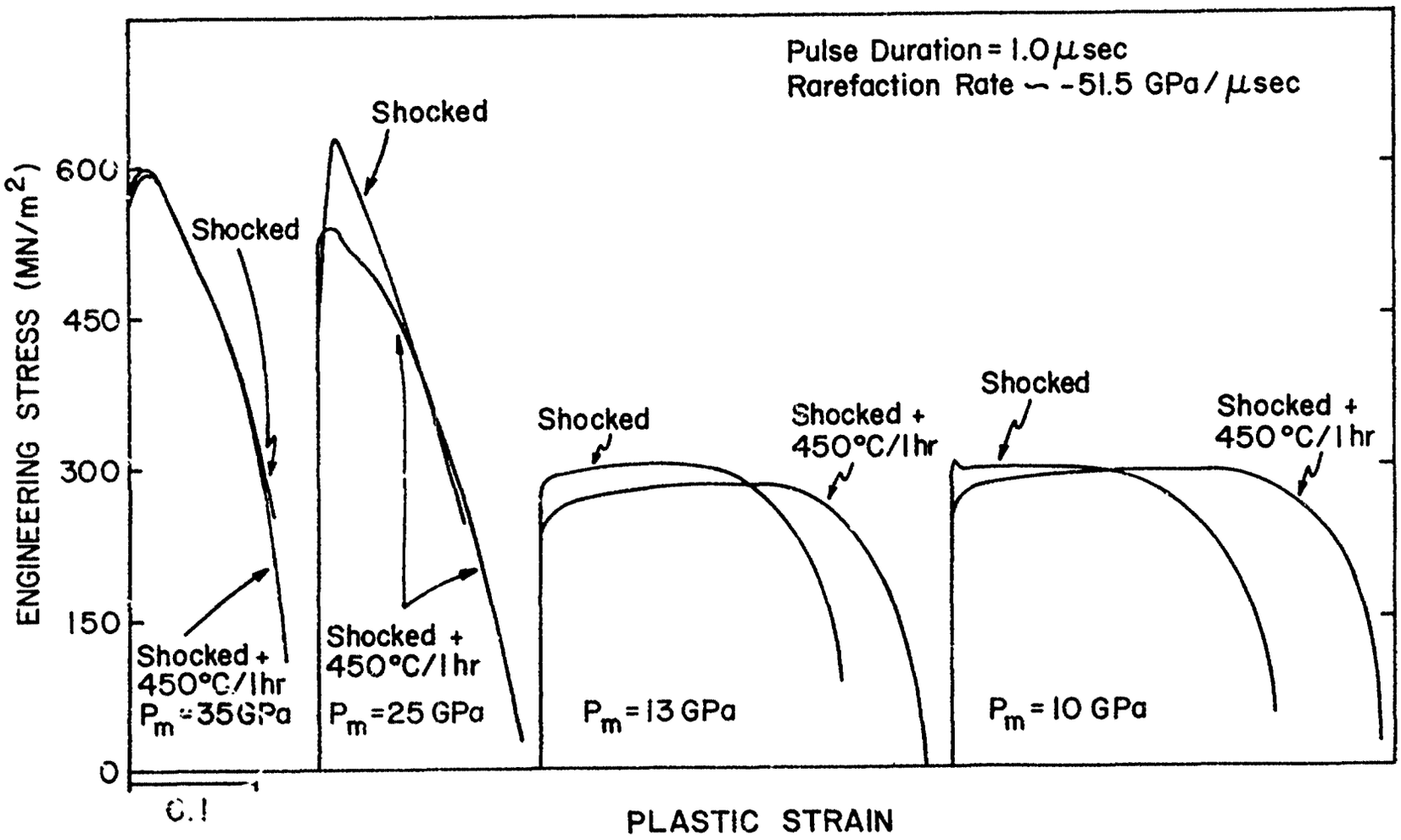

FIGURE 41. The Effects of Peak Pressure and Isochronal (1 hr) Annealing Temperature on the Tensile Properties of ARMCO Ingot Iron.

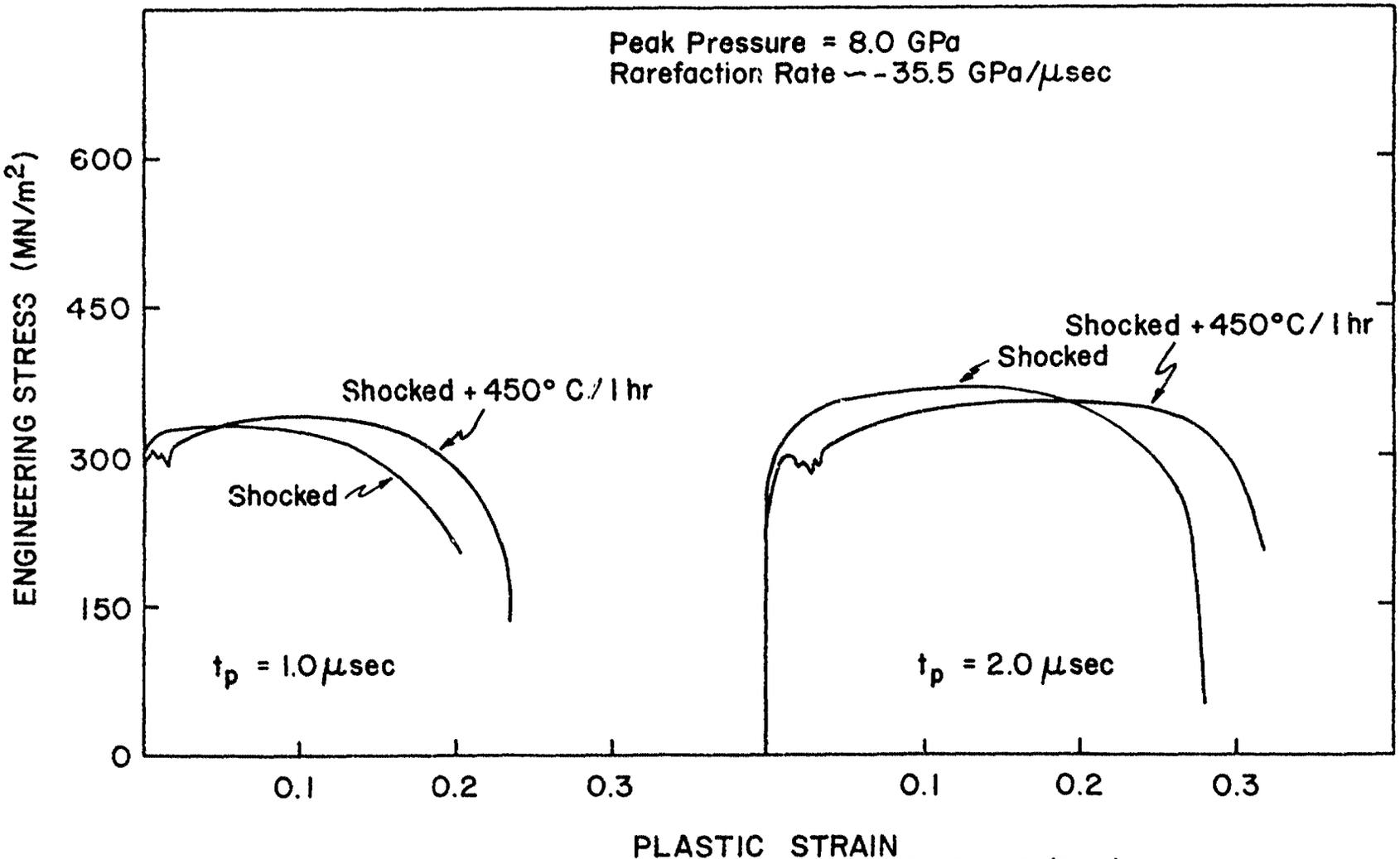

FIGURE 42. The Effects of Pulse Duration and Isochronal (1 hr) Annealing Temperature on the Tensile Properties of AISI 1008 Steel Shocked at 8 GPa.

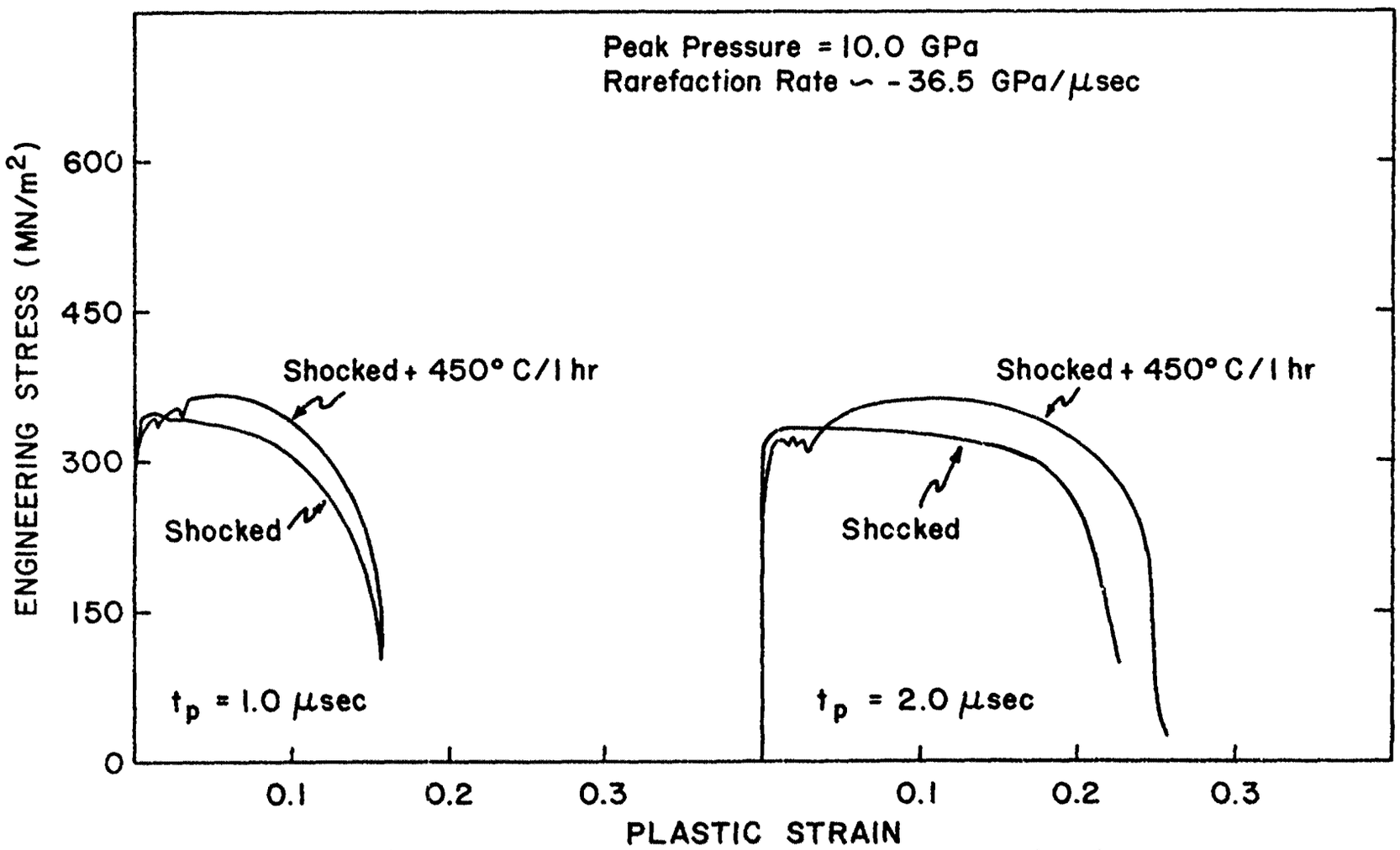

FIGURE 43. The Effects of Pulse Duration and Isochronal (1 hr) Annealing Temperature on the Tensile Properties of AISI 1008 Steel Shocked at 10 GPa.

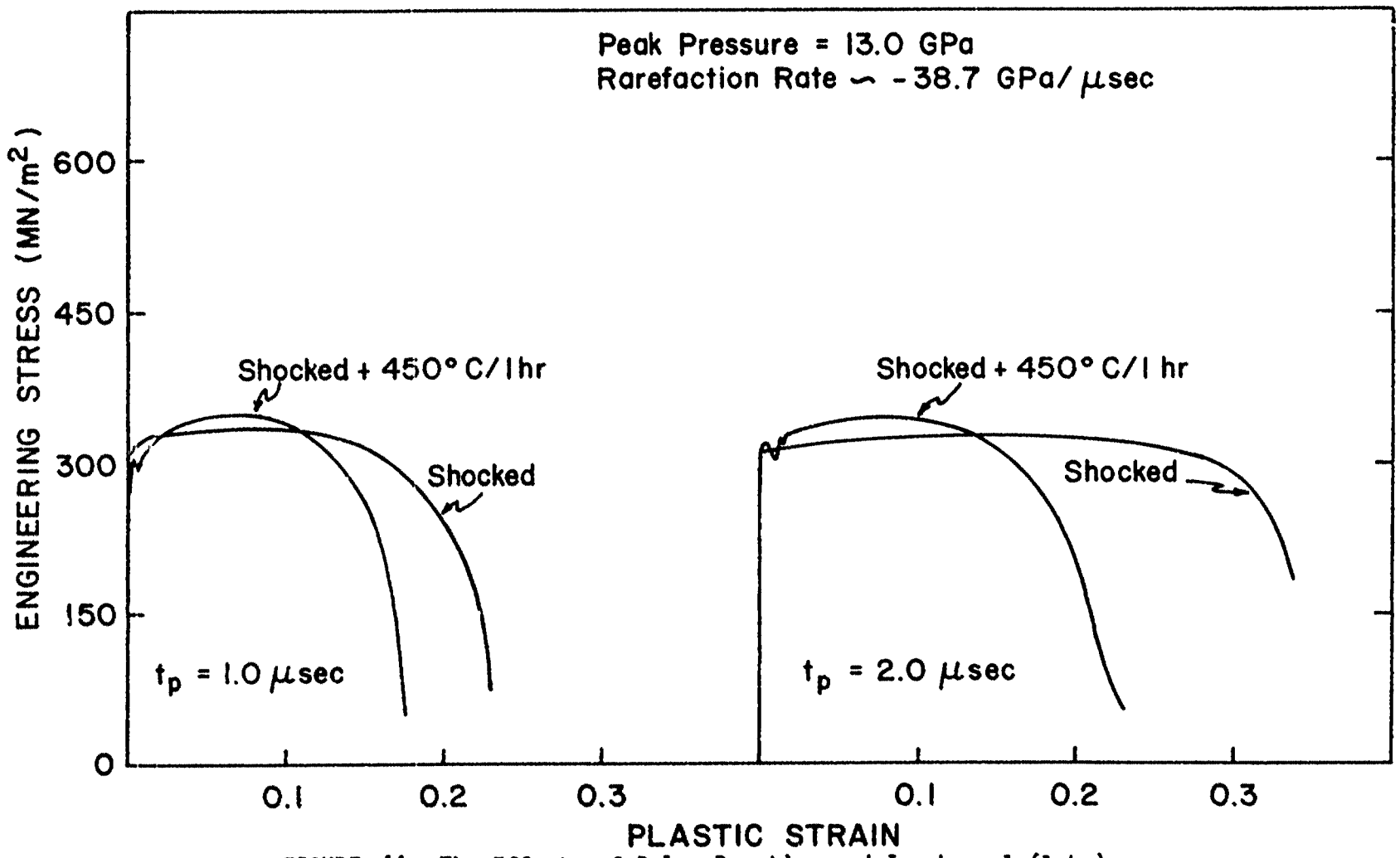

FIGURE 44. The Effects of Pulse Duration and Isochronal (1 hr) Annealing Temperature on the Tensile Properties of AISI 1008 Steel Shocked at 13 GPa.

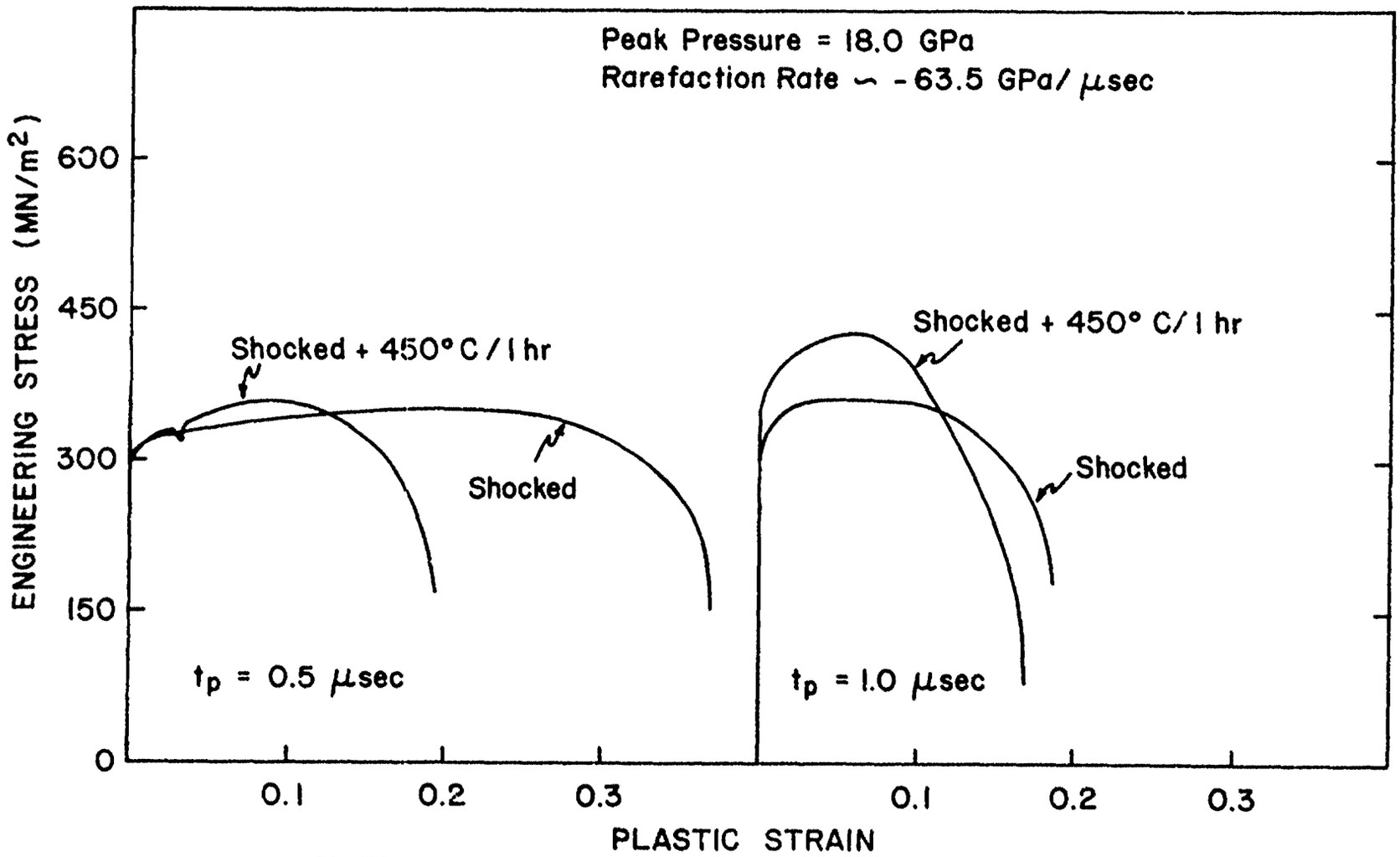

FIGURE 45. The Effects of Pulse Duration and Isochronal (1 hr) Annealing Temperature on the Tensile Properties of AISI 1008 Steel Shocked at 18 GPa.

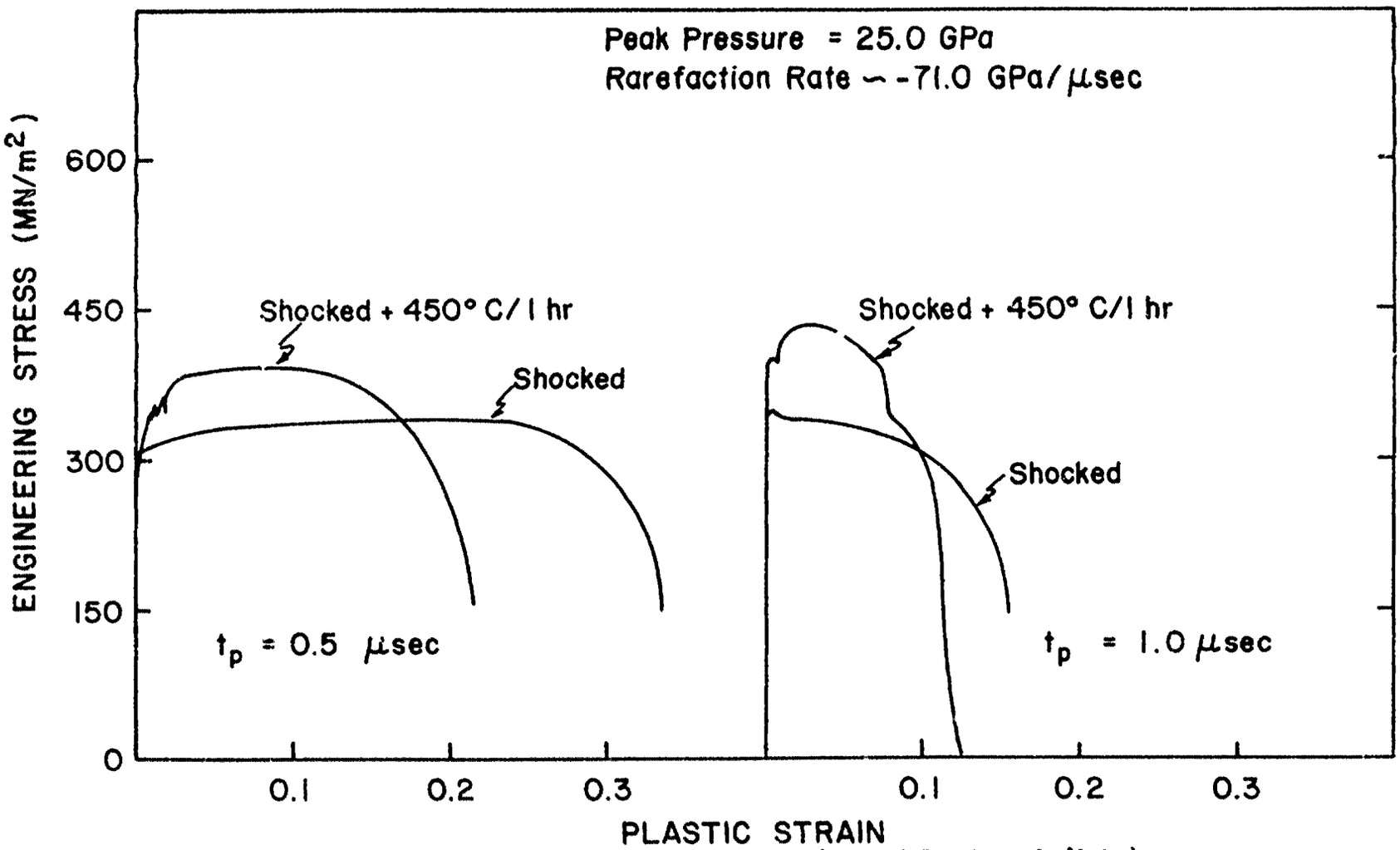

FIGURE 46. The Effects of Pulse Duration and Isochronal (1 hr) Annealing Temperature on the Tensile Properties of AISI 1008 Steel Shocked at 25 GPa.

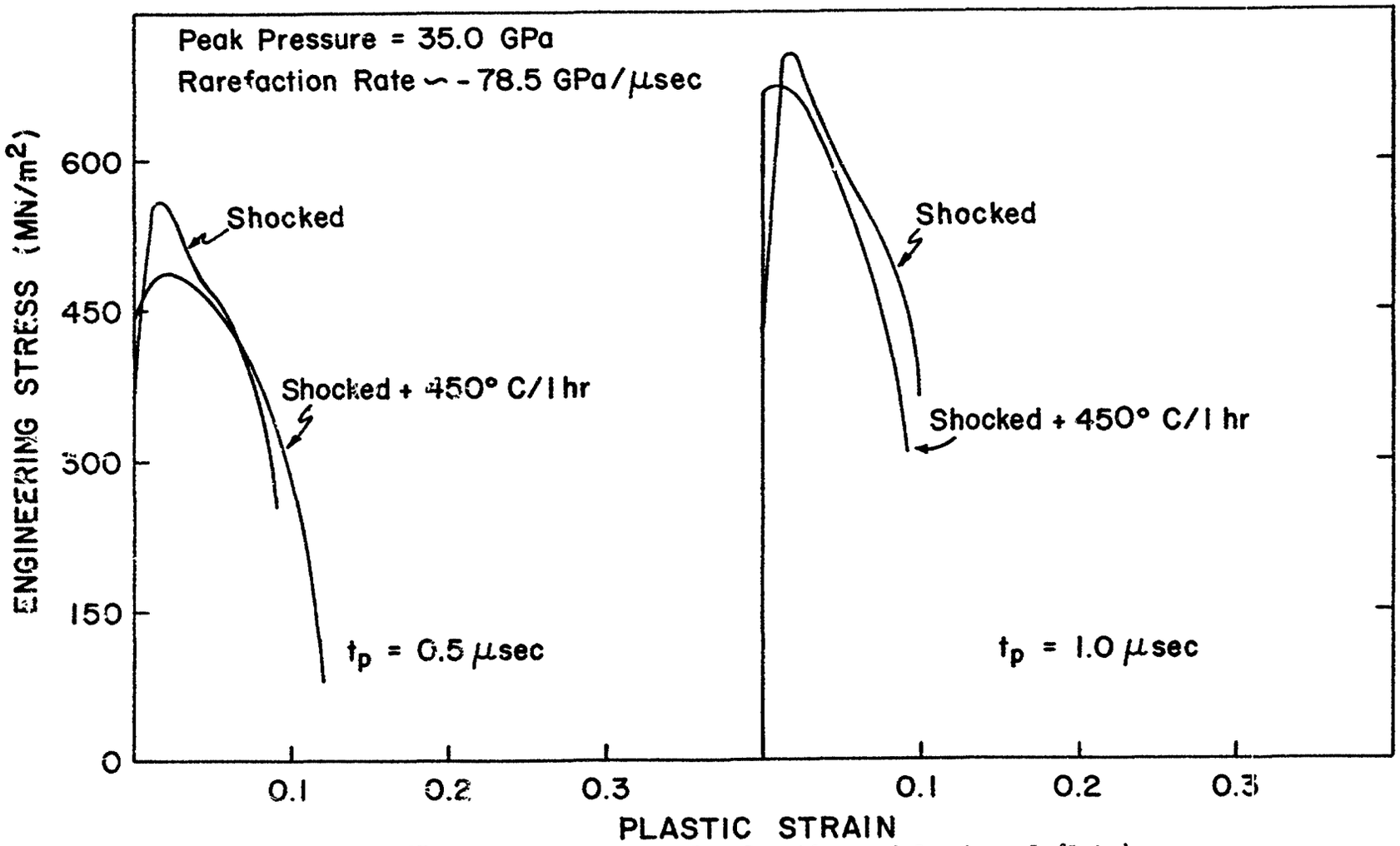

FIGURE 47. The Effects of Pulse Duration and Isochronal (1 hr) Annealing Temperature on the Tensile Properties of AISI 1008 Steel Shocked at 35 GPa.

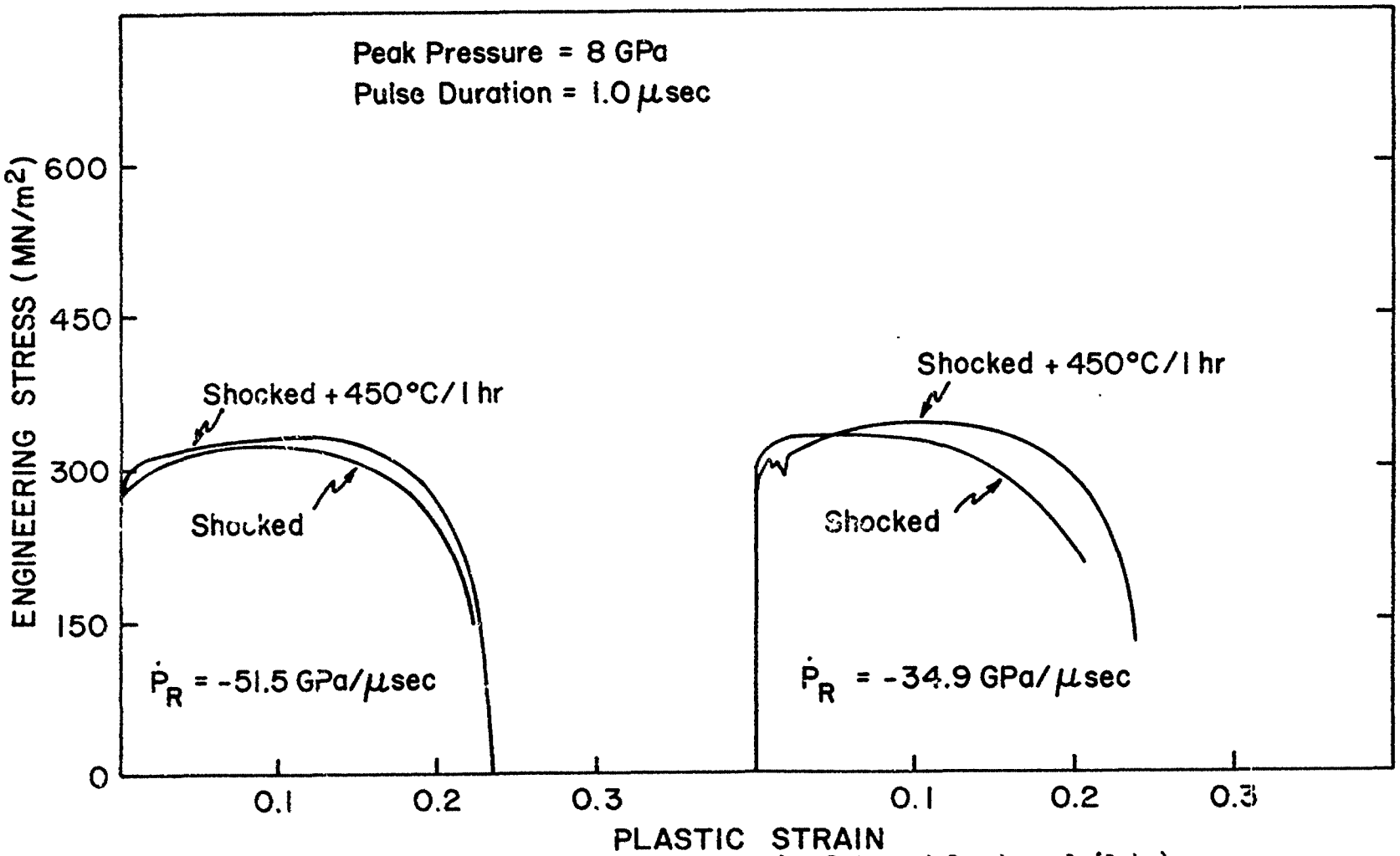

FIGURE 48. The Effects of Rarefaction Rate and Isochronal (1 hr) Annealing Temperature on the Tensile Properties of AISI 1008 Steel Shocked at 8 GPa.

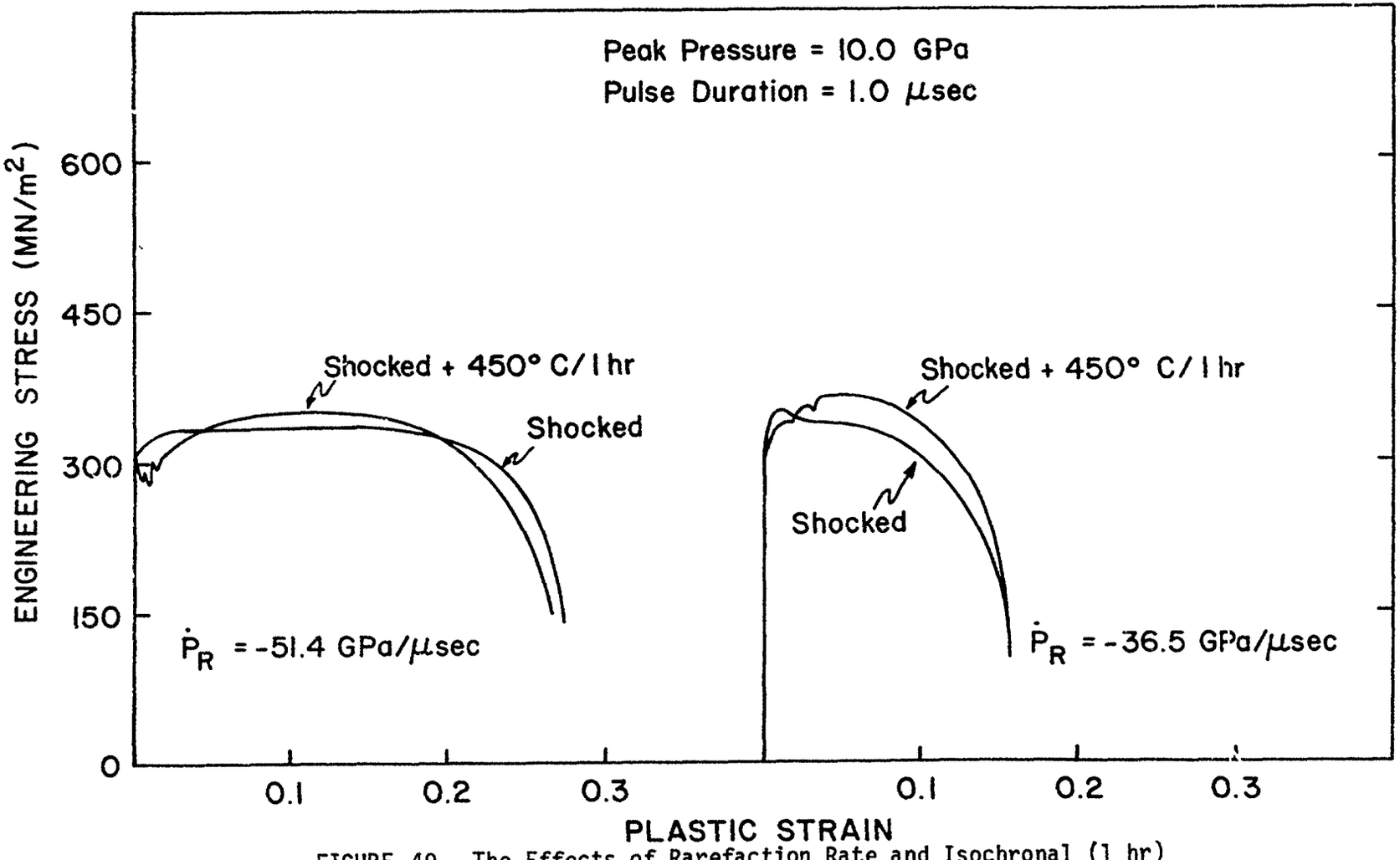

FIGURE 49. The Effects of Rarefaction Rate and Isochronal (1 hr) Annealing Temperature on the Tensile Properties of AISI 1008 Steel Shocked at 10 GPa.

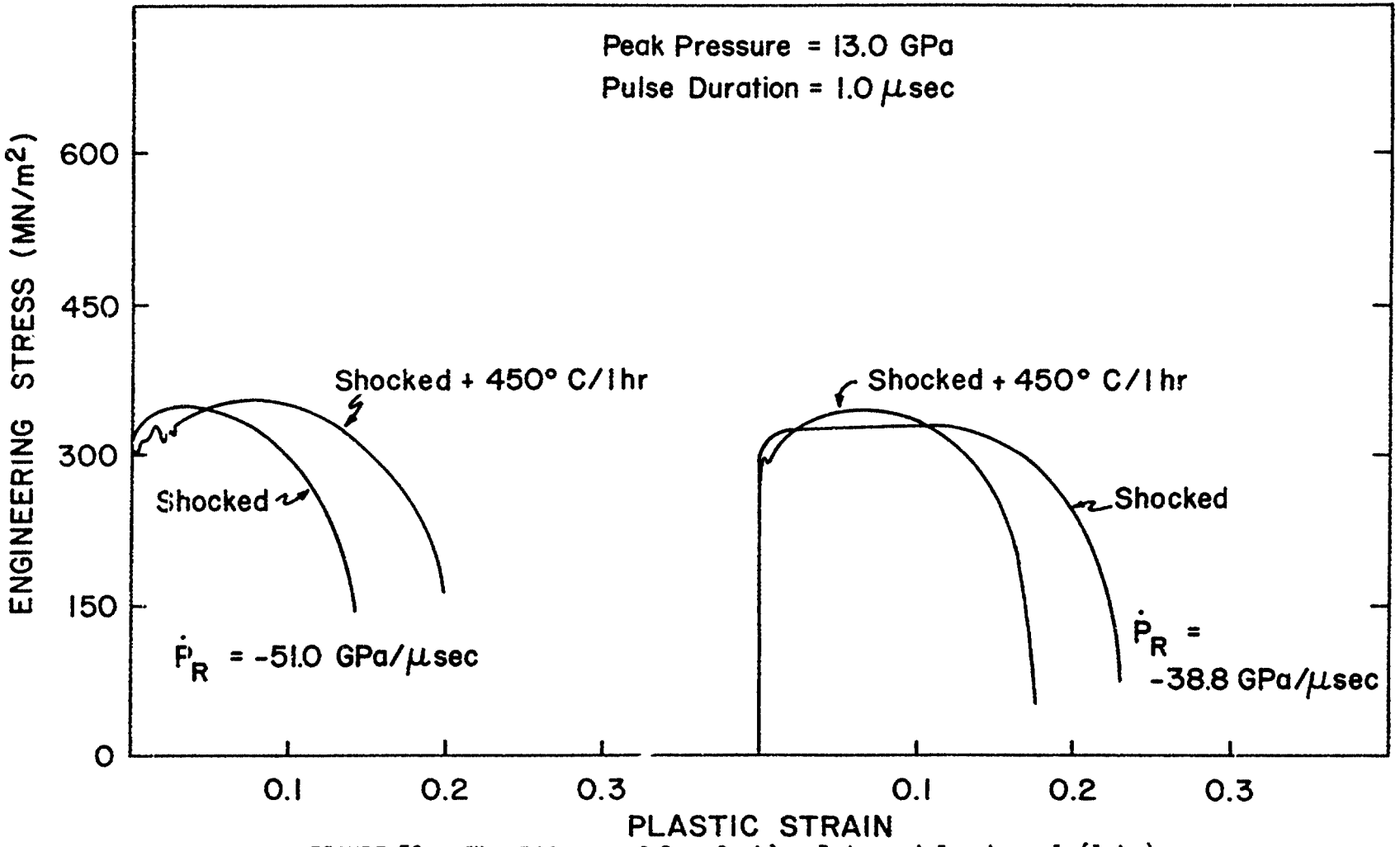

FIGURE 50. The Effects of Rarefaction Rate and Isochronal (1 hr) Annealing Temperature on the Tensile Properties of AISI 1008 Steel Shocked at 13 GPa.

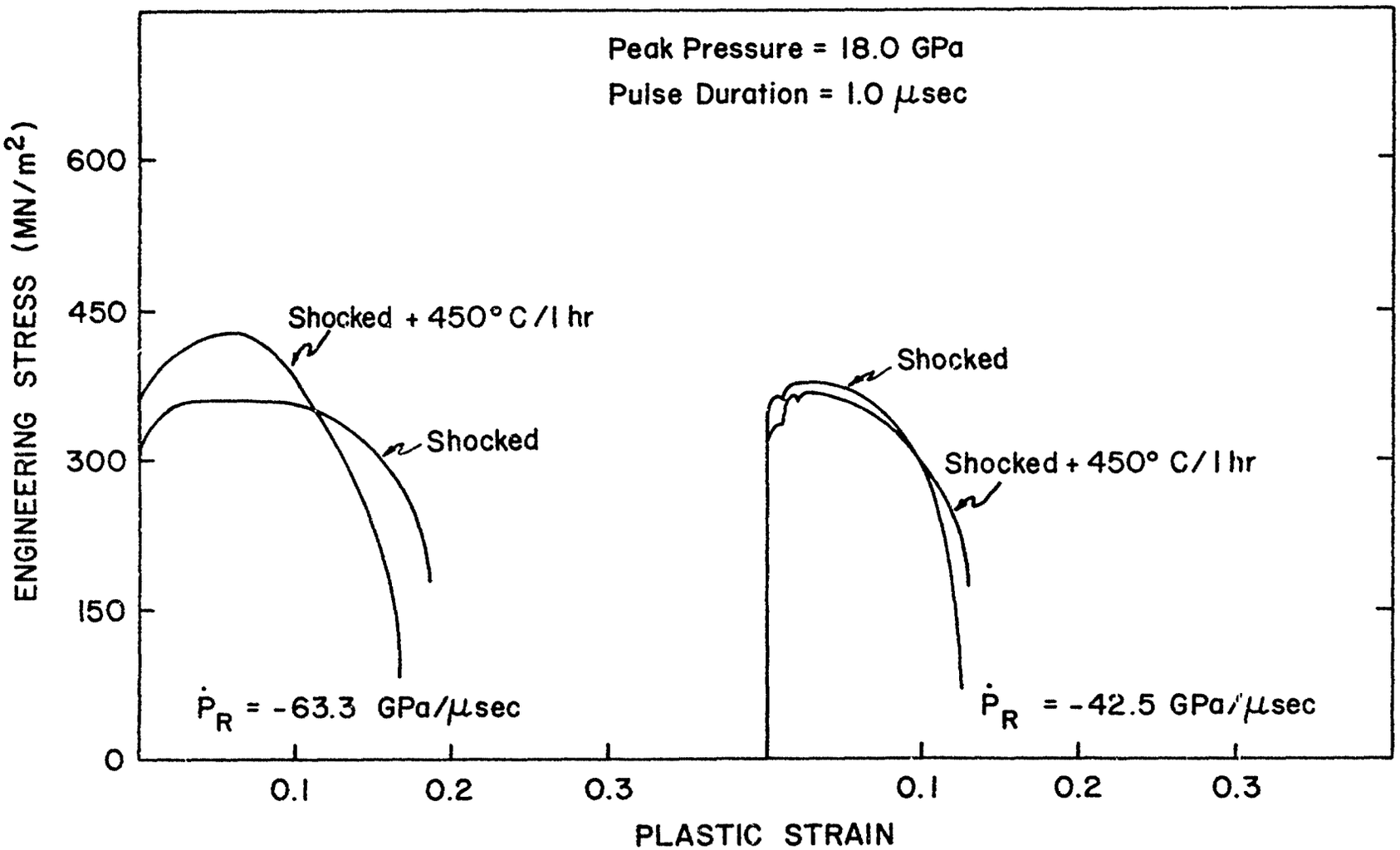

FIGURE 51. The Effects of Rarefaction Rate and Isochronal (1 hr) Annealing Temperature on the Tensile Properties of AISI 1008 Steel Shocked at 18 GPa.

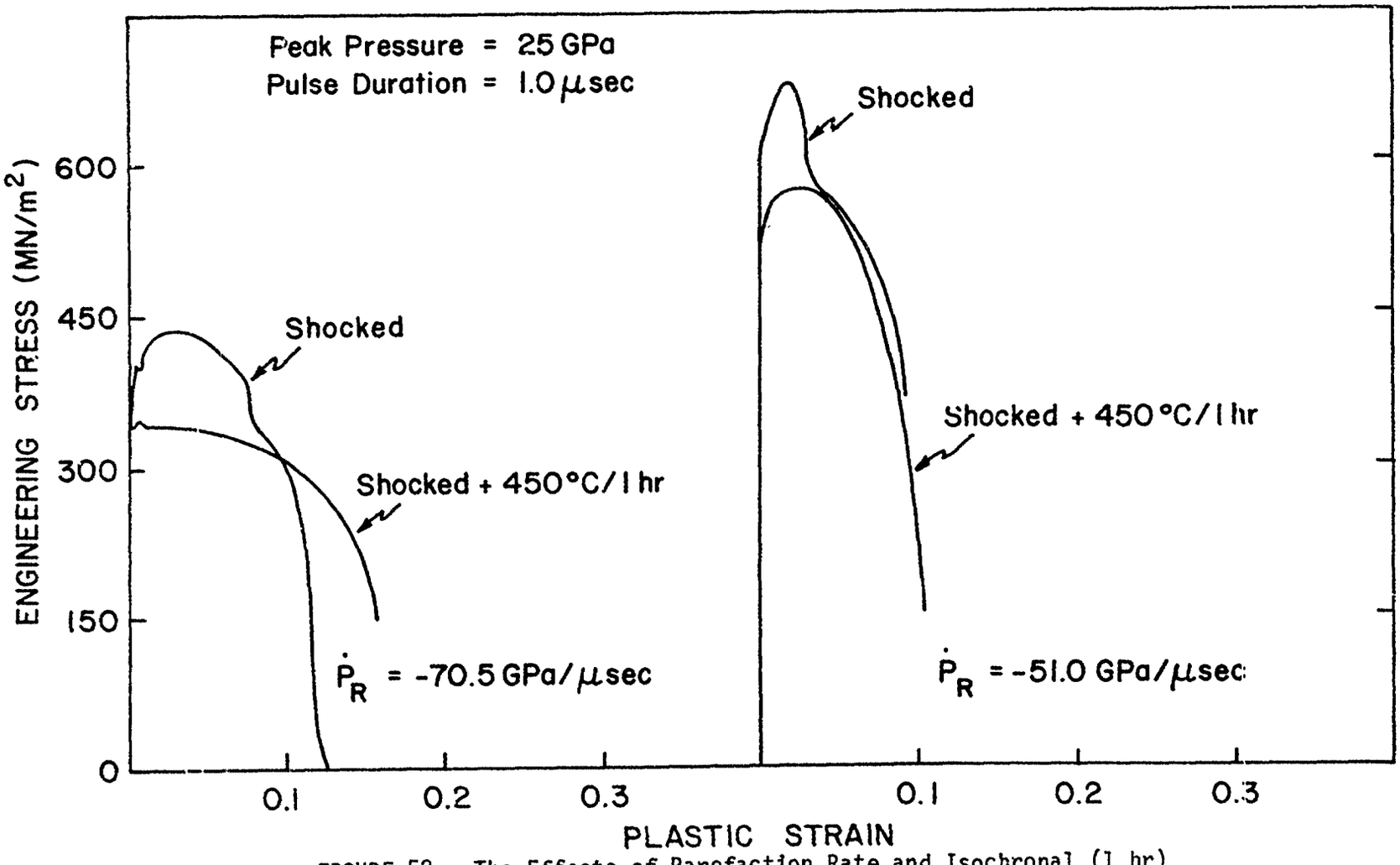

FIGURE 52. The Effects of Rarefaction Rate and Isochronal (1 hr) Annealing Temperature on the Tensile Properties of AISI 1008 Steel Shocked at 25 GPa.

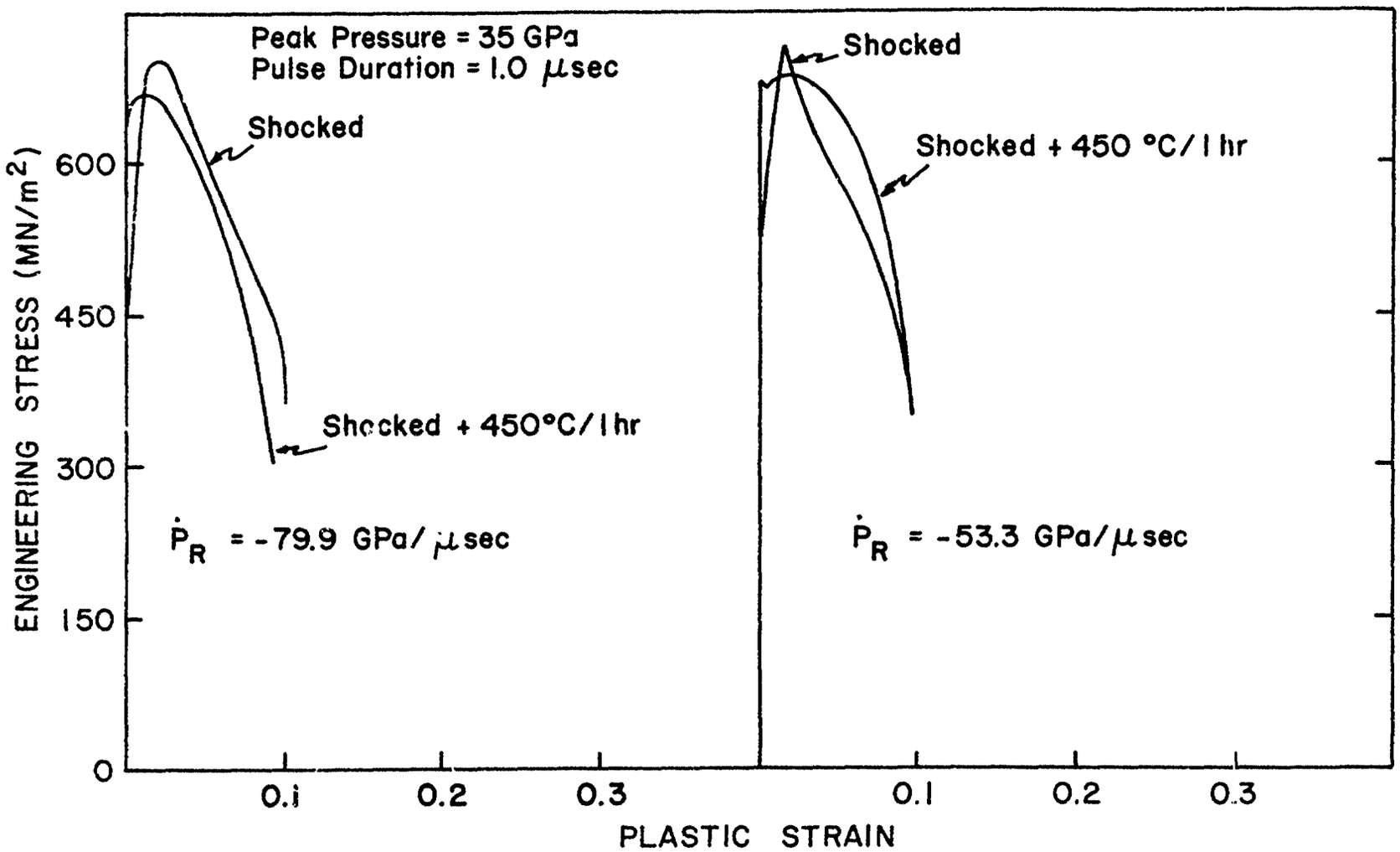

FIGURE 53. The Effects of Rarefaction Rate and Isochronal (1 hr) Annealing Temperature on the Tensile Properties of AISI 1008 Steel Shocked at 35 GPa.

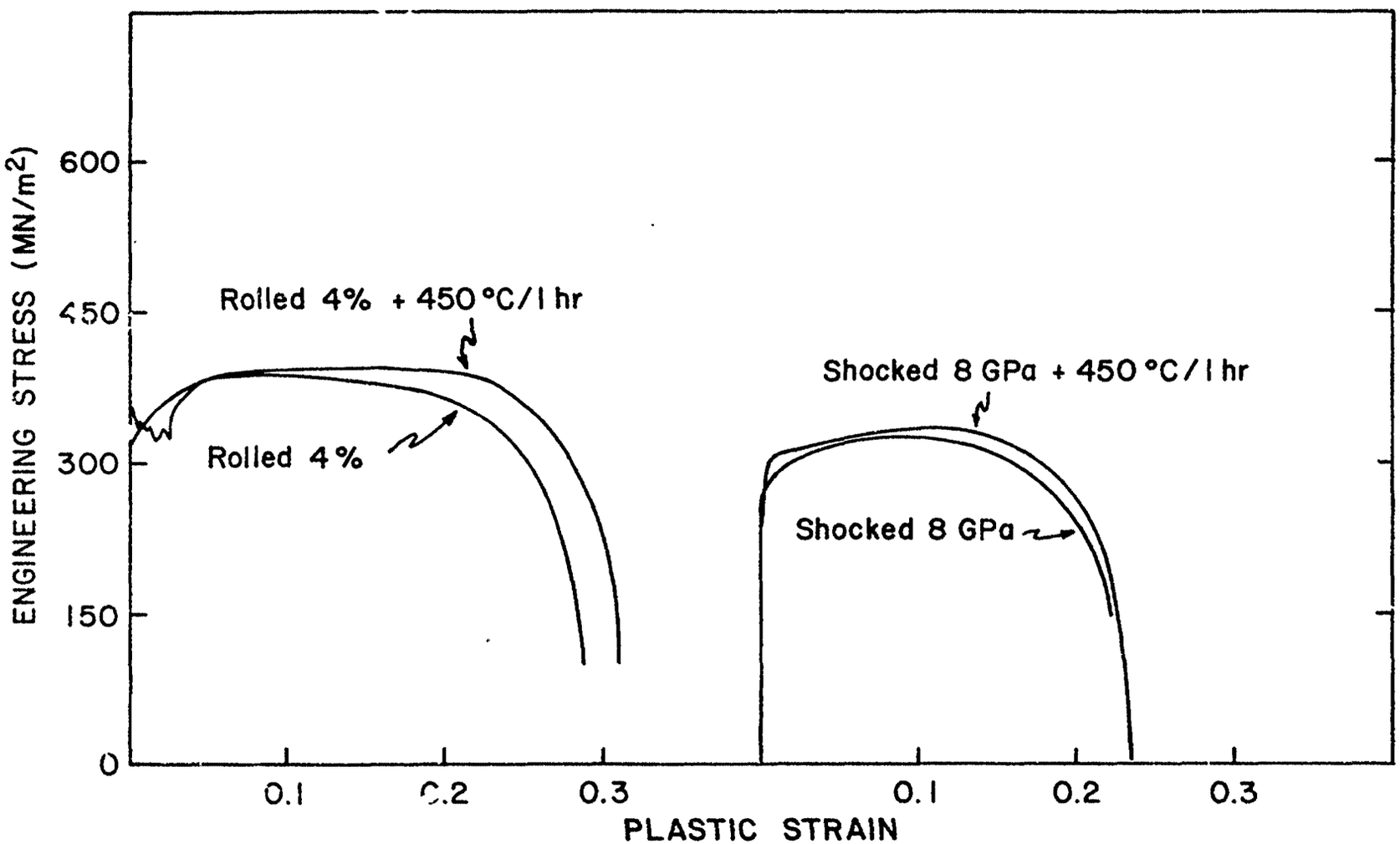

FIGURE 54. The Effects of the Mode of Deformation and Isochronal (1 hr) Annealing Temperature on the Tensile Properties of AISI 1008 Steel Shocked at 8 GPa and Cold-rolled 4%.

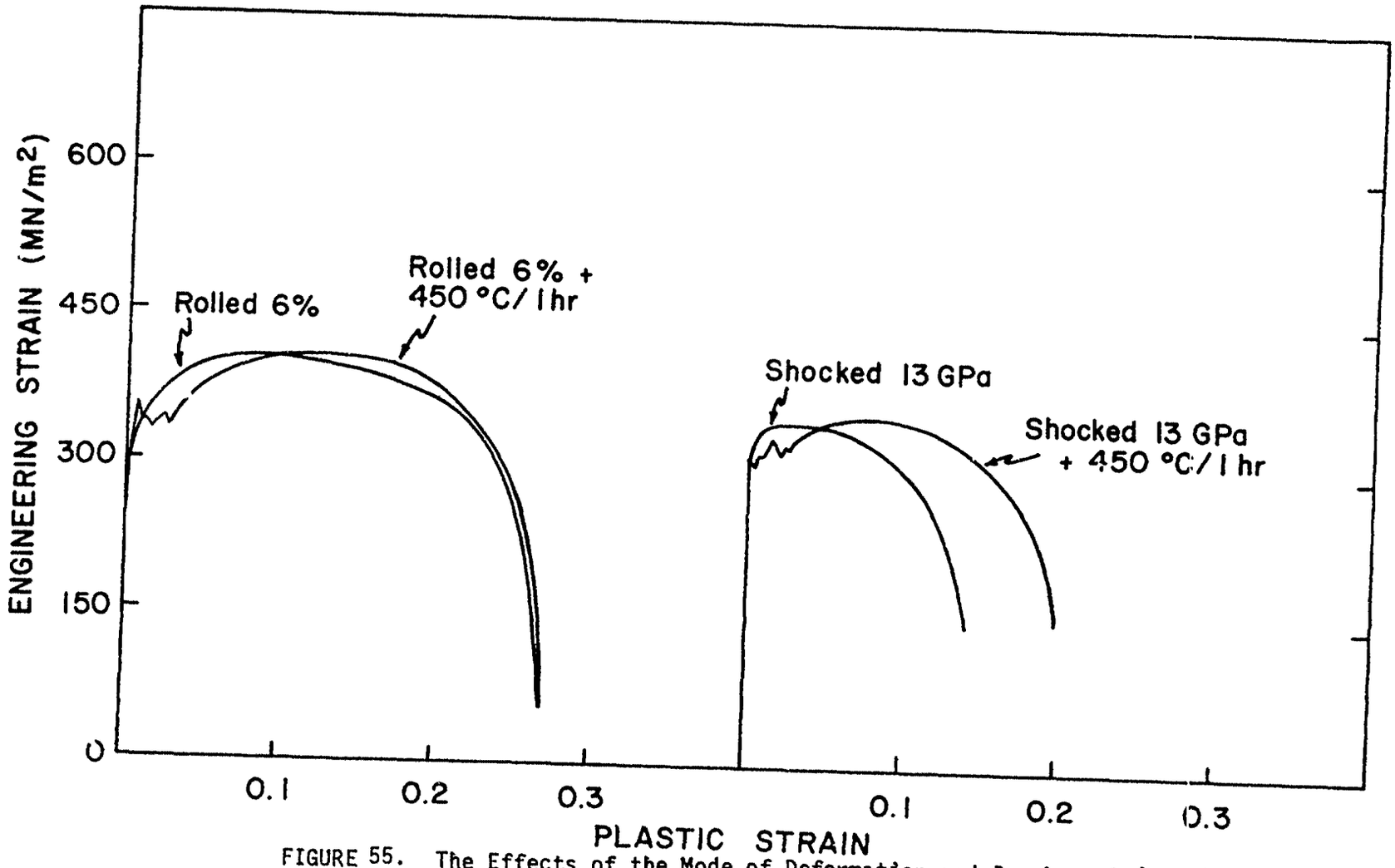

FIGURE 55. The Effects of the Mode of Deformation and Isochronal (1 hr) Annealing Temperature on the Tensile Properties of AISI 1008 Steel Shocked at 13 GPa and Cold-rolled 6%.

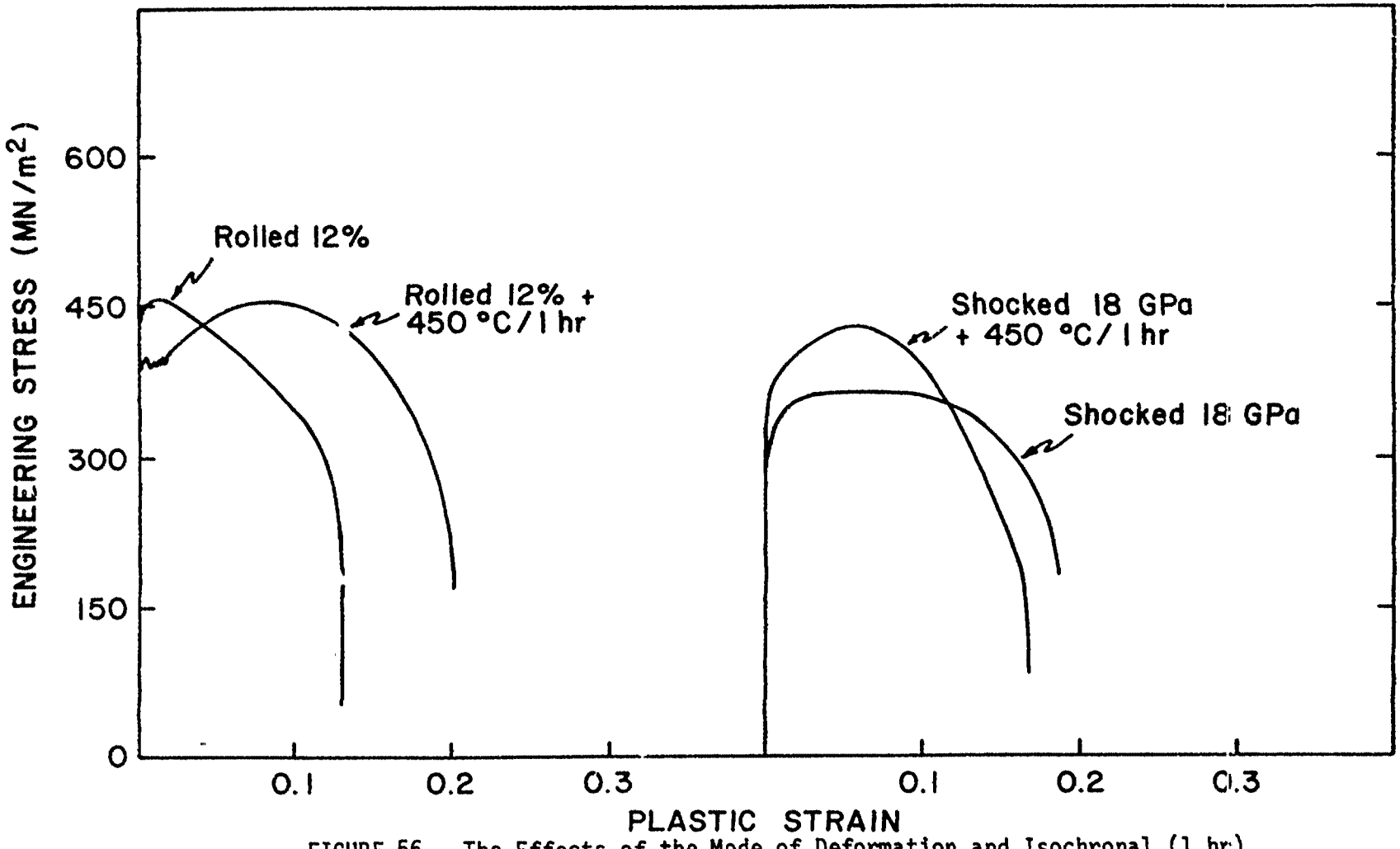

FIGURE 56. The Effects of the Mode of Deformation and Isochronal (1 hr) Annealing Temperature on the Tensile Properties of AISI 1008 Steel Shocked at 18 GPa and Cold-rolled 12%.

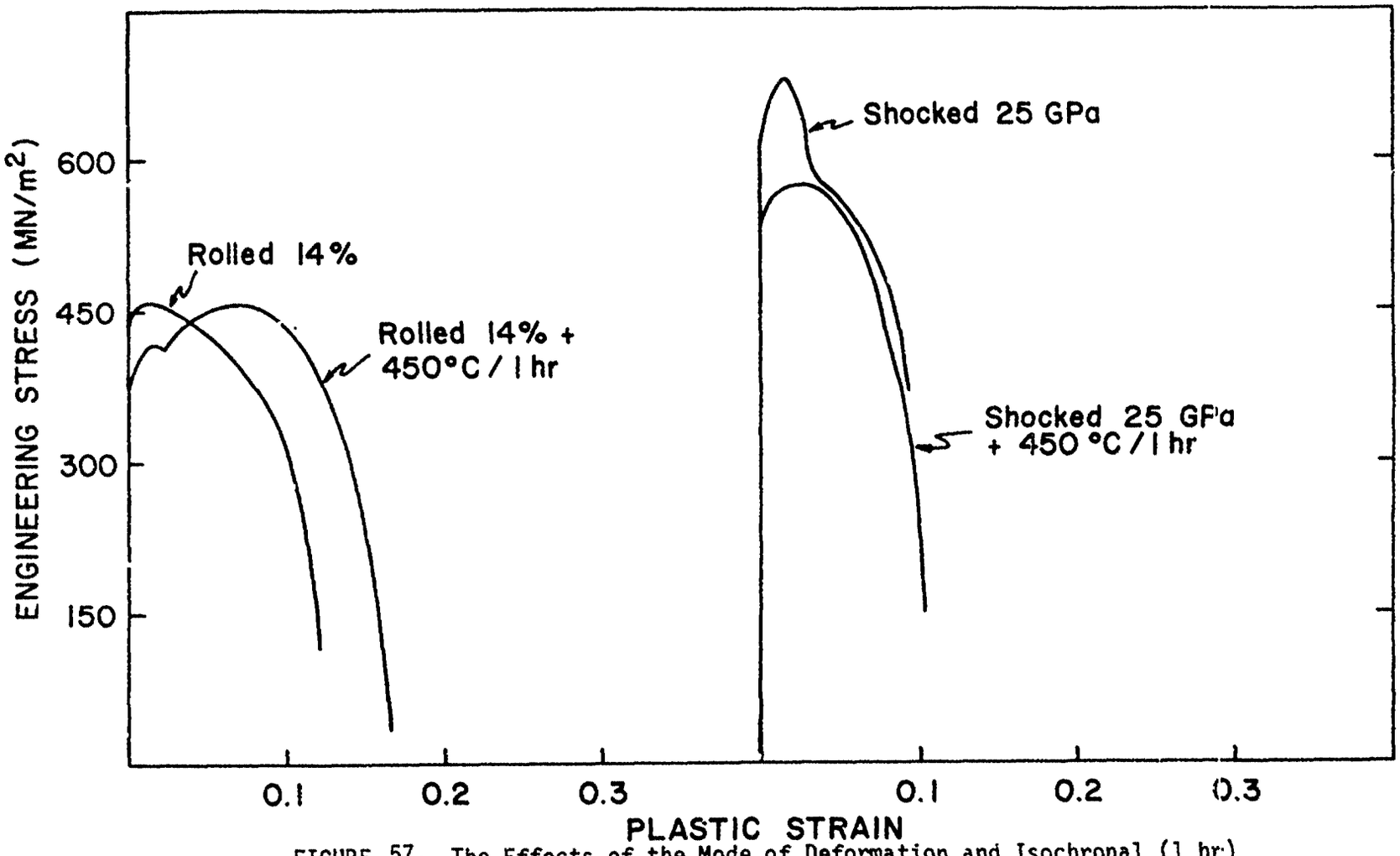

FIGURE 57. The Effects of the Mode of Deformation and Isochronal (1 hr) Annealing Temperature on the Tensile Properties of AISI 1008 Steel Shocked at 25 GPa and Cold-rolled 14%.

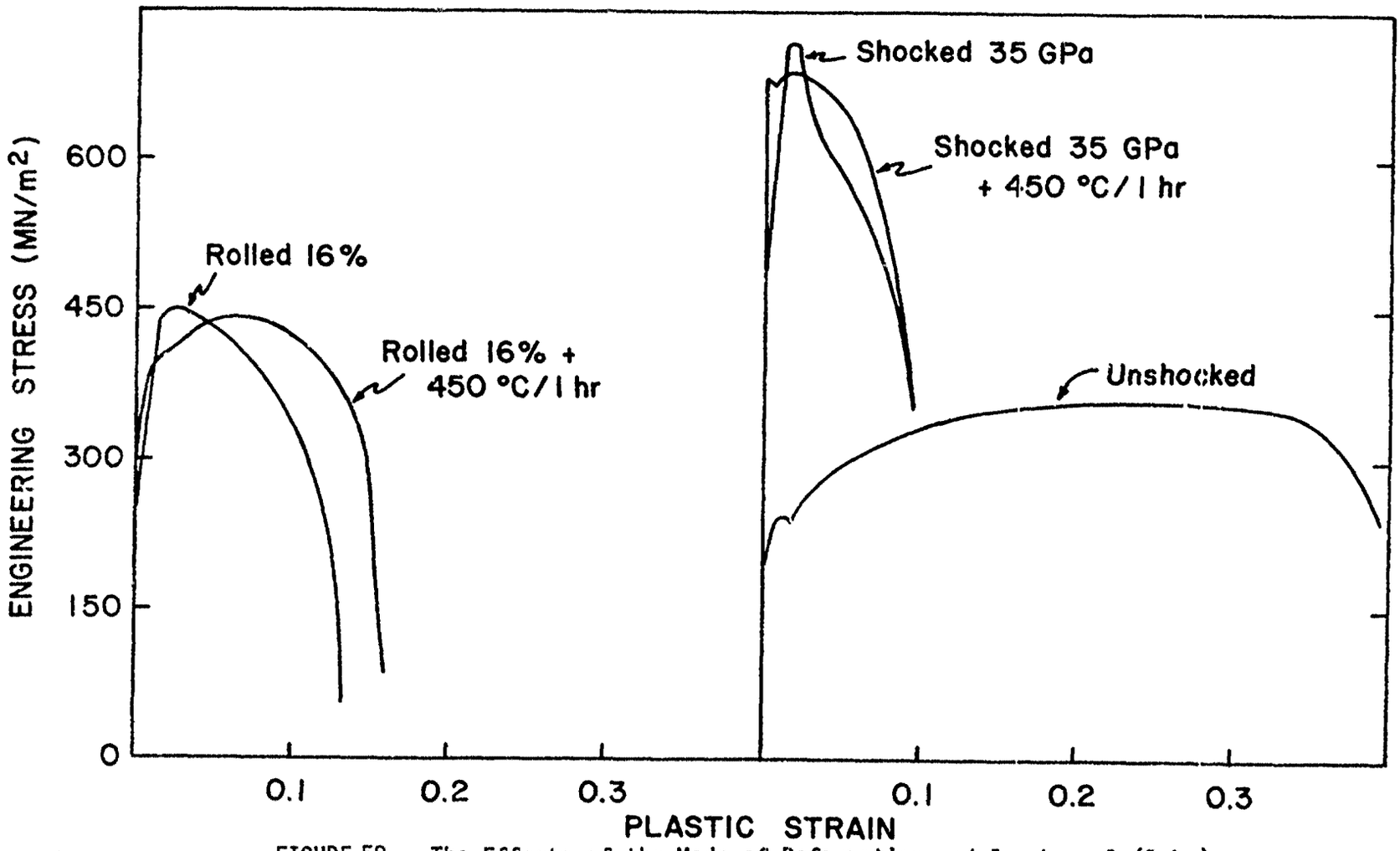

FIGURE 58. The Effects of the Mode of Deformation and Isochronal (1 hr) Annealing Temperature on the Tensile Properties of AISI 1008 Steel Shocked at 35 GPa and Cold-rolled 16%.

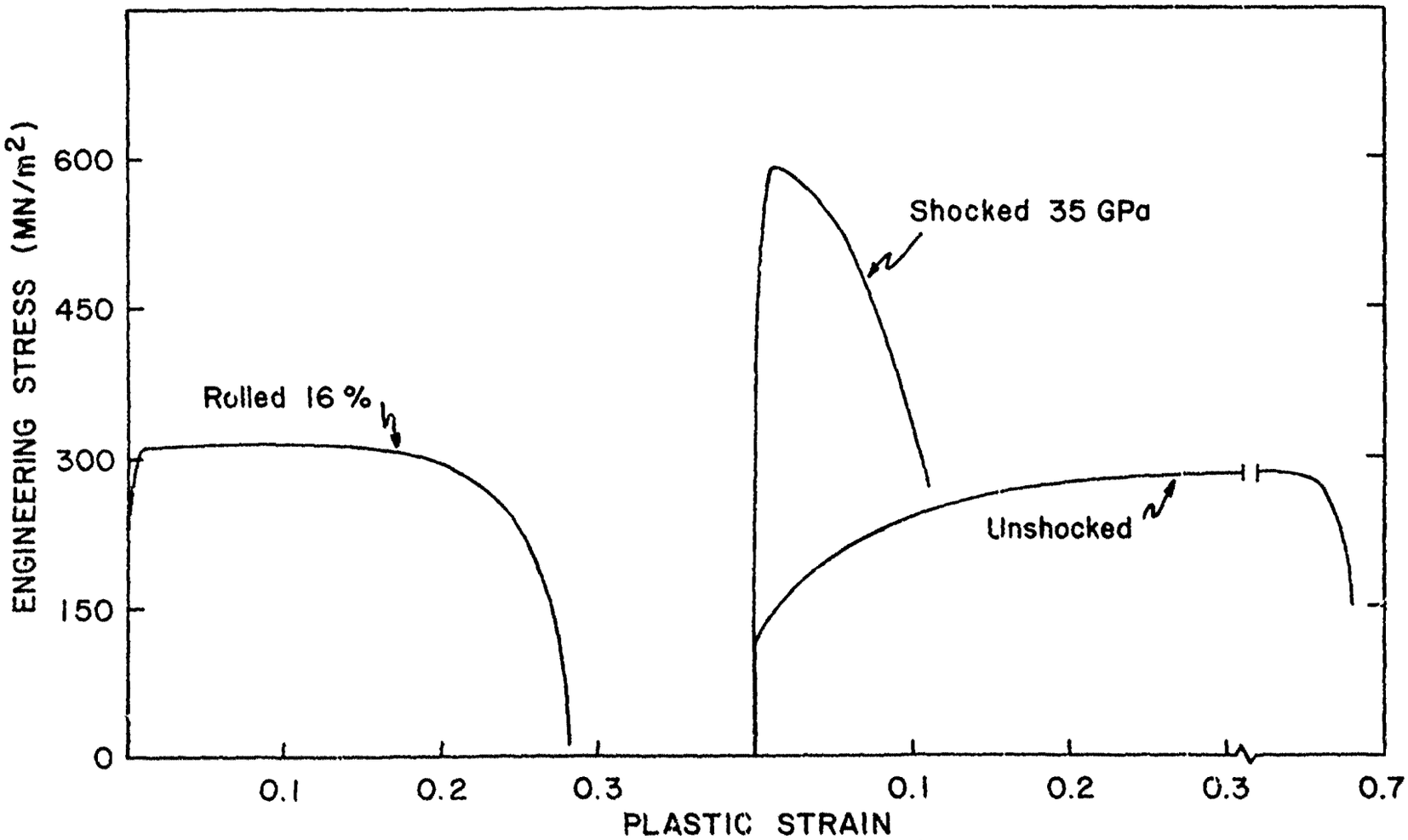

FIGURE 59. The Effects of the Mode of Deformation on the Tensile Properties of ARMCO Ingot Iron Shocked at 35 GPa and Cold-rolled 16%.

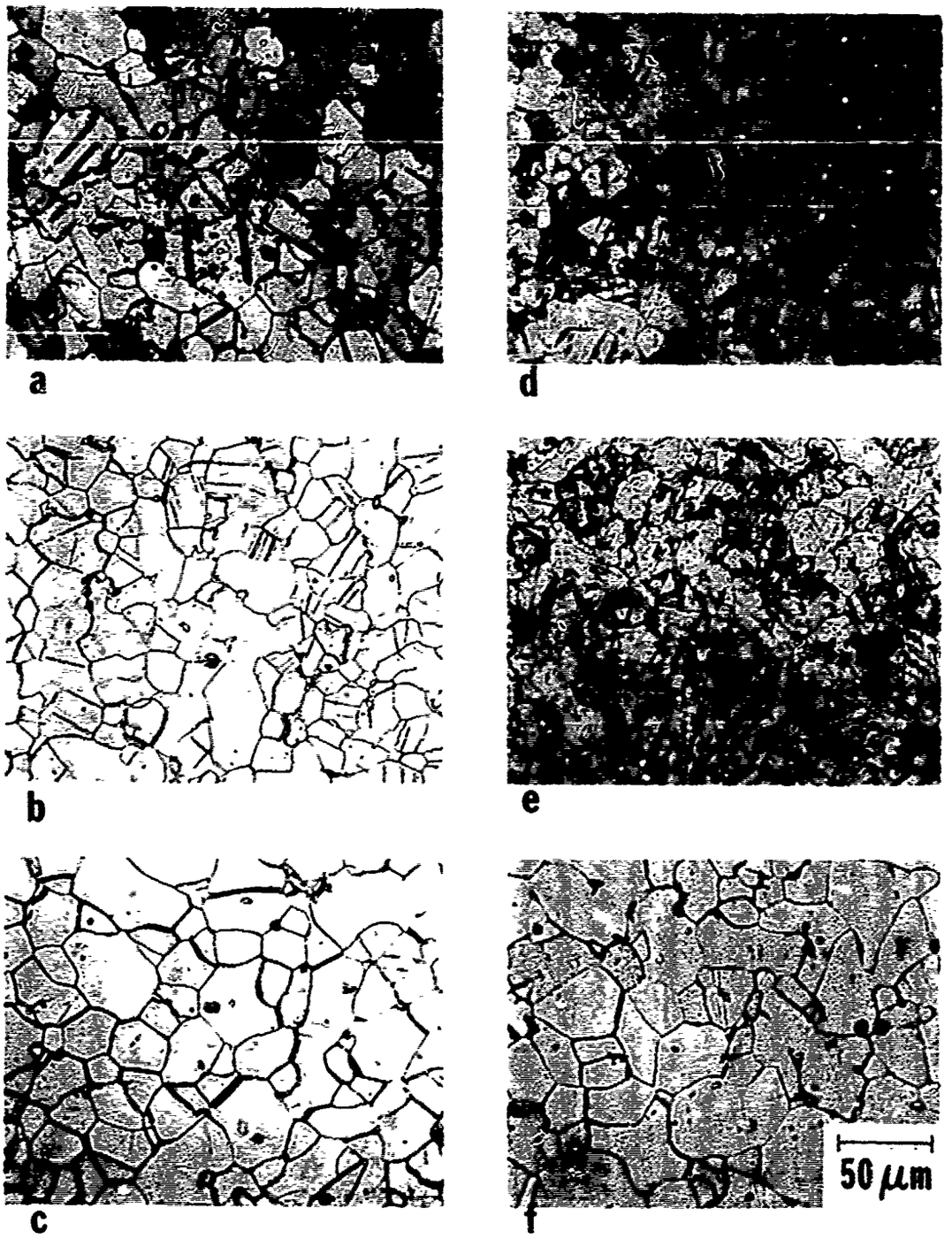

FIGURE 60. Microstructure of AISI 1008 Steel shocked at 1.0 μsec duration and ≈-51.5 GPa. sec rarefaction rate: (a) 13 GPa; (b) same as (a) plus 450°C/1hr; (c) same as (a) plus 600°C/1hr; (d) 25 GPa; (e) same as (d) plus 450°C/1hr; (f) same as (d) plus 600°C/1hr.

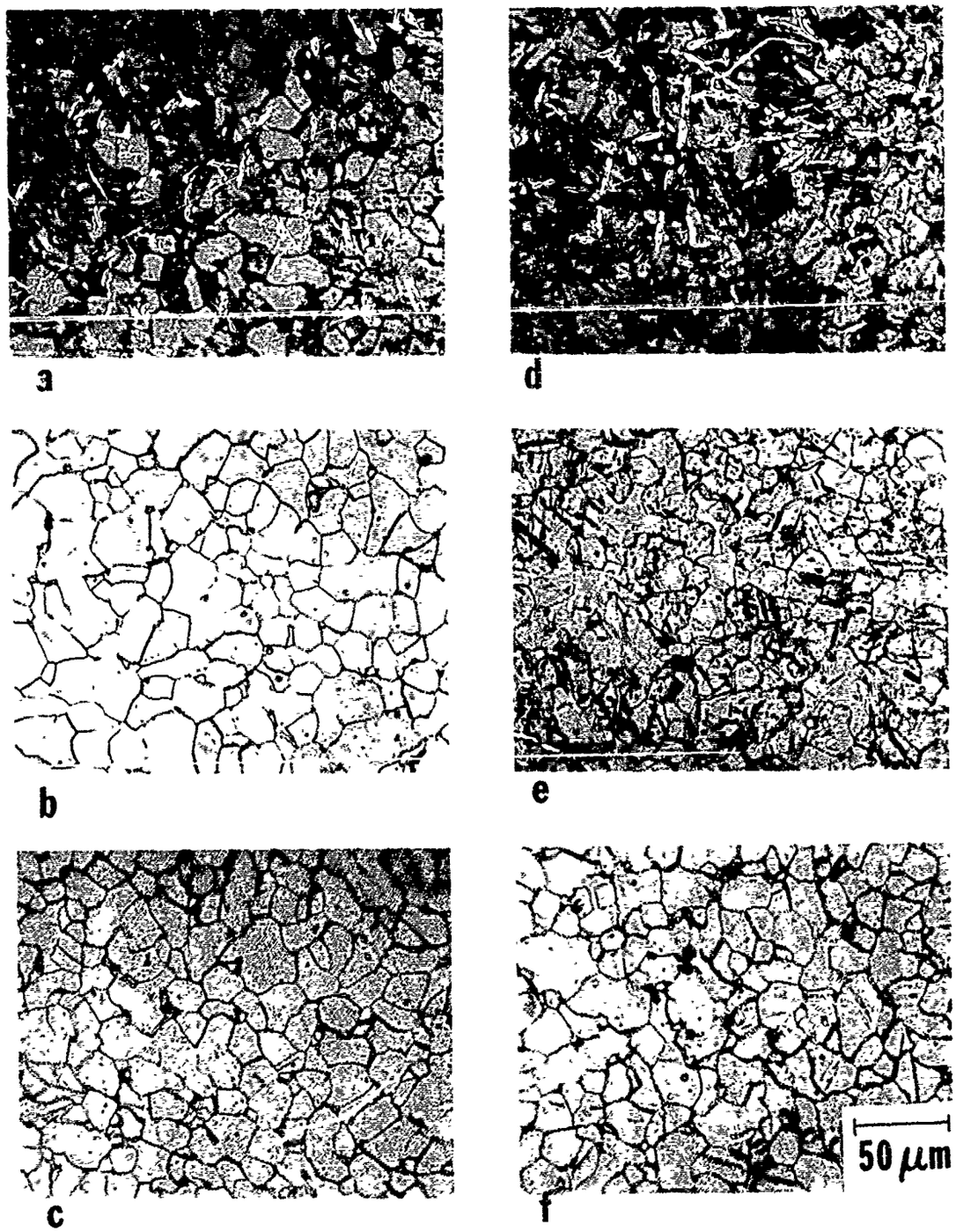

FIGURE 61. Microstructure of AISI 1008 Steel shocked at 18 GPa pressure and ≈63.5 GPa/μsec rarefaction rate: (a) 0.5 μsec duration; (b) same as (a) plus 450°C/1hr; (c) same as (a) plus 600°C/1hr; (d) 1.0 μsec duration; (e) same as (d) plus 450°C/1hr; (f) same as (d) plus 600°C/1hr.

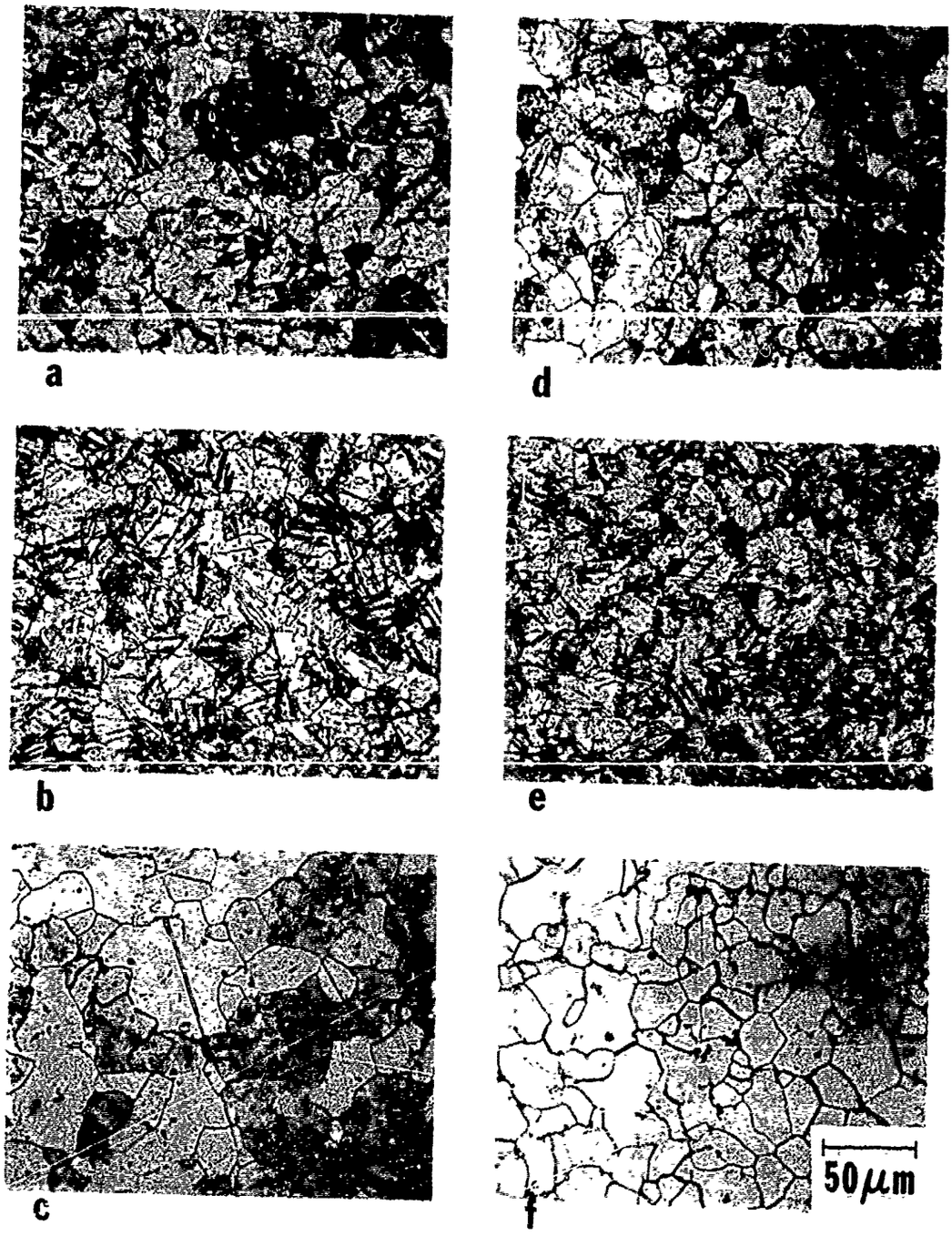

FIGURE 62. Microstructure of AISI 1008 Steel shocked at 35 GPa pressure and 1.0 μsec duration; (a) -79.9 GPa/μsec rarefaction rate; (b) same as (a) plus 450°C/1hr; (c) same as (a) plus 600°C/1hr; (d) -53.3 GPa/μsec rarefaction rate; (e) same as (d) plus 450°C/1hr; (f) same as (d) plus 600°C/1hr.

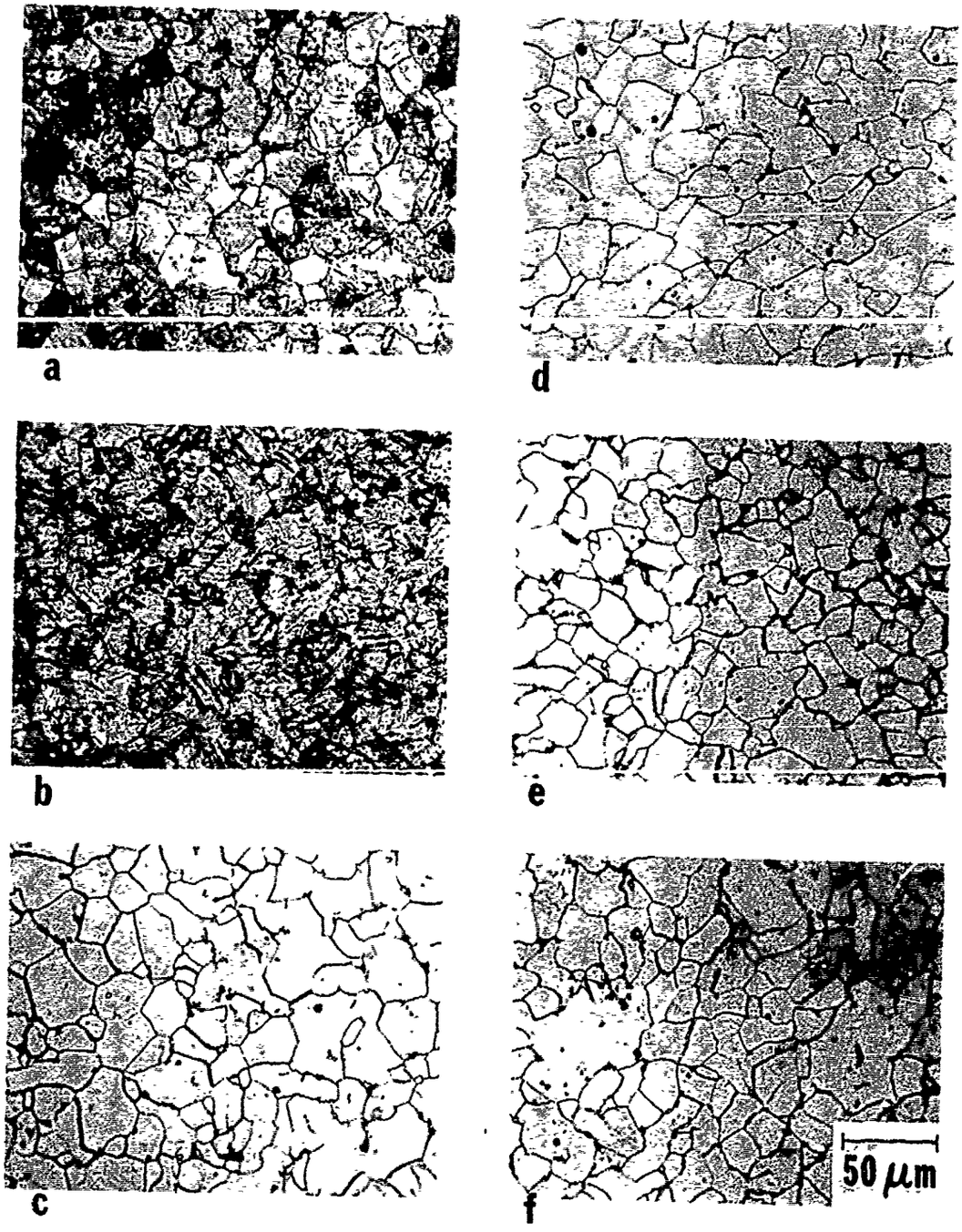

FIGURE 63. Microstructure of AISI 1008 steel: (a) shocked at 35 GPa pressure; 1.0 μsec duration and -53.3 GPa/μsec rarefaction rate; (b) same as (a) plus 450°C/1hr; (c) same as (a) plus 600°C/1hr; (d) cold-rolled 16%; (e) same as (d) plus 450°C/1hr; (f) same as (d) plus 600°C/1hr.

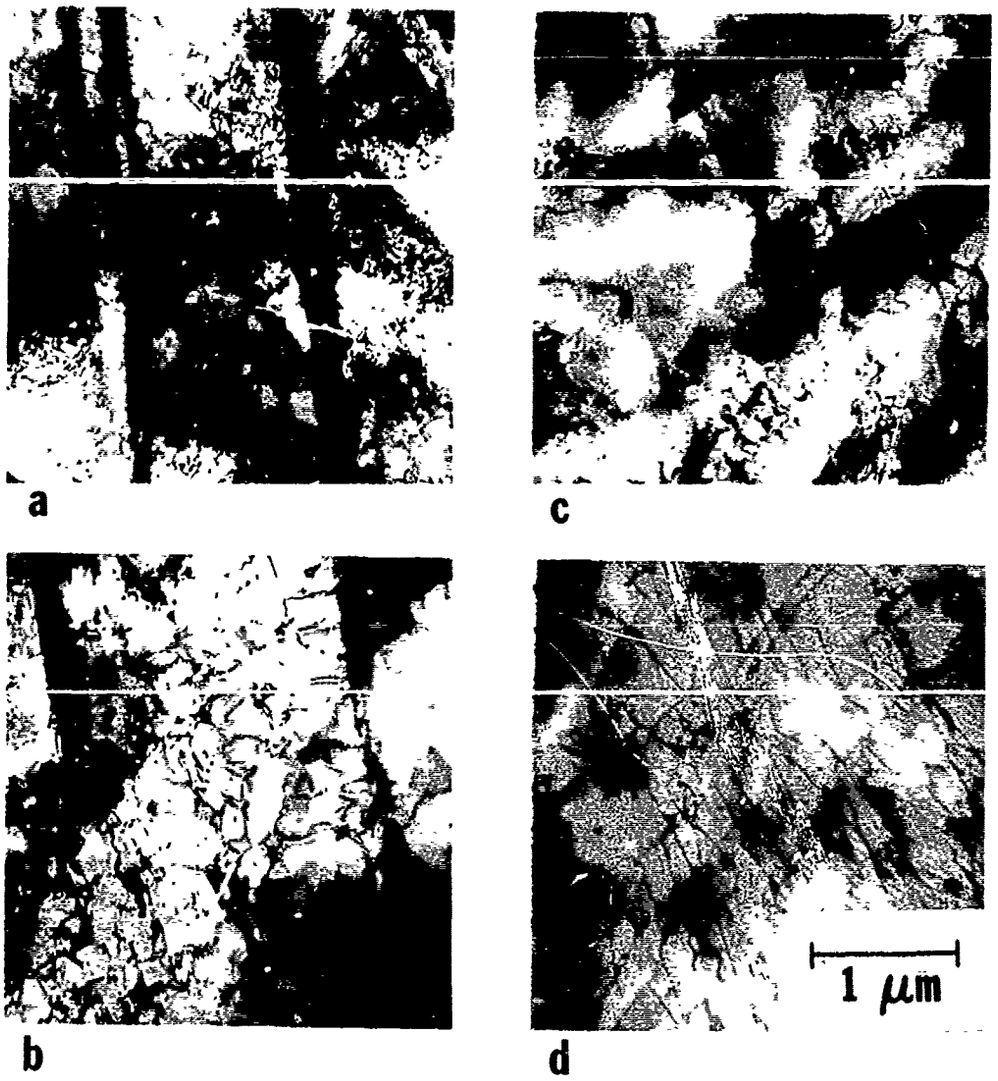

FIGURE 64. Substructure of AISI 1008 Steel shocked at 1.0 μsec duration and ≈-51.5 GPa/μsec rarefaction rate: (a) 10 GPa pressure; (b) same as (a) plus 450°C/1hr; (c) 13 GPa pressure; (d) same as (c) plus 450°C/1hr.

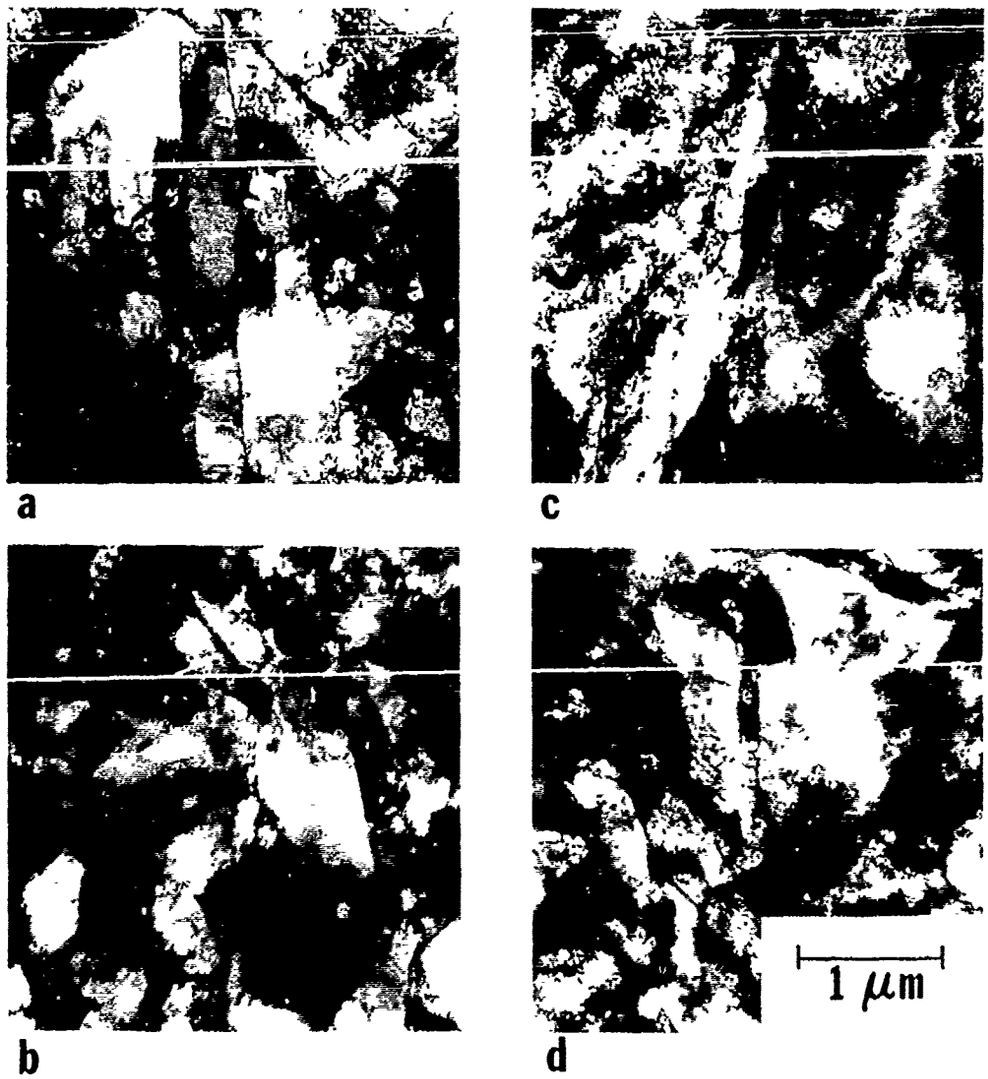

FIGURE 65. Substructure of AISI 1008 Steel shocked at 1.0 μsec duration and ≈-51.5 GPa/μsec rarefaction rate: (a) 25 GPa pressure; (b) same as (a) plus 450°C/1hr; (c) 35 GPa pressure; (d) same as (c) plus 450°C/1hr.

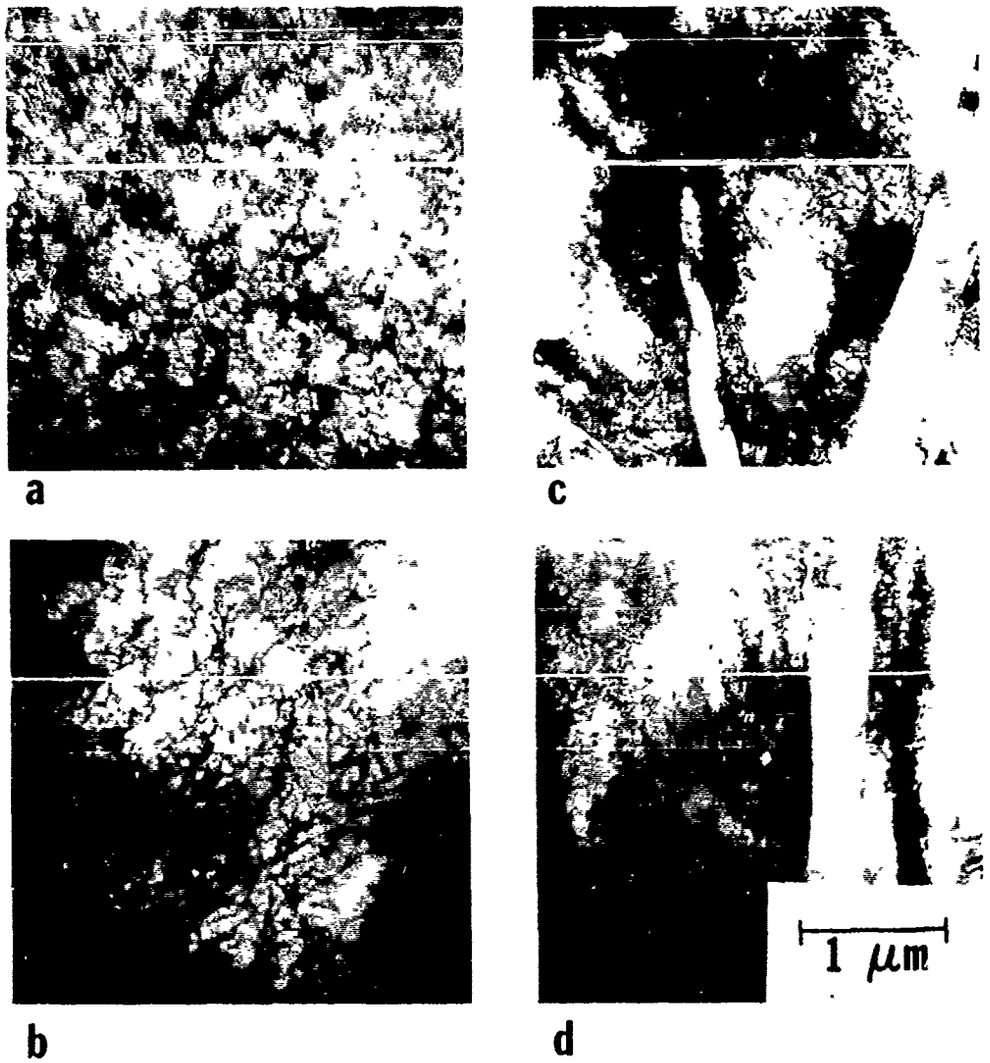

FIGURE 66. Substructure of AISI 1008 Steel shocked at 18 GPa pressure and ≈-63.5 GPa/μsec rarefaction rate; (a) 0.5 μsec duration; (b) same as (a) plus 450°C/1hr; (c) 1.0 μsec duration; (d) same as (c) plus 450°C/1hr.

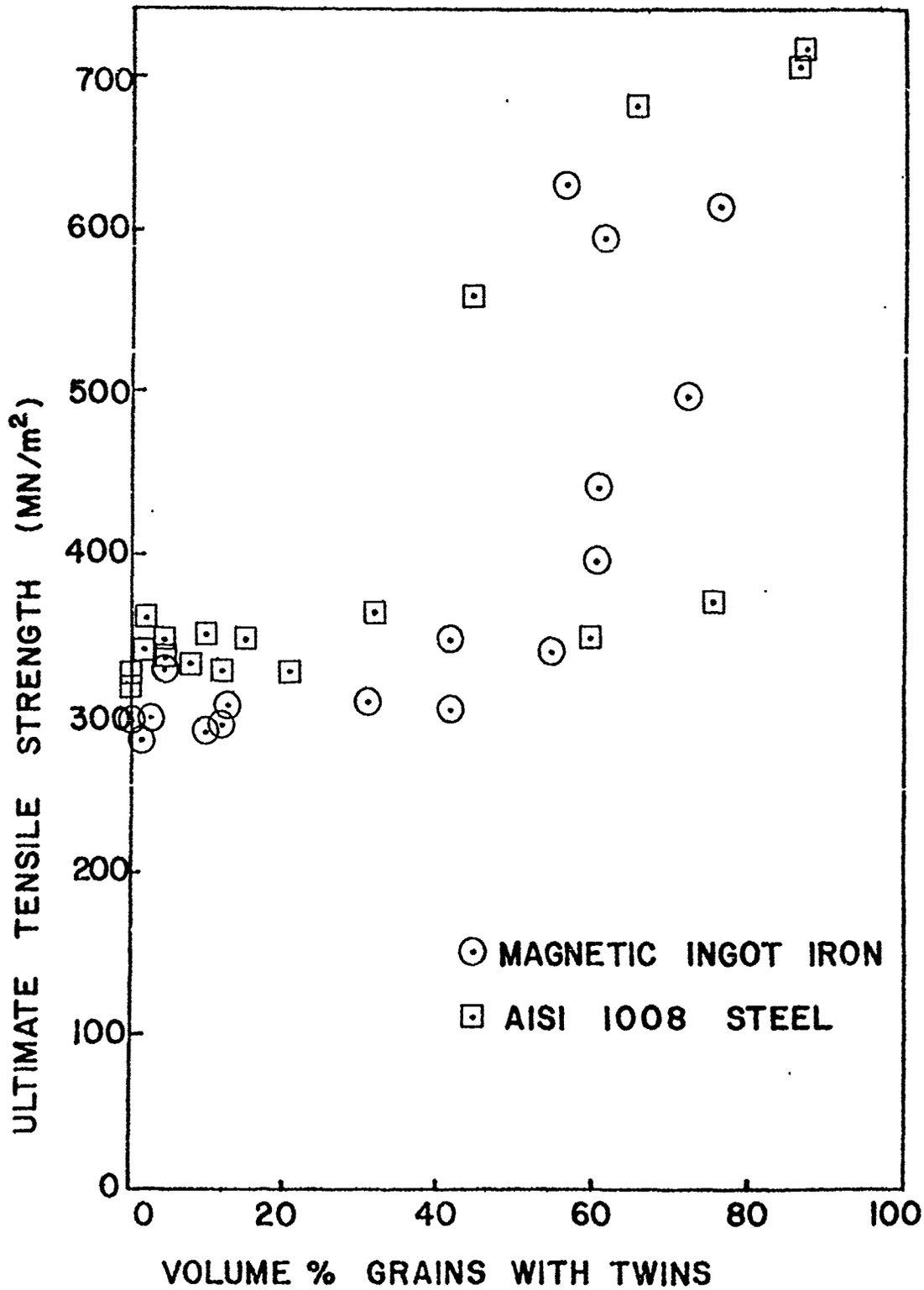

FIGURE 67. Volume Percent of Grains with Twins Versus Ultimate Tensile Strength.

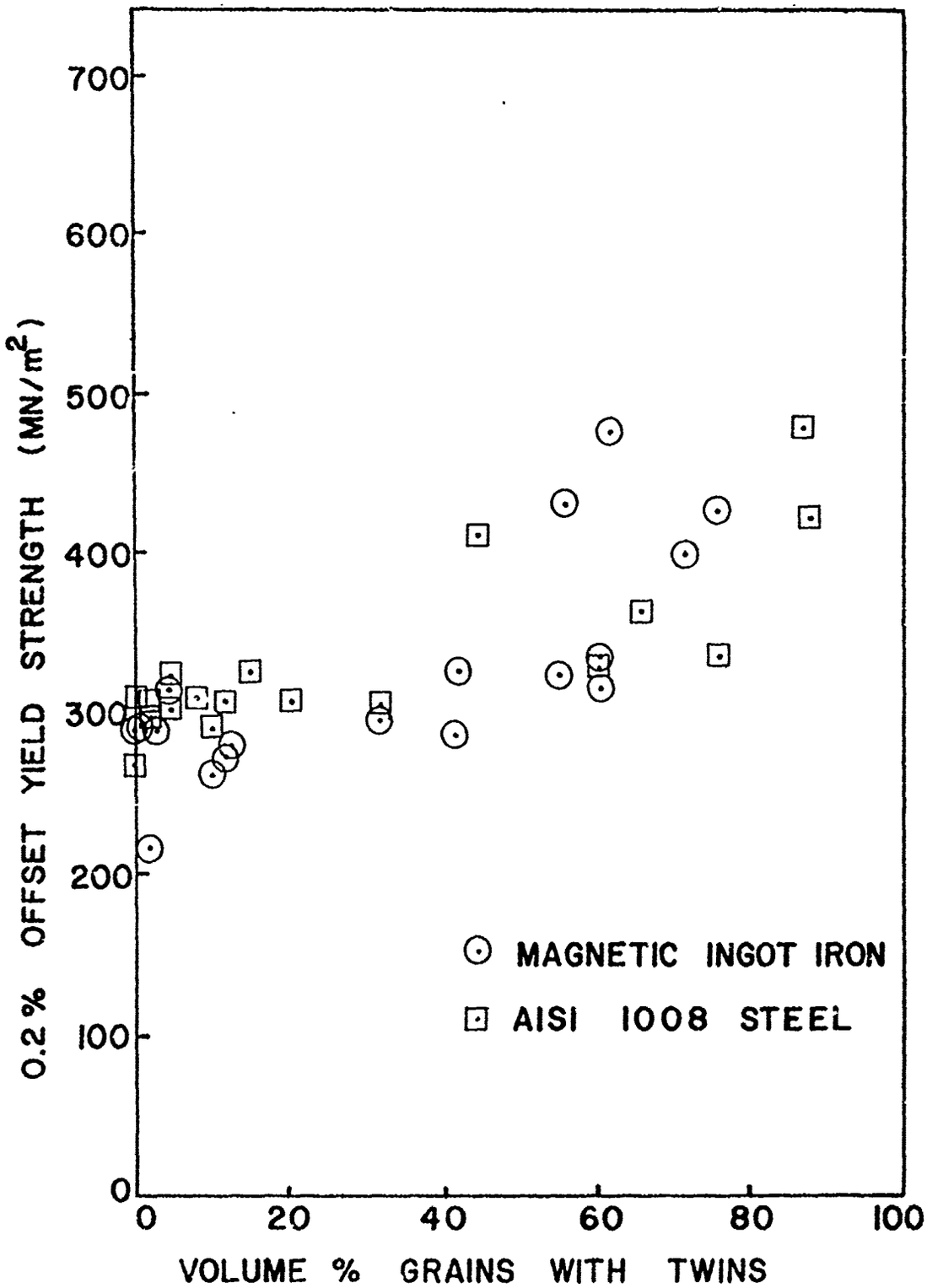

FIGURE 68. Volume Percent of Grains with Twins Versus 0.2% Offset Yield Strength.

Unclassified

SECURITY CLASSIFICATION OF THIS PAGE (When Data Entered)

REPORT DOCUMENTATION PAGE		READ INSTRUCTIONS BEFORE COMPLETING FORM
1. REPORT NUMBER ~~SMT-1-78~~	2. GOVT ACCESSION NO.	3. RECIPIENT'S CATALOG NUMBER
4. TITLE (and Subtitle) AN INVESTIGATION OF THE INFLUENCE OF SHOCK-WAVE PROFILE ON THE MECHANICAL AND THERMAL RESPONSES OF POLYCRYSTALLINE IRON		5. TYPE OF REPORT & PERIOD COVERED Final Technical Report 5 April 1976- 16 July 1978 6. PERFORMING ORG. REPORT NUMBER 2339
7. AUTHOR(s) G. A. Stone, R. N. Orava, G. T. Gray, A. R. Pelton		8. CONTRACT OR GRANT NUMBER(s) Grant DAAG29-76-G-0181
9. PERFORMING ORGANIZATION NAME AND ADDRESS Department of Metallurgical Engineering South Dakota School of Mines and Technology Rapid City, South Dakota 57701		10. PROGRAM ELEMENT, PROJECT, TASK AREA & WORK UNIT NUMBERS
11. CONTROLLING OFFICE NAME AND ADDRESS U. S. Army Research Office P. O. Box 12211 Research Triangle Park, NC 27709		12. REPORT DATE September 30, 1978 13. NUMBER OF PAGES 138
14. MONITORING AGENCY NAME & ADDRESS (if different from Controlling Office)		15. SECURITY CLASS. (of this report) 15a. DECLASSIFICATION/DOWNGRADING SCHEDULE N/A

16. DISTRIBUTION STATEMENT (of this Report)

Approved for public release; distribution unlimited.

17. DISTRIBUTION STATEMENT (of the abstract entered in Block 20, if different from Report)

18. SUPPLEMENTARY NOTES

The view, opinions, and/or findings contained in this report are those of the author(s) and should not be construed as an official Department of the Army position, policy, or decision, unless so designated by other documentation.

19. KEY WORDS (Continue on reverse side if necessary and identify by block number)

shock hardening; magnetic ingot iron; AISI 1008 steel, shock-wave profile; shock-pressure duration; shock rarefaction rate; strain aging; thermal recovery.

20. ABSTRACT (Continue on reverse side if necessary and identify by block number)

An investigation was conducted to determine the relative influence of shock-wave parameters on the strengthening of Magnetic Ingot Iron and AISI 1008 Steel. The independently-varied shock-wave parameters include peak pressure, peak pressure duration, and rarefaction rate. Eighteen shock-loading conditions were studied with peak pressures of 8, 10, 13, 18, 25 and 35 GPa. As peak pressure was increased, an increase of the 0.2% offset yield stress, hardness, twin density and the degree of room temperature

DD FORM 1 JAN 73 1473 EDITION OF 1 NOV 65 IS OBSOLETE

Unclassified

SECURITY CLASSIFICATION OF THIS PAGE (When Data Entered)

strain aging was observed. An increase of pulse duration caused an increase of twin volume fraction, yield strength, and strain aging. Rarefaction rate was found to produce no systematic changes in structure or properties.

A recovery study on the shock-hardened material was conducted and compared to samples which were cold-reduced to equivalent maximum shear strain. Isochronal (1 hr) anneals were conducted in the temperature range from 25 to 650°C. Recovery was monitored by hardness measurements, tensile tests, and optical and transmission electron microscopy. Annealing response is most influenced by peak pressure variations; however, increasing pulse duration can also effectively modify the recovery. Rarefaction rate shows no unifying trends on the softening of the shocked steel. One hour, 450°C recovery anneals eliminated work softening in the lower pressure shots, whereas the tensile properties of the higher pressure samples were only partially stabilized by aging. The annealed low-pressure and cold-rolled samples showed improved tensile properties compared to the asdeformed properties. The tensile properties of the high pressure shots were not improved by aging at 450°C.